PERFORMANCE OF SOLID DESICCANTS FOR FIXED-BED REGENERATOR APPLICATIONS

A Thesis submitted to the College of
Graduate and Postdoctoral Studies
In Partial Fulfillment of the Requirements
For the Degree of Master of Science
In the Department of Mechanical Engineering
University of Saskatchewan
Saskatoon

By

Teddy Okolo

ABSTRACT

Fixed-bed regenerators (FBRs) are a relatively novel type of energy recovery ventilator (ERV) used to reduce energy consumption in buildings. FBRs operate under cyclical conditions by storing heat and moisture in one recovery period and transferring the accumulated heat and moisture to an air stream in the next period. FBRs are very promising for heat recovery but are yet to be fully adapted for moisture transfer on a commercial scale. In order to enable moisture transfer, adsorptive materials known as desiccants can be coated on FBR plates for energy recovery. The primary goal of this thesis is to apply experimental and numerical methods to select desiccants for FBRs.

Desiccants remove moisture by an **ad**sorption process as opposed to **ab**sorption where molecules penetrate a bulk media. The sorption properties of the desiccant directly influence the latent effectiveness of FBRs during summer operation. The experimental results in this thesis showed that sorption kinetics is an important parameter for FBRs. A numerical model which includes the sorption kinetics was used to predict the dynamic behaviour of FBRs. The numerical results showed that selecting desiccants with a higher kinetic rate constant value leads to higher moisture transfer rates which in turn will increase the effectiveness of FBRs.

The main contribution of this thesis is that the results enable researchers to determine the recovery periods and parameters when sorption kinetics can be neglected, and an equilibrium model is acceptable for FBR applications. The results showed that a 5% relative error in latent effectiveness was achieved in the equilibrium model for a rate constant of at least 0.0014 1/s, thicknesses of up to 25 mm, effective diffusion coefficient of at least 2.9×10^{-5} m^2/s, and cycle periods of at least 60 s.

ACKNOWLEDGMENTS

DEDICATION

I dedicate this thesis to my father for being an outstanding role model in my pursuit of academic excellence, and to my mother for bringing me up in the way of the Lord.

TABLE OF CONTENTS

LIST OF TABLES

LIST OF FIGURES

NOMENCLATURE

Acronyms

BET	Brunauer-Emmett-Teller
ERV	Energy Recovery Ventilator
FBR	Fixed-bed regenerator
GSR	Gas-side resistance
GSSR	Gas and solid-side resistance
HVAC	Heating, ventilating and air-conditioning
IAQ	Indoor air quality
IUPAC	International Union of Pure and Applied Chemistry
LDF	Linear driving force
PGS	Pseudo gas-side resistance
RH	Relative humidity
SEM	Scanning Electron Microscopy

English symbols

A_{N_2}	Adsorbate cross sectional area for nitrogen (Å^2)
B	Systematic uncertainty
c_p	Specific heat (J/(kg·K))
C	Brunauer-Emmett-Teller (BET) constant
d	Diameter of desiccant particles (m)
D	Diffusion coefficient of water vapour in air (m^2/s)
D_{AB}	Binary diffusion coefficient of water vapour in air (m^2/s)

F_B	Mass corrections due to buoyant forces (g)
h_{fg}	Phase change energy due to adsorption/desorption (J/kg)
h_h	Convective heat transfer coefficient (W/(m$^2\cdot$K))
h_m	Convective mass transfer coefficient (m^2/s)
k	Sorption rate constant (1/s)
K	Thermal conductivity (W/(m$\cdot$K))
l	Representative elementary volume of characteristic length (m)
L	Thickness of desiccant (mm)
L_T	Characteristic length (m)
Le	Lewis number
m	Mass (g)
$\dot{m}$	Phase change rate (kg/(s$\cdot$m^3))
M	Molecular mass (g/mol)
n	Degree of freedom
N	Avogadro's number
Nu	Nusselt number
P	Pressure (Pa)
P_o	Saturation pressure (Pa)
P_X	Random uncertainty
Q	Quantity of gas adsorbed (cm^3/g)
r_p	Pore size (nm)
R	Specific gas constant (J/(kg$\cdot$K))

R_P	Particle size (mm)
Ra	Rayleigh number
S_{BET}	Brunauer-Emmett-Teller surface area (m^2/g)
S_t	Total surface area (m^2)
t	Time (s)
t_s	Student t-factor
T	Temperature (K)
u	Moisture content (g/g)
u_r	Relative moisture content
u_t	Dynamic moisture content (g/g)
U	Total uncertainty
V	Volume (cm^3)
V_l	Liquid molar volume (cm^3)
V_m	Molar volume (cm^3)
W_m	Weight of adsorbate as monolayer (g)
x	Length direction perpendicular to the desiccant (m)
z	Compressibility factor

Greek symbols

α	Thermal diffusivity (m^2/s)
α_m	Moisture diffusivity (m^2/s)
β	Water vapour adsorption in IGA-002 (g/g)
γ	Surface tension of liquid nitrogen (N/m)

Δ	Difference between adsorption and desorption moisture contents
ε	Volume fraction
λ	Error in equilibrium model assumption
ρ	Density (kg/m^3)
σ	Standard deviation
τ	Tortuosity
ψ	General transport variable

Subscripts

a	Air
ads	Adsorption period
anl	Analytical model
ave	Average
cycle	Cycle
d	Desiccant
des	Desorption period
eff	Effective porous media property
equ	Equilibrium
g	Gas
i	Initial
k	Kinetics
l	Liquid
num	Numerical model
o	Original

sat	Saturation
t	Time
v	Vapour
w	Water

CHAPTER 1

INTRODUCTION

1.1   MOTIVATION

People generally spend over 90% of their time indoors [1], which makes good indoor air quality (IAQ) vital for the occupants in buildings. The World Health Organization (WHO) cautions that long-term exposure to inadequate IAQ may not only result in cardio-vascular and respiratory disorders but can also affect our cognitive behaviour [2]. Thus, for maintaining acceptable indoor conditions in buildings – heating, ventilating and air-conditioning (HVAC) systems have been employed for space heating and cooling [3], ventilation [4], humidity control [5] and air purification [6].

Surveys in Canada have shown that HVAC systems account for over 50% of building energy consumption [7], resulting in a total operational energy cost of approximately $29 billion in 2013 [8]. Considering that cooling demand is estimated to increase by a factor of 30 from the year 2000 to 2100 [9], better systems are required given the high operational energy costs of the conventional HVAC equipment. In order to improve the energy efficiency of conventional systems, energy recovery ventilators (ERVs) have been employed in HVAC systems to reduce energy consumption by recovering heat and moisture from the exhaust air stream [10]. This energy recovery process results in a reduction of the size, energy requirement and operational cost of HVAC systems [11]. This thesis examines a relatively new ERV known as a fixed-bed regenerator (FBR).

ERVs are broadly classified into regenerators and recuperators [12]. Generally, regenerators have a higher effectiveness than recuperators [12]. Fixed-bed regenerators (FBRs) are relatively new to the HVAC field and were recently introduced in 2018 as an informative appendix in the CSA standard 439-2018 for ERV testing [13]. Previous research however, has shown FBRs to be a very

1

promising ERV for HVAC applications, chiefly due to their high sensible effectiveness (> 80%) and energy savings (> 15%) [14]. Figure 1.1 contains a schematic of a single flow channel of an FBR as it transfers heat and moisture between two airstreams. As depicted in Figure 1.1, the FBR operates by recovering the heat and moisture from the exhaust air stream in one period and then transferring the accumulated heat and moisture to the supply/ventilation air stream in the second period [15]. This storage and release of heat and moisture by the FBR is typically within a total cycle of about 120 seconds (*i.e.* 60s for exhaust air and 60s for supply air) [16]. Thus, due to this short recovery period, the transient heat and moisture transfer performance is vital for the effectiveness of FBRs.
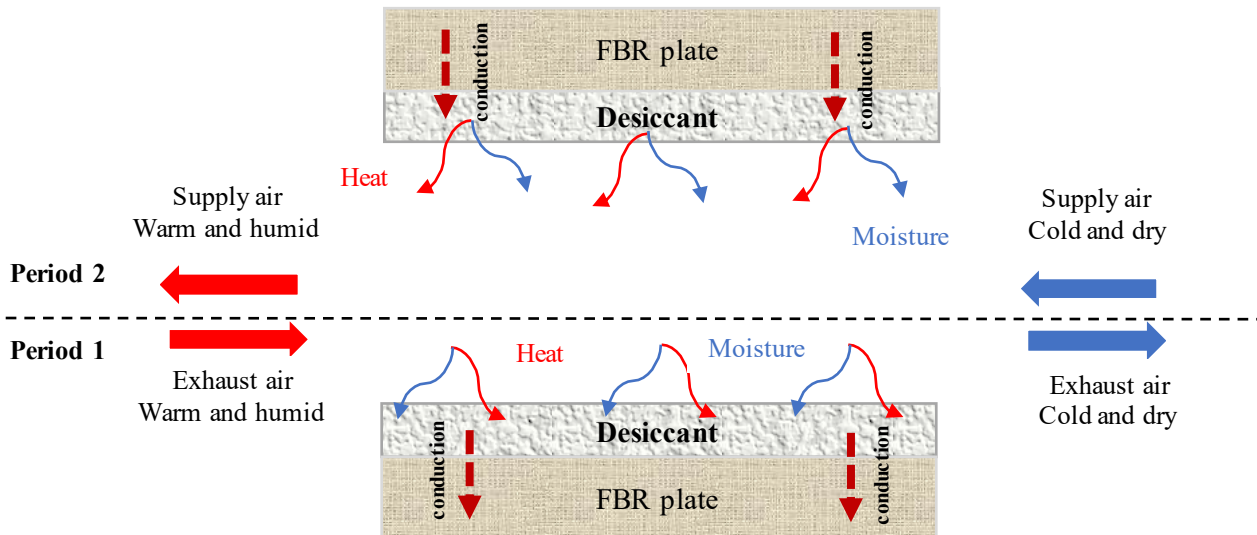
Figure 1.1. A schematic of the heat and moisture transfer in a fixed-bed regenerator.

In order to allow the FBR to transfer moisture, hygroscopic materials known as desiccants may be coated on the FBR plates. These desiccant materials remove moisture via an **ad**sorption process [17]. The **ad**sorption process of a desiccant is a surface phenomenon unlike **ab**sorption where molecules enter the bulk of the porous media. In general, the type of desiccant (*i.e.,* its sorption properties) plays a very significant role in the moisture transfer performance of desiccant coated FBRs. Recent studies have shown that the pore structure and surface area directly affect the steady-state (sorption isotherm) and transient (sorption kinetics) performances of desiccants [18], [19]. As such, FBR performance would be different with individual desiccants, because each desiccant has a distinct surface area and porous structure. Thus, this MSc study aims to present a method to

test and recommend desiccants for FBRs based on their sorption properties, porosimetry (pore sizes, surface area, etc.), and coupled heat and moisture transfer performance.

1.2   BACKGROUND

The theoretical background to this research is divided into four parts, giving a general insight into the experimental and numerical investigations carried out in Chapters 2 and 3 of this thesis. The first part (Section 1.2.1) explains molecular adsorption, which is the primary basis for desiccant-moisture interactions. The second part (Section 1.2.2) classifies desiccant materials with typical examples. The third part (Section 1.2.3) presents the desiccant performance and characterization parameters to be measured while the fourth part (Section 1.2.4) provides the basis for the modelling approach adopted in this thesis.

1.2.1   Molecular Adsorption

As discussed in Section 1.1, adsorption is a surface process where the adsorbate (molecules adsorbed) does not penetrate the bulk of the media. The theory of 'true adsorption' was first illustrated by Irving Langmuir [20] in 1918, presenting that molecules adhere or condense on surfaces with a thickness of a mono-molecular layer as shown in Figure 1.2(a). Further studies on adsorption [21], showed that gaseous molecules can also 'condense' in multi-molecular layers at higher relative pressures (or relative humidity in the case of air) as shown in Figure 1.2(b).
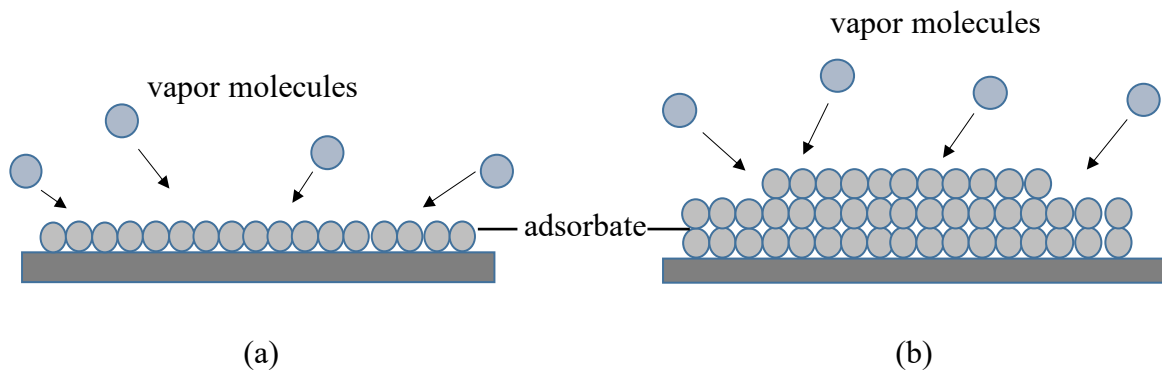
Figure 1.2. Molecular adsorption in (a) monolayer formation and (b) multi-layer formation.

Generally, molecular adsorption may occur in the form of either physisorption (physical adsorption) or chemisorption (chemical adsorption). Physisorption is a reversible process (*i.e.,* adsorption/desorption) whereby the molecules on the desiccant surface are held together by weak

Van Der Waal's forces [22]. Chemisorption on the other hand, is an irreversible process with very high heats of adsorption and activation energies [23]. Table 1.1 summarizes the major differences between physisorption and chemisorption. Physisorption is the most relevant in HVAC given its applications in porosimetry analysis (surface area, pore volume, pore width, etc.) and water vapour sorption, while chemisorption finds its major application in heterogenous catalysis.

Table 1.1. Differences between physisorption and chemisorption [22], [24].

Property	Physisorption	Chemisorption
Bonding force	Van Der Waals	Chemical bonds
Isothermal reversibility	Complete	Usually not possible
Activation energy	No energy barrier	60 – 100 kJ/mol
Differential heat of adsorption	< 40 kJ/mol	50 – 200 kJ/mol
Molecular adsorption type	May form multilayers	Monolayer formation

1.2.2 Desiccant materials

Solid desiccants are usually porous materials which remove water vapor molecules (moisture) from an air stream by adsorption. Figure 1.3 depicts the classification of solid desiccant materials with their common examples compiled from Refs. [17], [25], [26].

Solid desiccant materials

Conventional desiccants

- Silica gel
- Zeolites
- Molecular sieves
- Activated alumina
- Activated carbon

Composite desiccants

- Silica gel-host composites
- Mesoporous silicate-based composites
- Carbon-host composites
- Natural rock-host composites
- Binary salt-based composites

Polymer desiccants

- Polyelectrolytes
- Metal-organic frameworks (MOFs)

Figure 1.3. Classification of solid desiccants with common examples.

Highlighted properties of some conventional solid desiccants are summarized as follows:

- Silica gel is widely used in many industrial applications for drying due to its nominal cost and porous nature, however, it has the minor drawback of odour complications at high relative humidities (RH) [27].

- Natural zeolites and molecular sieves (synthetic zeolites) perform better than silica gel at lower RH (< 40%) but are a more expensive option [28]. However, they are prevalent in many HVAC applications, as they do not possess the musty odour and mould complications that plagues silica gel.

- Activated carbon is best suited for higher RH (> 70%) due to its low hydrophobicity [19]

- At any RH, the sorption uptakes of silica gel and activated alumina present acceptable results for HVAC applications [29].

In general, conventional desiccants have presented acceptable performances in many industrial applications. However, in order to achieve greater sorption uptakes and mitigate the limitations of conventional desiccants, recent studies have been developed in composite and polymer desiccant materials. These 'novel' desiccants have about 3 – 12 times higher sorption capacities in

comparison to the conventional desiccants but generally with the drawback of greater costs [30]–[33].

1.2.3 Desiccant performance and characterization

The performance of solid desiccants for HVAC applications are dependent on their steady-state and transient moisture uptakes (*i.e.,* sorption isotherm and sorption kinetics) [25]. However, these sorption performances are also dependent on their textural properties (such as the pore size and surface area) which describe the desiccant's sorption attributes [27].

1.2.3.1 *Sorption isotherm and sorption kinetics*

The sorption isotherm of a desiccant represents its steady-state moisture uptake as a function of air relative humidity at a constant temperature. Generally, for the same mass of desiccant, the equilibrium moisture uptake (at steady-state) is higher at lower temperatures [34], [35]. In many applications, the moisture uptake is best represented as a normalized mass ratio in units of g/g or kg/kg (*i.e.,* the mass of water vapor adsorbed by the mass of dry desiccant). As delineated by the International Union of Pure and Applied Chemistry (IUPAC) [22], the sorption isotherms are classified into six types according to their shapes, where the type I isotherm represents monolayer adsorption while types II – VI represent multilayer adsorption of gases on porous/non-porous desiccants.

The sorption kinetics of a desiccant describes the transient moisture uptake at a particular temperature and air relative humidity. In simpler terms, the sorption kinetics defines how quickly the desiccant is capable of removing moisture from or releasing moisture to the air at a specific operating condition. In a solid desiccant system, sorption kinetics is a vital parameter because it affects the recovery period required for moisture transfer [36] which is also important for FBRs where the total cycle is about 120 seconds [16].

1.2.3.2 *Desiccant characterization*

The sorption performance of solid desiccants depends on their material and geometric (textural) characteristics. Various techniques can be used to characterize desiccants and identify the dominant phenomena responsible for their unique sorption attributes. Table 1.2 highlights a few of the common characterisation techniques in the literature. The most prevalent in HVAC

applications are the surface imaging and nitrogen adsorption techniques. Thus, in this thesis, only nitrogen adsorption and scanning electron microscopy (SEM) imaging are used to characterize the desiccants selected for application on the FBR.

Table 1.2. Summary of common characterization techniques for solid desiccants.

Characterisation Technique	Equipment	Function
Scanning Electron Microscopy (SEM)	Scanning electron microscope	Provides a 3D pictorial representation of the external surface structure
Transmission Electron Microscopy (TEM)	Transmission electron microscope	Provides a 2D pictorial representation of the internal structure
X-Ray Photoelectron Spectroscopy	Monochromatic XPS system	Presents the elemental composition of materials and their unique binding energies
X-Ray Diffraction	X-Ray diffractometer	Depicts the molecular structure by virtue of its diffraction patterns
FT-IR Spectroscopy	Spectrophotometer	Presents the spectral signature of materials in order to identify functional groups responsible for high intensity adsorption bands
Nitrogen Adsorption Isotherm	Sorption analyser	Evaluates textural properties such as: surface area, pore width, pore volume, etc.

1.2.4   Heat and mass transfer modelling

Several numerical methods have been developed over the years to analyze and solve the coupled heat and mass transfer problems in various applications. These methods can be divided into three types as depicted in Figure 1.4 and as summarized from Refs. [37]–[39] namely: (i) Gas side resistance (GSR), (ii) Gas and solid side resistance (GSSR), and (iii) Pseudo gas and solid side resistance (PGS) models.

```mermaid
flowchart TD
    A[Modelling approach] --> B[Gas-side resistance GSR]
    A --> C[Gas and solid side resistance GSSR]
    A --> D[Pseudo-gas-side resistance PGS]
```

Modelling approach

Gas-side resistance (GSR)

Gas and solid side resistance (GSSR)

Pseudo-gas-side resistance (PGS)

Advantages

- Least computation time
- No requirement for desiccant diffusion terms

Advantage

- Best accuracy as it includes desiccant diffusion and conduction terms

Advantage

- Lesser computational time than GSSR

Disadvantage

- Diffusion and conduction within the desiccant bulk is neglected (*i.e.,* assumed to be infinite)

Disadvantage

- Highly complex model with longer computational times

Disadvantage

- Requires a lumped heat and mass transfer coefficient which can only be obtained through experiments

Figure 1.4. Overview of modelling techniques summarised from Refs. [37] – [39].

The GSR method solves the heat and mass transfer between the air stream and the desiccant surface, neglecting the diffusion and conduction resistance within the solid side (*i.e.,* desiccant bulk) [40]. The GSSR method on the other hand is generally the most preferred, as it includes the inter/intra-crystal diffusion through and between the pores (on the gas and solid side), thereby resolving the entire porous media problem [38] of the desiccant. This method would be referred to as porous media modelling in the later sections of this thesis. The PGS method, which is typically

a compromise between the first and second methods, uses a lumped heat and mass transfer coefficient (obtained experimentally) to represent the gas (air-side) and solid side (desiccant bulk) resistances [38].

The coupled heat and mass transfer process in a desiccant coated layer or a desiccant bed is a complex process involving many physical phenomena which occur simultaneously. Many numerical studies assume instantaneous diffusion with a uniform moisture content in the desiccant (*i.e.*, GSR method) [41], however, this does not accurately capture the physical problem. This is chiefly due to two major reasons: (i) there is a delay in adsorption due to the sorption kinetics (*i.e.,* adsorption is not instantaneous) and (ii) diffusion governs the moisture transfer within the porous desiccant (*i.e.,* desiccant moisture content is not uniform) [42]. As a result, the moisture content in the bulk desiccant is not uniform and in equilibrium with the air due to this transient process, resulting in a coupling between the kinetics (delay in adsorption) and diffusion within the porous desiccant [42]. Neglecting this physical concept could potentially lead to errors in estimating performance of the desiccant coated FBR, given that the total cycle is only about 120 seconds. It should also be noted that sorption kinetics occurs at a much faster rate than molecular diffusion [43], which makes kinetics a vital piece for any adsorption model. In this study, a porous media approach (GSSR) is used to resolve the complex heat and mass transfer problem by also incorporating a sorption kinetic model (*i.e.,* the LDF model).

1.3 LITERATURE REVIEW

The adsorption phenomena of desiccant materials has been adopted in many industrial processes and fields such as in agriculture [44]–[47], gas separation [48], [49], chemical processing [50]–[53], and HVAC [54]–[57]. Thus, the available literature regarding desiccant materials and adsorption systems is diverse and copious. Nevertheless, considering that this thesis presents a methodology to recommend desiccants for FBRs in HVAC, applications of desiccants in other fields (*i.e.,* chemical and mining engineering) are not reviewed in detail. Figure 1.5 shows a statistical analysis of articles published in the past 25 years via numerous databases. The articles are divided into 3 search criteria: (i) desiccant studies, (ii) desiccant studies in HVAC (a sub-set of the first item) and (iii) solid desiccant materials in energy exchanger applications (a sub-set of the second item).

In all three search criteria, the results were generated using their respective keywords as shown in Table 1.3 and for all publications between the years 1995 – 2020 via following online databases: Engineering Village (www.engineeringvillage.com), Scopus (www.scopus.com), Web of Science (www.webofscience.com), Science Direct (www.sciencedirect.com) and ASME publications (asmedigitalcollection.asme.org). It should also be noted that duplicate and irrelevant articles from all databases were removed from the search results.
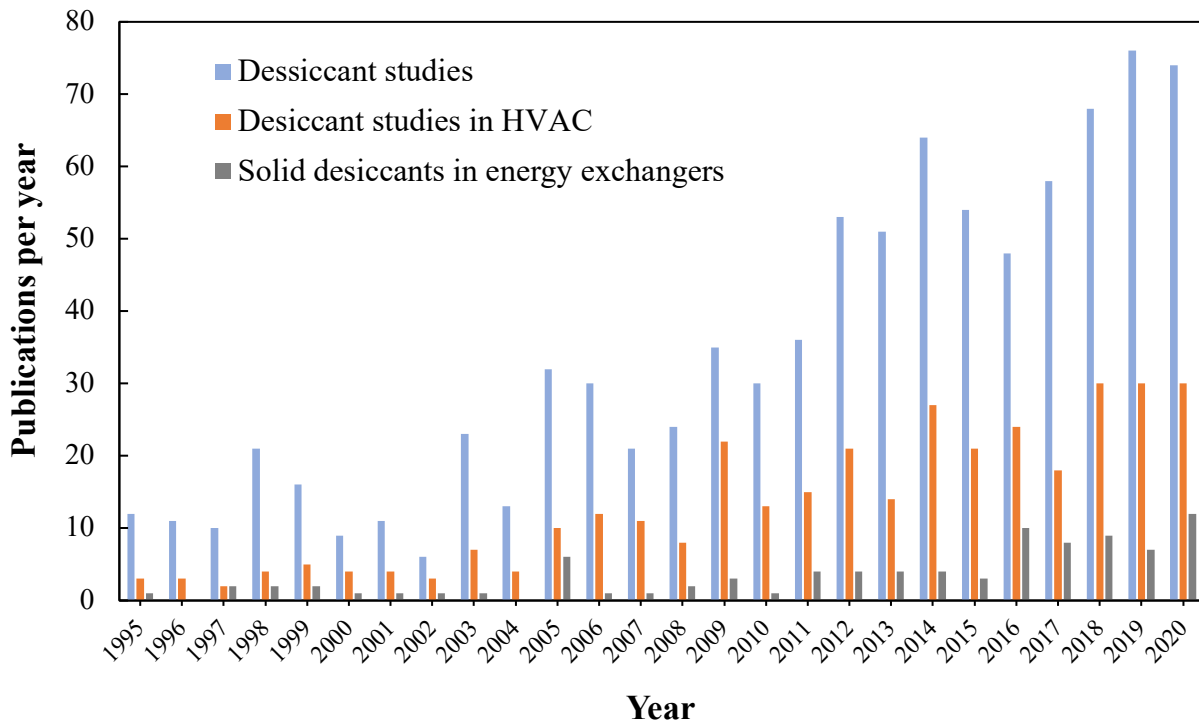
Figure 1.5. Classification of the 886 publications on the sorption performance of desiccant materials between the years 1995 – 2020 in Engineering Village, Scopus, Web of Science, Science Direct and ASME databases.

Table 1.3. Search criteria and keywords used for literature review.

Search Criterion	Keywords
Desiccant studies	"adsorption", OR "desorption", OR "sorption" AND "desiccant".
Desiccant studies in HVAC	"adsorption", OR "desorption", OR "sorption" AND "desiccant" AND ("heating" OR "air-conditioning").
Solid desiccant studies in energy exchanger applications	"adsorption", OR "desorption", OR "sorption" AND "solid desiccant" AND "energy exchanger".

Considering Figure 1.5, an overall increasing trend can easily be observed in desiccant material research as would be expected, likewise the recent interest in energy exchanger applications from the year 2016 can also be noticed. Figure 1.6 highlights the methodologies used for desiccant studies in energy exchanger applications.
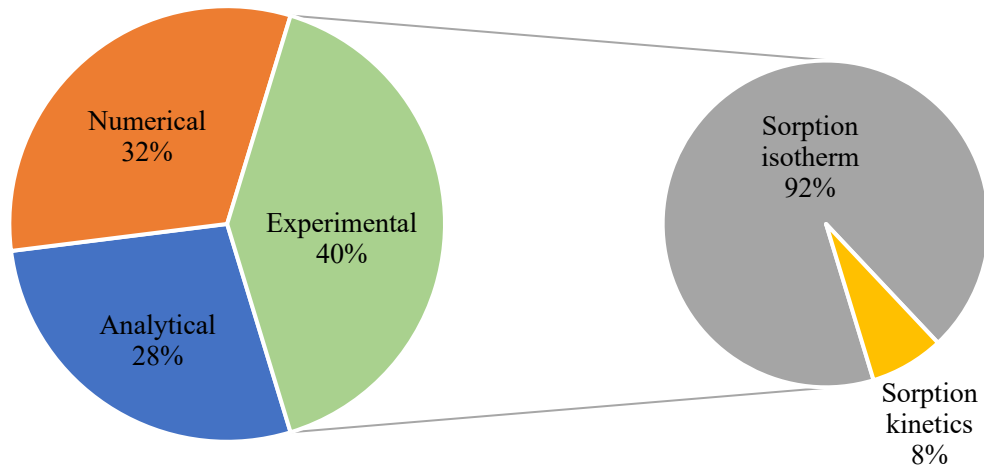
Figure 1.6. A classification of the desiccant studies in energy exchangers between 1995 – 2020 in 90 journal papers.

It can be observed that the numerical and analytical studies (60%) exceed the experimental studies (40%) published on energy exchanger applications. However, very few of those experimental studies focused on the sorption kinetics (only 8%). Additionally, it should also be noted that there are no available numerical models at this time investigating sorption kinetics in energy exchangers; however, sorption kinetics has been presented in other fields such as in chemical and mining

engineering. This shows that there are limited studies investigating the sorption kinetics for energy exchanger applications. Therefore, this MSc study targets the gap in the literature for energy exchangers, presenting both experimental and numerical investigations into the kinetics of desiccant moisture interactions for FBR applications.

1.4 RESEARCH OBJECTIVES

The main objectives of this thesis are to address the gap (*i.e.,* limited numerical studies on sorption kinetics in energy exchangers) in the literature as highlighted previously in Section 1.3, in order to develop a methodology to select desiccants for FBR applications. To meet the main objectives, two major tasks are set and carried out sequentially in order to evaluate the desiccant performance for FBR applications and address the literature gap as delineated in Figure 1.7. Additionally, in order for a thorough methodology to be presented in this thesis, both experiments and numerical analysis were conducted.

MAIN OBJECTIVES: Develop a methodology to select desiccants for fixed-bed regenerators (FBRs).
Literature gap: limited studies on sorption kinetics for FBRs.

Major tasks:

Ch.2
- Measure the relevant properties (textural, sorption isotherm, sorption kinetics) of a few selected desiccants for FBRs and determine their uncertainty.

Ch.3
- Develop and verify a porous media numerical model to determine the heat and moisture transfer performance of a desiccant-coated layer for FBR applications.

Figure 1.7. Research objectives and chapter numbers where corresponding tasks are addressed.

1.5 THESIS STRUCTURE

This MSc thesis is written in manuscript-style, consisting of a total of four chapters and four appendices. The first chapter consists of the thesis introduction, while the final chapter consists of the summary, conclusions and recommendations for future research. The two middle chapters

(*i.e.,* Chapter 2 and Chapter 3) contain the experimental and numerical studies respectively as outlined in the Figure 1.7.

The appendices of this thesis contain the supplementary information. Appendix A provides the detailed uncertainty analysis for the property measurements described in Chapter 2. Appendix B presents the local volume averaging and local thermal equilibrium methods used to develop the porous media numerical model in Chapter 3. Appendix C contains the discretized governing equations used in the porous media model and the MATLAB program. Lastly, the reliability (*i.e.,* sensitivity study) in the selection of grid size, time step, convergence criterion, and residuals of the MATLAB simulation program are presented in Appendix D.

CHAPTER 2

MEASUREMENT OF DESICCANT PROPERTIES

2.1   OVERVIEW

This chapter addresses one of the major tasks of the thesis, which is "*to measure the relevant properties (textural, sorption isotherm, sorption kinetics) of a few selected desiccants for FBR and determine their uncertainty*". This chapter presents an experimental method to evaluate desiccant properties (*i.e.,* textural and sorption) for FBR applications. The textural properties (porosimetry) were measured using an Accelerated Surface Area and Porosimetry (ASAP) instrument while the sorption properties were measured using a gravimetric (IGA-002) sorption analyzer.

The results in this chapter shows that the desiccants' surface area and pore size directly influence both the equilibrium sorption capacity and the kinetics of the desiccant during moisture transfer. A sorption rate constant (k) is also defined which represents the kinetic properties of the desiccant at specific operating periods.

The manuscript in this chapter has been submitted to the Industrial and Engineering Chemistry Research Journal. The authors of the manuscript are Teddy Okolo (M.Sc. Student) who conducted the tests and wrote the manuscript, Easwaran Krishnan (PhD student) who performed the scanning electron microscopy (SEM) experiments, Gurubalan Annadurai (Post-Doctoral Fellow) who provided feedback and comments on the manuscript, and Carey J. Simonson (M.Sc. Supervisor) who critically reviewed the manuscript and supervised the study.

Water vapour sorption and kinetic properties of solid desiccant coatings for fixed-bed regenerators

T.I. Okolo, E.N. Krishnan, G. Annadurai, C.J. Simonson

2.2 ABSTRACT

Fixed bed regenerators (FBRs) are relatively novel energy exchangers in the HVAC field which operate by storing and releasing energy with an airstream over a total cycle of 120 seconds. FBRs can be adapted for energy exchange (*i.e.,* heat and moisture transfer) by coating the FBR plates with hygroscopic desiccants. The primary aim of this chapter is to develop an experimental method for testing desiccants for FBR applications.

The proposed methodology in this chapter recognises the fact that FBRs are transient devices, and as such, the sorption kinetics of a desiccant at the initial stages of adsorption and desorption are vital for FBR performance. Furthermore, a crucial parameter for sorption kinetics known as the kinetic rate constant was identified and its roles for FBR applications were discussed.

The results indicated that since FBR operates within a cycle of only 120 seconds (*i.e.,* 60 s adsorption and 60 s desorption), selecting desiccants with faster kinetics during the first 60 s of adsorption is the more preferred option, as opposed to selecting desiccants with higher moisture uptakes over an equilibrium process.

2.3   INTRODUCTION

The recent COVID-19 global pandemic has driven the need to increase building ventilation rates in order to reduce concentrations of aerosol and viral contaminants in indoor spaces [58]. Heating, ventilating and air-conditioning (HVAC) systems are generally employed for maintaining adequate indoor air quality (IAQ) in buildings [59]. However, increasing ventilation rates to improve IAQ increases building energy consumption and costs. For example, a recent study [60] on the impact of COVID-19 on HVAC systems reported up a 128% increase in energy consumption. In addition, one of the key recommendations for reducing household energy costs during the pandemic was the use of energy recovery ventilators (ERVs) to precondition the fresh air supplied to the building [60], [61].

Fixed-bed regenerators (FBRs) are a relatively novel type of ERV with high sensible effectiveness and energy savings potential [16]. FBRs consist of several desiccant coated plates and operate by recovering heat and moisture from the exhaust air stream in one period and then transferring the accumulated heat and moisture to the supply/ventilation air stream in the second period [15]. This storage and release of heat and moisture occurs within a total cycle of about 120 seconds (*i.e.* 60s for exhaust air and 60s for supply air) [16]. The heat and moisture transfer performance of any ERV (including the FBR) is dependent on two major factors [62], [63]: (i) the intrinsic properties of the adsorptive material (*i.e.* sorption isotherm, sorption kinetics, textural properties) and (ii) the design and operating parameters of the equipment (*i.e.* plate geometry, hydraulic diameter, corrugation angles). However, this thesis focuses on FBR applications based on properties of the adsorptive material known as desiccants.

Desiccants are the primary adsorptive materials used in coating FBRs to enable moisture interactions with the air stream via an **ad**sorption process [37]. The theory of adsorption and motivations for investigating the properties of solid desiccants have been discussed previously in Chapter 1. Research studies on solid desiccant based ERVs are copious, with increasing interest over the past few decades [10], [38], [56], [62]–[65]. However very few of these studies are focused on FBRs [29], [65], and no known studies at this time were focused on the effect of intrinsic desiccant properties on FBR performance.

Previous solid desiccant studies on ERVs [56] showed that the driving force for moisture transfer is the relative humidity (or relative pressure) gradient between the surface of the desiccant and the air stream. The relative humidity at the surface is determined from the equilibrium moisture content of the desiccant via the sorption isotherm [56], [63]. However, in FBRs which have a short operating period, the equilibrium capacity of the desiccant may not be reached due to the kinetic delay of moisture transfer into the desiccant pores and internal sorption sites [27]. Thus, selecting desiccants for use in FBR based on an equilibrium sorption process could potentially lead to errors. In this regard, this chapter aims to present a method to test and recommend desiccants for FBR applications based on their sorption performance (kinetics and isotherm) and textural properties (pore sizes, surface area, etc.). These characteristics can then be used as input parameters to model the performance of desiccant coatings or a desiccant coated layer in FBR as shown later in Chapter 3. This chapter presents a better understanding of the kinetic performance of solid desiccants, which in turn will enable a better design of desiccant coated FBRs.

2.4   THEORY

2.4.1   Porosimetry

The term porosimetry refers to the methods or techniques used in quantifying the porous structure of a material [66]. The quantifiable parameters evaluated for porosimetry analysis were the average pore width, pore size distribution, pore volume, and available surface area. According to the International Union of Pure and Applied Chemistry (IUPAC), physisorption is the best suited method for porosimetry analysis [22]. As described earlier in Section 1.2, physisorption is a reversible process whereby molecules are adsorbed on the desiccant surface by virtue of weak Van der Waal's forces. As a result, physisorbed molecules adhere on the external surface area and porous network without penetrating the desiccant or changing its physical properties via chemical reactions. In many applications, 'non-reacting' adsorbates such as noble gases (argon, krypton, xenon, etc.) are used for porosimetry analysis. However, due to the high cost of these noble gases, a cheaper alternative – nitrogen, has been used extensively in the literature. In addition to cost, the popularity of nitrogen is primarily due to its stable adsorption/desorption isotherms at 77 K.

In practice, the amount (*i.e.,* volume or mass) of gas adsorbed on the desiccant surface at any relative pressure is determined by the difference between the amount of adsorbate gas dosed into

the sample chamber and the gas remaining in the sample chamber [67]. Over several decades, many correlations have been developed to evaluate desiccant surface area and pore sizes respectively. Some of these methods and their assumptions are highlighted as follows:

1. Langmuir method: This method is used to evaluate the surface area of a desiccant with the assumption that the entire adsorption process occurs in an adsorbate monolayer [20]. The hypothesis of this method is never truly fulfilled and typically leads to an overestimation of the desiccant's surface area [68].

    The oversight in this theory can be explained using figure 2.1. In the figure, the quantity adsorbed reaches a near steady value at a certain relative pressure much less than the saturation pressure in the type I (Langmuir type) isotherm below. As such, the assumption that there is still available surface area for monolayer adsorption at the remaining relative pressures up to saturation would result in an overestimated value. Due to this reason, this method was not adopted in this thesis.
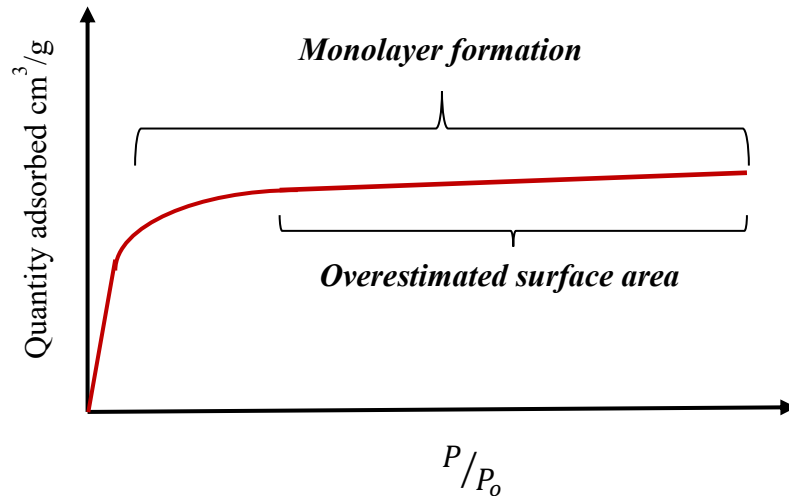
Figure 2.1. Langmuir method for surface area estimation (type I isotherm only)

2. Brunauer-Emmett-Teller (BET) method: This method is an extension of the Langmuir model [21]. It enables a more accurate evaluation of the available surface area in a desiccant regardless of the isotherm type. As a result of its robustness, this model was used for all surface area evaluations in this thesis. Theoretically, the BET method assumes that even for a multilayer isotherm, the available surface area for the first monolayer is between the relative pressure range of $0.05 - 0.35$ [24] as depicted in the figures 2.2(a) and 2.2(b).

18
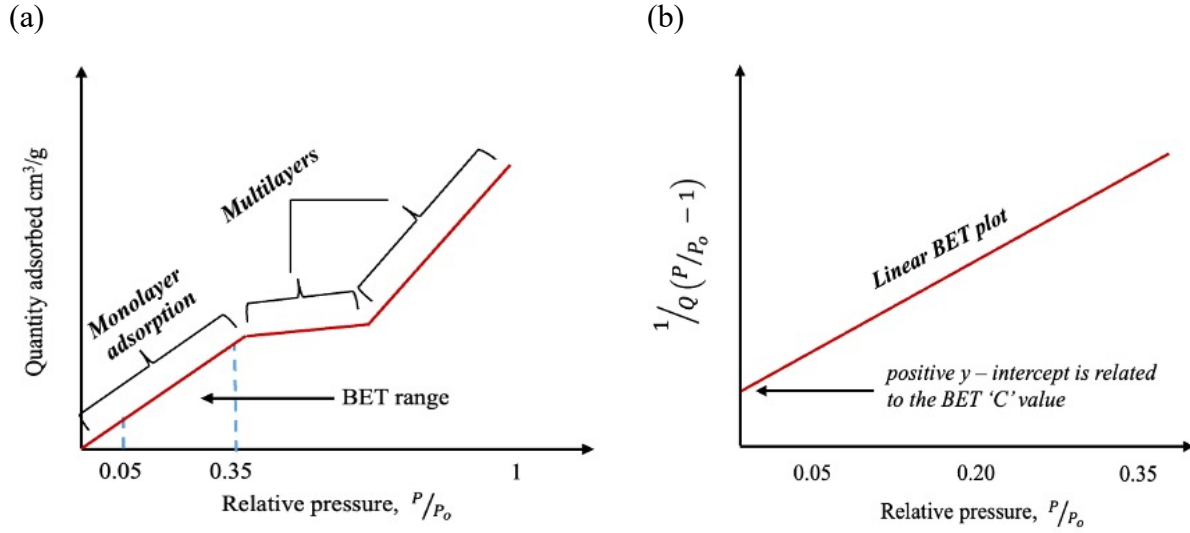
Figure 2.2. Brunauer-Emmett-Teller (BET) surface area estimation for a type II desiccant showing the (a) isotherm, and (b) transform plot.

The BET equation states that the amount of gas adsorbed is proportional to the relative pressure and heat of adsorption (related to the C constant) required to form a monolayer [21]. It is expressed by:

$$\frac{1}{Q\left(P/P_o - 1\right)} = \frac{1}{W_m \cdot C} + \frac{C-1}{W_m \cdot C} \cdot \left(P/P_o\right) \tag{2.1}$$

In Equation (2.1), the BET constant (C) is related to the heat of adsorption of the adsorbate and its value must always be positive for a physically realistic surface area plot. In order to evaluate the surface area, a linear plot of $1/Q(P\,/\,Po - 1)$ against $P\,/\,Po$ is required as shown in figure 2.2(b). The weight of gas adsorbed as a monolayer (W_m) is related to the BET plot by:

$$W_m = \frac{1}{slope + intercept} \tag{2.2}$$

The total surface area (S_t) available for adsorption by the desiccant can then be evaluated in accordance with Avogadro's law, in relation to the molecular weight (M) and molecular cross-sectional area for nitrogen gas (A_{N_2}) or any other gas used for physisorption.

$$S_t = \frac{W_m N A_{N_2}}{M} \qquad (2.3)$$

In many applications [24], the BET area (S_{BET}) is represented as a specific surface area for comparison purposes with other materials. Equation (2.3) can thus be simply expressed as a ratio of the total surface area to the sample mass (m) in units of m²/g as shown below:

$$S_{BET} = {S_t}/{m} \qquad (2.4)$$

3. Barrett-Joyner-Halenda (BJH) method: This method is widely used to determine the pore volume, average pore size and pore size distribution of porous materials [69]. It is based on the Kelvin equation which is best suited for mesoporous and macroporous desiccants [24]. According to IUPAC [22], pore sizes are classified using the nomenclature presented in Table 2.1.

Unlike the BET surface area method, the BJH method is valid for a relative pressure range of $0.1 - 1$ [69]. The lower limit of this range is 0.1 because micropore filling is assumed to be complete at this relative pressure, while the upper limit is the saturation point (P/P$_o$ ≈ 1) where capillary condensation of the liquid adsorbate takes place in the desiccant pores. Figure 2.3 shows the process of determining the pore volume from an isotherm with hysteresis, and a pore size distribution plot after implementing the Kelvin equation.

Table 2.1. Classification of micro, meso and macropores based on pore size [22].

Classification	Average pore size
Microporous	< 2 nm
Mesoporous	2 – 50 nm
Macroporous	> 50 nm
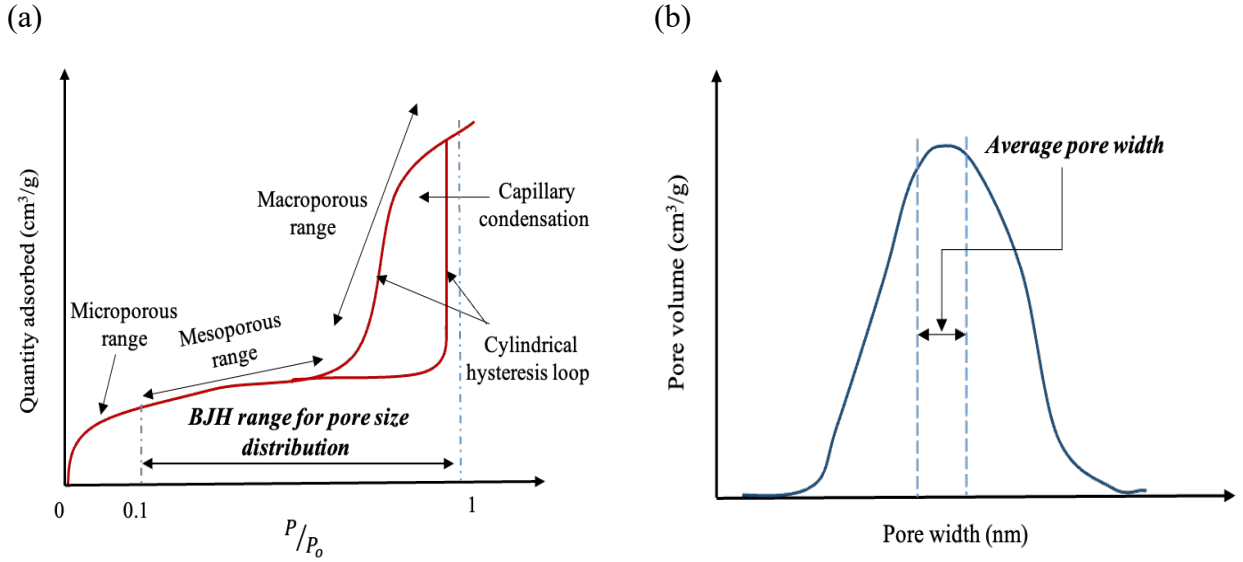
Figure 2.3. Barrett-Joyner-Halenda (BJH) pore analysis method for a type IV desiccant showing the (a) isotherm (b) pore size distribution plot

The BJH method is based on two major assumptions from the Kelvin equation [19]. Firstly, the pores of the desiccant are assumed to be cylindrical as noted in the adsorption/desorption hysteresis loop in figure 2.3(a). Secondly, fluid-wall interactions are negligible (*i.e.,* negligible film thickness) in the desiccant pores. The pore radius (r_p) can then be evaluated using the Kelvin equation [69]:

$$ln \frac{P}{P_o} = \frac{-2\gamma V_l}{r_p RT} \tag{2.5}$$

4. Horvath-Kawazoe method: Unlike the BJH method, which is accurate for mesoporous and macroporous desiccants, the Horvath-Kawazoe method is used to accurately determine the micropore volume and pore size distribution of a desiccant [70]. As a result, this model was used for micropore analysis in this thesis. Theoretically, it is based on the assumption that the porous network is of a slit-pore type geometry. Similar to the BJH method, a pore size distribution plot of pore volume against pore width is obtained. The H-K model can be expressed mathematically as [43]:

$$R \cdot T \cdot ln \frac{P}{P_o} = E_o + Y \tag{2.6}$$

21

where E_o is the potential function which represents the adsorbent-adsorbate interactions and Y represents the adsorbate-adsorbate-adsorbent interactions.

2.4.2 Sorption performance

The sorption performance of a desiccant is usually presented in terms of its steady-state (sorption isotherm) and transient (sorption kinetics) gaseous uptake. A typical water vapour sorption isotherm is plotted as the moisture uptake (amount adsorbed) against relative humidity at a particular temperature. The equilibrium moisture content (u) is evaluated by:

$$u = \frac{m_{eq} - m_o}{m_o} \tag{2.7}$$

where: m_{eq} is the desiccant mass at the end of a sorption process (*i.e.,* equilibrium sorption quantity), and m_o is the initial or original dry mass of the desiccant as defined in the nomenclature.

The sorption kinetics on the other hand is typically presented as the dynamic moisture content (u_t) which is evaluated by [27]:

$$u_t = \frac{m_t - m_o}{m_o} \tag{2.8}$$

where m_t is the mass at any given time (t) since the start of the sorption process.

Sorption kinetics may also be represented in terms of a normalized relative moisture uptake (u_r) which is evaluated by:

$$u_r = \frac{m_t - m_o}{m_{eq-} m_o} \tag{2.9}$$

2.4.3 Linear driving force model

The linear driving force (LDF) model is a classical method proposed by Glueckauf in 1955 [71] and is used to describe the kinetics and dynamic behaviour of adsorption-based systems. The LDF model gives a good approximation for the overall kinetics mass transport (*i.e.,* kinetics and diffusion) without solving the more complex Fickian diffusion equations [72]–[75]. This

advantage of simplicity makes it a widely used method for kinetics approximations in the literature [76]. It is represented mathematically as:

$$\partial u_t / \partial t = k(u - u_t) \tag{2.10}$$

Equation (2.10) shows that the rate of adsorption is directly proportional to the difference between the dynamic moisture content (u_t) at a given time (t) and the equilibrium moisture content (u). In other words, Equation (2.10) represents how quickly the moisture content in the desiccant reaches its equilibrium sorption quantity as described by a proportionality constant (k).

where k is the kinetic rate constant of the desiccant

Rearranging Equation (2.10) and applying the Napierian logarithm,

$$-\ln\left(1 - \frac{u_t}{u}\right) = kt \tag{2.11}$$

The rate constant (k) can then be evaluated by curve fitting $-\ln\left(1 - \frac{u_t}{u}\right)$ against t in Eq. (2.11).

2.5   EXPERIMENTS

2.5.1   Materials

This section addresses the first objective task of this thesis – which is to present an experimental method for testing and evaluating the sorption properties of desiccants for FBR applications. Three of the desiccants analyzed in this thesis were extracted from three desiccant coated FBR samples, manufactured by Wieland Metal Services, Warwick. The FBRs were coated with a 3Å molecular sieve (MS) desiccant impinged with three different binders. In this thesis, the three coating samples are referred to as white, green and blue as seen in Figure 2.4(a). The white MS + binder sample is a common type of 3Å MS desiccant coating used in ERVs. The blue is the same MS desiccant and binder, but with a cross linking agent to prevent flaking/cracking (*i.e.,* better durability). Lastly, the green MS + binder is also the same MS + binder as the white and blue, however, an optimum desiccant-binder mixing ratio was used to achieve a higher performance as reported by the manufacturer. The exact chemical composition and mixing ratio of the binder is not reported due to confidentiality; however, this thesis strictly focuses on the method of evaluating desiccant

performance for FBR as opposed to desiccant/binder synthesis. In this regard, the methodology presented in this thesis can be used for other desiccants.

In addition to the 3 MS + binder samples, a silica gel desiccant shown in Figure 2.4(b) from Thermo Fisher Scientific (United States) was also tested and analyzed for comparison with the 3Å MS samples. In this chapter, experiments were conducted on the four desiccants shown in Figure 2.4 in order to measure their textural properties (porosimetry and surface structure), sorption isotherm and sorption kinetics. It should be noted that the 3 MS + binder samples shown in Figure 2.4(a) are very brittle (*i.e.,* brake easily upon handling), and as a result, the samples were tested in a powder form.

(a)

(b)
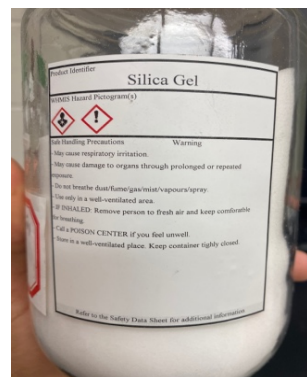
Figure 2.4. Photographs of the (a) white, green, and blue molecular sieve (MS) desiccants, and the (b) silica gel desiccant.

2.5.2 Experimental methods

The textural properties of all 4 samples were characterized using porosimetry and surface imaging techniques. The surface imaging was conducted via Scanning Electron Microscopy (SEM) by using a Hitachi SU8010 field emission instrument whereas the porosimetry analysis was conducted using an Accelerated Surface Area and Porosimetry instrument (Micromeritics ASAP 2020). In order to obtain the pore size distribution and surface area of the samples, nitrogen adsorbent at 77K was used for porosimetry analysis. The surface areas were evaluated using the BET method [21], while the pore size distributions were evaluated using the Horvath-Kawazoe [70] and BJH methods [69] for the MS + binder samples and silica gel respectively. It should also be noted that

the porosimetry parameters were evaluated using the required equations and transform plots as illustrated in Section 2.4.

Although, physisorption data provides a detailed insight into the amount of adsorbate removed by a desiccant sample, such data is insufficient for HVAC applications. This is because an FBR is exposed to moisture not nitrogen, and as such, water vapour sorption data is essential. Previously, correlations for effectiveness in ERVs [55], [62] showed that a sorption isotherm with a linear slope at the operating relative humidity (typically 30% – 50% in HVAC) gives the highest performance. Recently, these correlations were used to predict latent and total effectiveness in FBR [77], showing very good agreement with experiments. In this regard, a good indicator of a high performing desiccant for FBR applications would be a linear isotherm slope at the operating relative humidity. The test method developed for desiccant selection in this chapter is to evaluate the textural properties, and then the sorption isotherm and kinetics, which are the primary indicators of the desiccants moisture transfer properties that influence latent effectiveness in FBRs.

In addition to the sorption isotherm data, sorption kinetics is also vital given that it has the potential to affect the selection of the recovery period. FBRs typically operate in a complete cycle of 120 s (60 s adsorption/60 s desorption), and as a result, a desiccant may never reach its equilibrium sorption capacity during a given period. This chapter presents a method to quantify the sorption kinetics during the first 60 s of adsorption, which in turn, provides a better understanding of desiccant kinetic performance during the 60 s periods. Given that FBRs are transient devices, moisture transfer measurements using humidity sensors pose several difficulties for performance evaluations [77]. In order to determine desiccant performance for FBR, this chapter identifies crucial parameters such as the sorption rate constant (k), from which a numerical model can be used to evaluate the effects and roles of the sorption kinetic delay on FBR performance. This rate constant represents the overall mass transfer coefficient that includes both sorption kinetics and diffusion, which makes it useful for predicting performance. It should be noted that this thesis presents a general method which can be used for any type of solid desiccant.

2.5.3 Water vapour sorption measurements

2.5.3.1 Test facility

Two general methods are used to measure the amount of adsorbed water vapour in desiccants [75]. They are the gravimetric and volumetric methods. The gravimetric method measures the change in mass of the desiccant sample due to adsorption [78]. In this method, a high precision microbalance located inside the sample chamber is used to measure the mass increase due to water vapour sorption as the desiccant is exposed to air at a step-change increase in relative humidity. The volumetric method on the other hand, measures the volume of water vapour adsorbed by the calculating the difference between the amount of water vapour dosed and the amount remaining in the sample chamber [67], [79].

The experimental test facility used for water-vapour sorption measurements in this thesis uses the gravimetric technique as opposed to the volumetric method. The gravimetric technique, unlike the volumetric method, does not accumulate errors with each step-increase in relative humidity. This typically results in a lower experimental uncertainty value [80]. Recently, inter-laboratory comparisons of both gravimetric and volumetric methods showed a lower reproducibility and larger errors in high pressure measurements when the volumetric method was adopted [81]–[83]. In this regard, the gravimetric technique was recommended as the preferred option for sorption measurements.

The test facility shown in Figure 2.5 is an intelligent gravimetric sorption analyser (IGA-002) manufactured by Hiden Isochema, United Kingdom. It is a semi-automated device, capable of highly reproducible water-vapour sorption measurements at both isobaric and isothermal conditions. In addition, unlike the Schlenk line method [84], ISO 12571 and ASTM E104-85 methods [85], this instrument enables simultaneous transient and steady-state sorption measurements. IGA-002 conducts isobaric measurements monitored via the pressure transducer regulated within the range of $0 - 10$ bar, and isothermal measurements monitored via the type K thermocouple regulated within the range of $273 - 353$ K [86]. Table 2.2 below shows a list of the labelled components in Figure 2.5 and their respective functions.

Figure 2.5. IGA-002 test facility

Table 2.2. Major components of the IGA-002 test facility

S/N	Component	Function
1	Microbalance and pressure chamber	Contains the microbalance and pressure instruments
2	Anti-condensation temperature control	Prevents condensation by regulating temperature
3	Reactor	Houses the sample during the experiment
4	Windows PC	Runs the *HIsorp* program for inputting test conditions
5	Water bath	Regulates water jacket temperature
6	Gas handling	Enables flow of gas to and from the reactor
7	Water jacket	Regulates sample temperature in the reactor
8	Furnace	Controls sample temperature
9	Furnace power controller	Controls the sample environment thermostat

2.5.3.2   Test procedure

The IGA-002 was used to conduct simultaneous water vapour sorption isotherm and kinetics experiments. In order to ensure accurate results, the mass balance was first adjusted to a zero point to confirm stability between the counterweight and sample container. Shortly after, ca. 50 mg of

each desiccant was measured on a scale and loaded into the sample chamber (located in the reactor) for each test-run. A 50 mg mass was chosen to allow enough room for sorption (*i.e.,* at least 75% of free space in the sample environment) given that the sample chamber capacity is only 200 mg. After loading the sample in the chamber, the sample was degassed. Degassing was the most crucial step in the procedure because it was essential to ensure that all samples were void of contaminants (or pre-adsorbed gases) before testing. Degassing was done at a low pressure (*i.e.,* vacuum pressure) and room temperature by selecting the required experimental sequence on the computer software.

In order to generate the sorption data, the equilibrium temperature and number of relative humidity step changes were inputted using the computer software. The selected equilibrium temperature was 298 K, while 6 relative humidity step changes was used for all tests samples. The relative humidity step changes used for the samples were 0-16% RH, 16-31% RH, 31-47% RH, 47-63% RH, 63-80% RH, and lastly 80-95% RH. It should be noted that in the experimental sequence, equilibrium sorption quantity at each RH step change was set to be attained when the sample mass had no increase for over 5 minutes. In addition, the time interval for the data acquisition to generate the sorption data was set at 1 s. A total of three repeatability runs were conducted per sample. Furthermore, in order to ensure an overall quality in the experiment, system/instrument calibrations, leak tests, and gasket changes were all conducted before the start of the experiment.

2.5.3.3 *Instrumentation and uncertainty*

The major components in the IGA-002 are the temperature, pressure and mass related instruments as shown in the Figure 2.6. Any errors associated with these instruments are propagated into the sorption results, providing a degree of uncertainty in the measurements. As a result, the overall uncertainty is evaluated from the uncertainty contributions of all required instruments. Specifications of the required instruments and their corresponding uncertainty values are presented in Table 2.3.
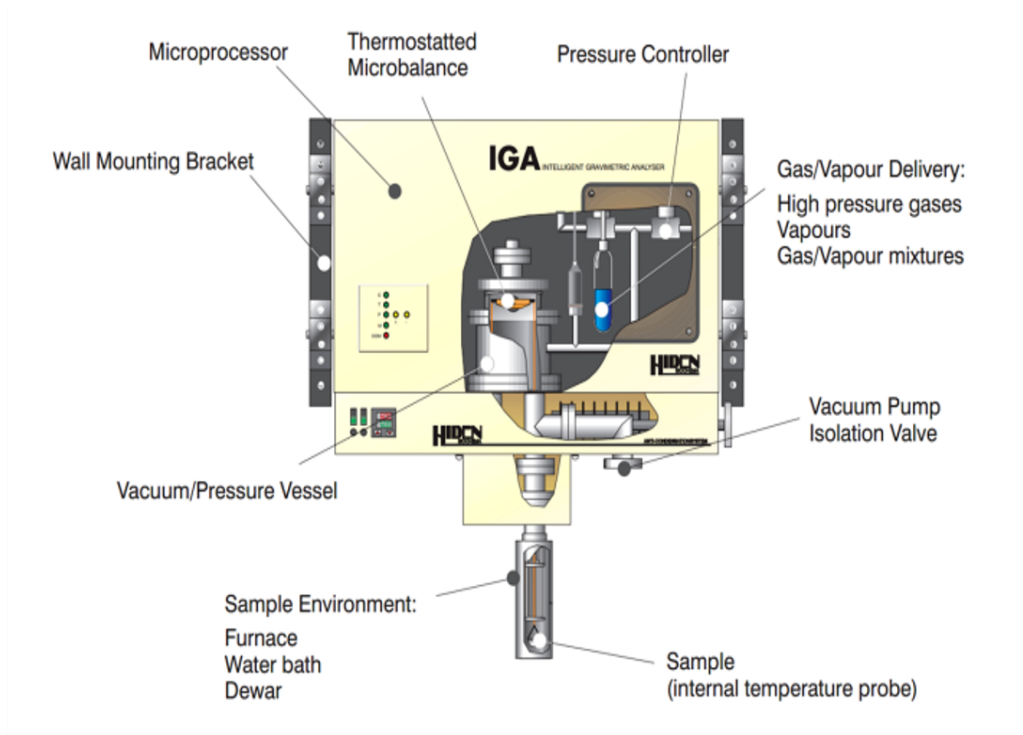
Figure 2.6. A Schematic of the IGA-002 device [86]

The overall uncertainty of the IGA-002 instrument was not specified by the manufacturer. However, the measurement uncertainty of any gravimetric instrument such as the IGA-002 mainly results from the mass measurements and corrections compensating for buoyant forces [79]. The total uncertainty in the mass measurements were very close to zero, given that the microbalance resolution was 0.1 μg in the measurement range of 0 – 200 mg [86]. Nevertheless, the uncertainty was assumed to be a conservative value of $\pm$ 1 μg. In addition, the uncertainty in the microbalance measurements was found to be much less than $\pm$ 1% in all cases when including buoyancy corrections at each instantaneous mass uptake. As such, a conservative value of $\pm$ 1% was assumed as shown in Table 2.3. The equation for the corrections compensating for the buoyant forces (added to microbalance readings) and the complete uncertainty propagations are presented in the Appendix A of this thesis.

Table 2.3. Specification and uncertainty contributions of the IGA-002 weight, pressure and temperature instruments.

Instrument	Parameter	Measurement range	Total uncertainty
IGA-002 microbalance (including buoyancy corrections)	Mass (weight)	0 – 200 mg	± 1%
Pressure transducer	Pressure	0 – 10 bar	± 0.004 bar
Type-K thermocouple	Temperature	3 – 1273 K	± 0.03 K

The total uncertainty in the instruments were derived from both systematic (B) and random uncertainties (P) for a 95% confidence level according to ASME PTC standard 19.1 [87]:

$$U = \sqrt{B^2 + P^2}$$

(2.12)

The random uncertainty (P) associated with all measured sorption data is determined by:

$$P_X = \frac{t_s \cdot \sigma}{n}$$

(2.13)

where: t_s is the student t-factor at a 95% confidence level for a degree of freedom of $(n-1)$, σ is the standard deviation of the sorption measurements.

The overall uncertainty in the IGA-002 instrument is then evaluated using the uncertainty propagation method [88]:

$$U_o = \left[\sum_{i=1}^{j} \left(\frac{\partial I}{\partial P_i} \cdot UP_i \right)^2 \right]^{1/2}$$

(2.14)

where: U_o, $\frac{\partial I}{\partial P_i}$ and UP_i are the overall uncertainty, sensitivity coefficient of parameter P_i and uncertainty associated with parameter P_i respectively.

2.6 RESULTS AND DISCUSSION

2.6.1 Desiccant characterization

The SEM images of the silica gel sample and the MS + binder samples are shown in the Figure 2.7. The monitor scales of the silica gel images are shown at 1 mm and 400 μm, while the green, blue and white MS samples are all shown at 100 μm and 20 μm scales respectively.

(a)
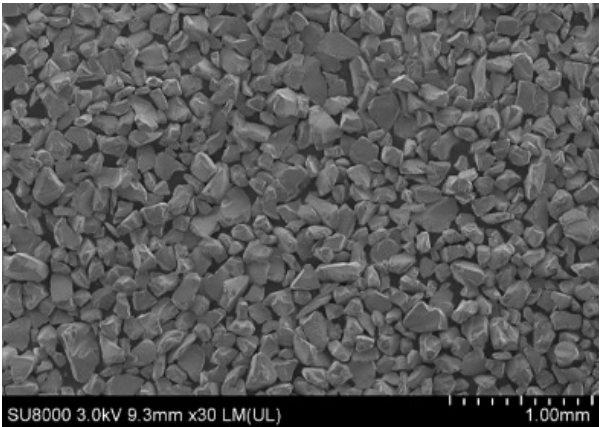
(b)
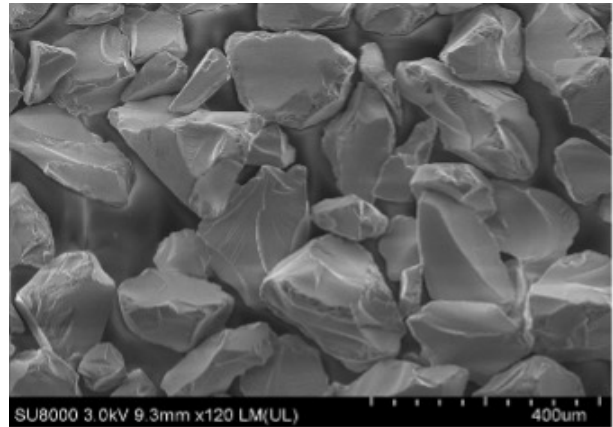
(c)
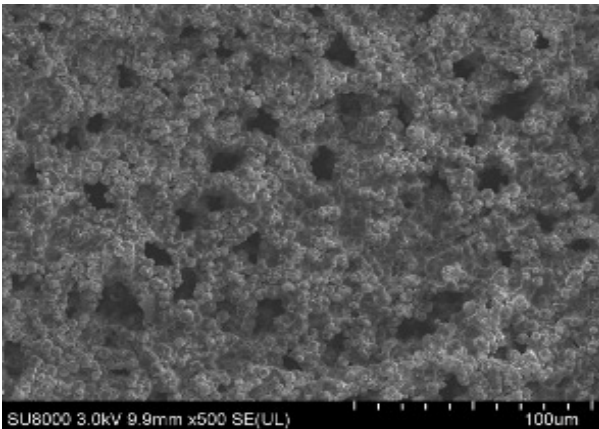
(d)
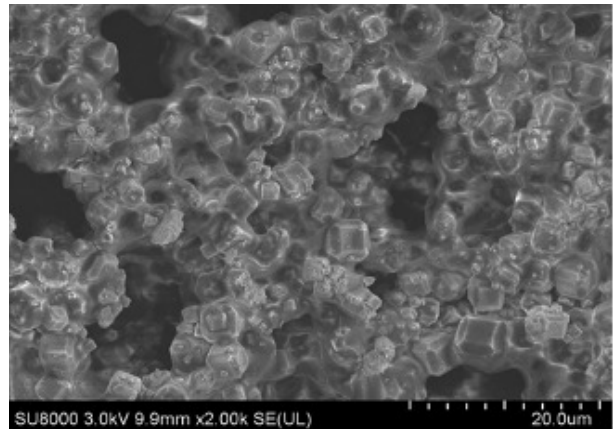
(e)
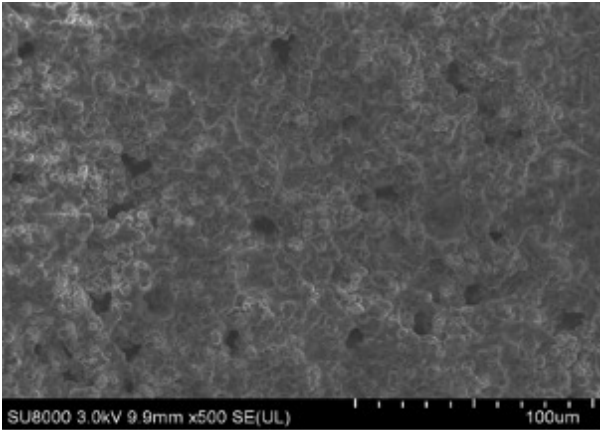
(f)
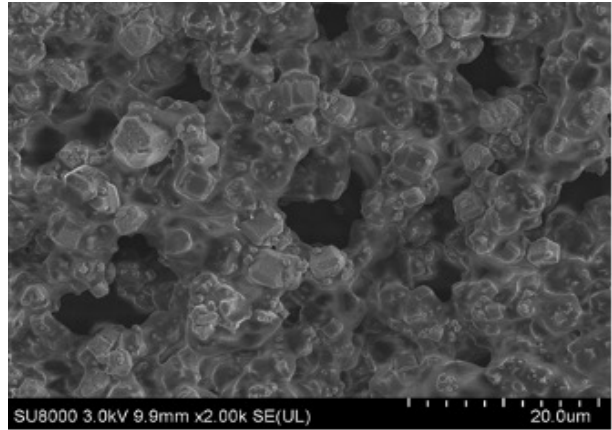
(g)
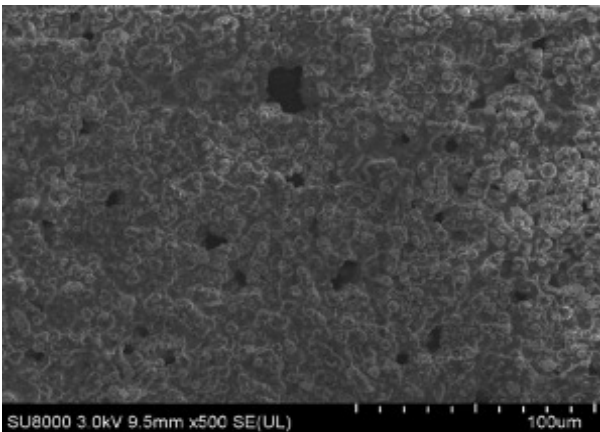
(h)
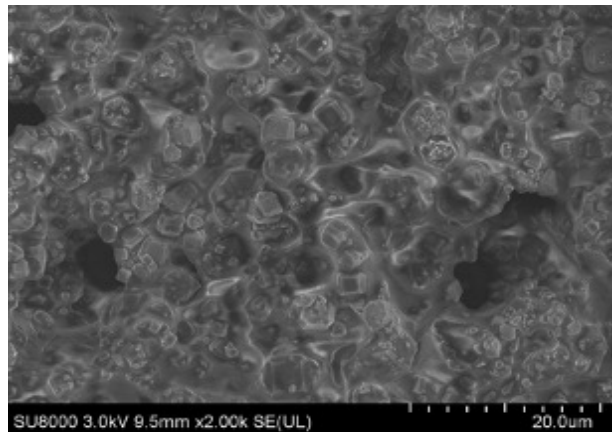
Figure 2.7. SEM images of (a) silica gel at 1 mm, (b) silica gel at 400 μm, (c) green at 100 μm, (d) green at 20 μm, (e) blue at 100 μm, (f) blue at 20 μm, (g) white at 100 μm, and (h) white at 20 μm monitor scales respectively.

In Figures 2.7(a) – (b) the silica gel particles depicted an amorphous form of irregular framework, interlocking to create a porous network of disordered particles. This surface morphology of silica gel presented was also consistent with that in the literature [56], [89]. However, in Figure 2.7(c) – (h), the extracted MS + binder samples showed an interesting surface structure, forming linkages with other individual particles as seen from the 20 µm scales. These linkages or 'clusters' were as a result of the binder compound impinged in the MS desiccant prior to the FBR coating process. As seen from the figure, the binder compound created lumps of disproportionate pore blockages, exhibiting a different surface structure from a typical pure MS desiccant in which individual particles interlock to create a uniform porous network [51]. Thus, it could be inferred that the

difference in surface structure between a pure MS sample and the MS + binder was attributed to binder impignment. Furthermore, similar studies have also reported alterations in both the textural and sorption properties of the parent desiccant due to binder impingement [36]. However, despite the fact that this phenomena is very intriguing, this thesis focuses on a method that can be applied to even unkown desiccants and binders, as opposed to the chemistry of desiccant/binder mixtures. As such, for a better understanding of the textural properties of the samples, further characterisation via porosimetry analysis was conducted to evaluate parameters such as the surface areas and pore widths as shown in Figure 2.8. Figure 2.8 also shows the BET transform plots generated by the Micromeritics ASAP 2020 computer software, from which the surface areas were evaluated. It should also be noteworthy that surface area for all samples were calculated using the BET method described in Section 2.4.

(a)

(b)

(c)

(d)
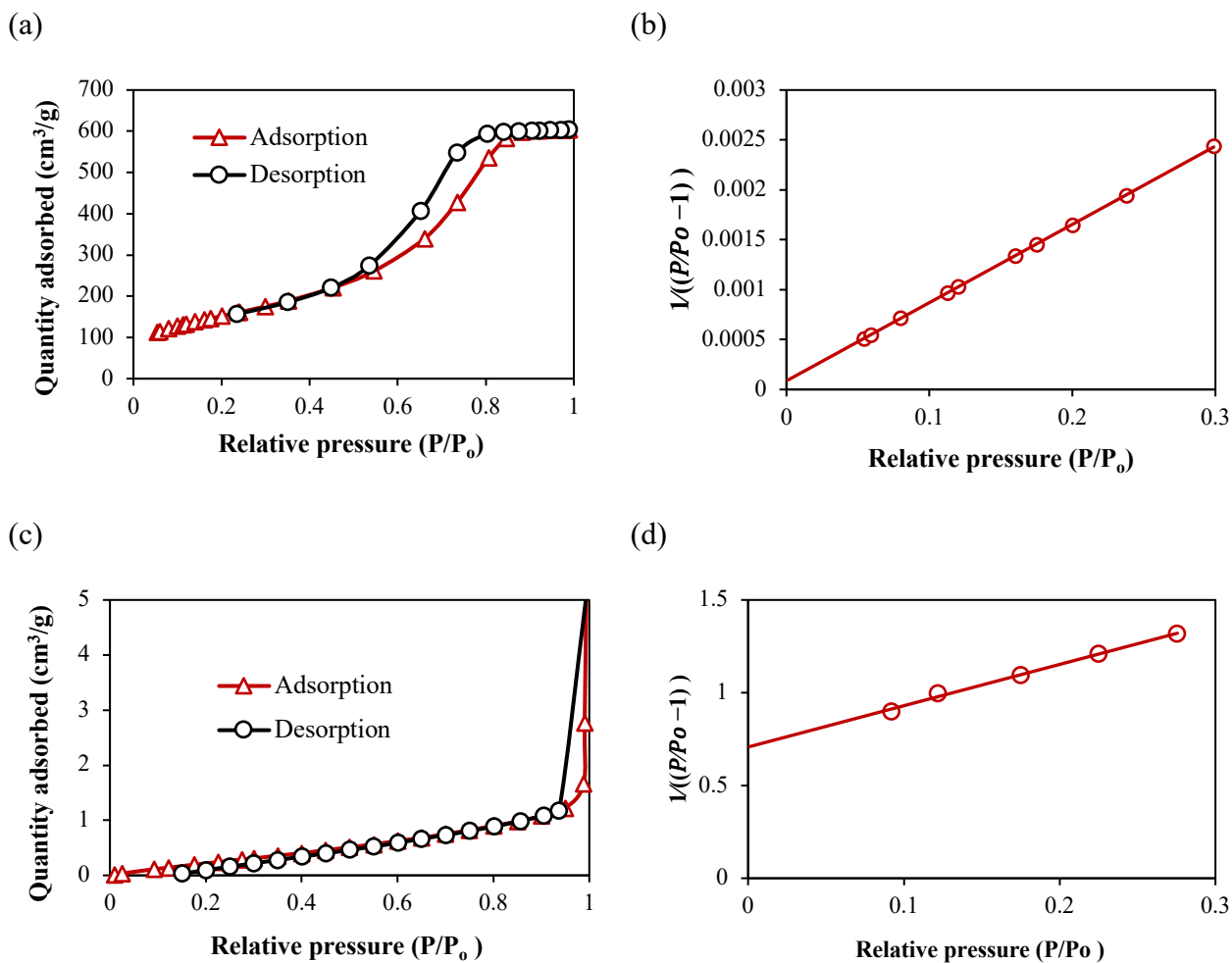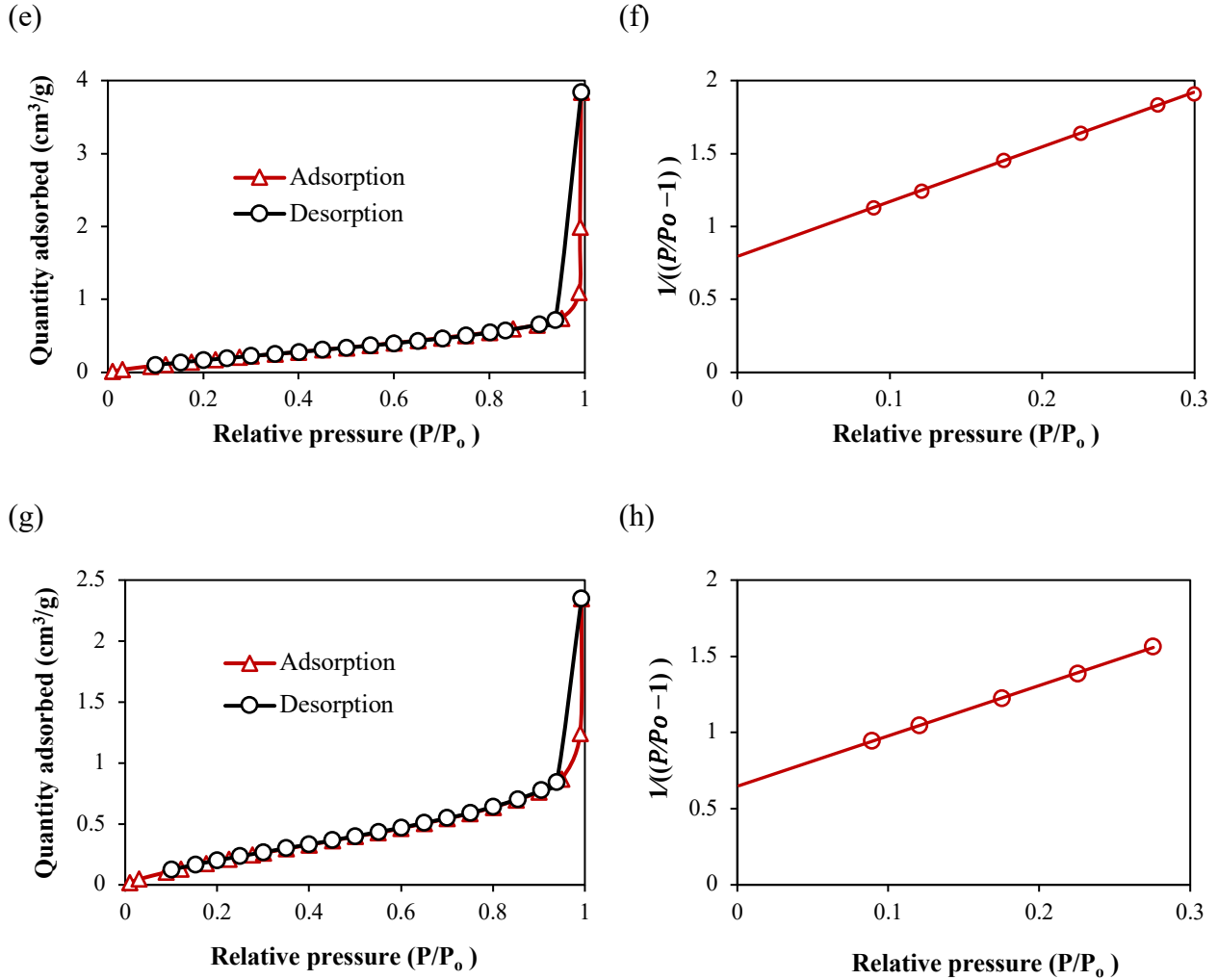
Figure 2.8. Nitrogen sorption isotherms and BET transform plots of (a)-(b) silica gel, (c)-(d) green, (e)-(f) blue, and (g)-(h) white samples at 77 K respectively.

The nitrogen sorption isotherms for the 4 desiccants show the amount of adsorbed and desorbed nitrogen during the sorption process. It can easily be observed that silica gel adsorbed the most amount of nitrogen per unit mass amongst all 4 desiccants. Meanwhile, amongst the 3 MS + binder desiccants, the green sample showed the highest adsorption quantity per unit mass, followed by the blue sample, and then the white sample. According to BET method, the higher the amount of physisorbed gases in a monolayer, the greater the available surface area for adsorption. Thus, indicating that the surface area of silica gel would be significantly larger than that of all MS + binder samples as shown in Table 2.4. Additionally, it can also be observed in Figure 2.8 that the curve fits of the BET transform plots show a good agreement with a positive y-intercept for all samples. As described earlier in Section 2.4, obtaining a positive y-intercept in the BET plot is

crucial because it indicates that the calculated surface area represents a physically realistic value with a positive heat of adsorption.

Table 2.4. BET surface area of silica gel, green MS, blue MS, and white MS desiccant samples.

Sample	BET surface area	R^2 correlation coefficient
Silica gel	549.2 ± 1.2 m^2/g	0.9999
Green	1.48 ± 0.04 m^2/g	0.9979
Blue	1.10 ± 0.01 m^2/g	0.9999
White	0.96 ± 0.01 m^2/g	0.9998

It can easily be observed from Table 2.4 that the surface area of silica gel was significantly higher than that of the MS + binder samples. This lower surface area was attributed to the binder impingement as observed in several other studies [36], [90], [91], when compared to that to of a pure MS desiccant. However, a recent comparative study [36] of an MS desiccant + binder and a pure MS desiccant showed that the use of binder coating method has a negligible effect on the water vapour sorption and sorption kinetics performance. This indicates that even with a lower surface area due to binder impingement, strong interactions still exist between the water vapor molecules and desiccant due to chemical affinity and functional groups, which can enhance sorption properties.

In order to further characterize the desiccants, the pore size distributions were evaluated using two different pore models – BJH (Barrett Joyner Halenda) and H-K (Horvath-Kawazoe) models. The BJH model was used to characterize the silica gel while the H-K model was used for the MS + binder samples as shown in Figure 2.9. Average pore sizes and classification of the desiccant samples in terms of their average pore widths according to IUPAC nomenclature are presented in Table 2.5.

Table 2.5. Average pore widths and volumes of silica gel, green, blue and white samples.

Sample	Classification	Average pore width	Average pore volume
Silica gel	Mesoporous	5.06 nm	9.3×10^{-1} cm^3/g
Green	Microporous	1.22 nm	3.0×10^{-4} cm^3/g
Blue	Microporous	1.21 nm	2.3×10^{-4} cm^3/g
White	Microporous	1.18 nm	2.6×10^{-4} cm^3/g
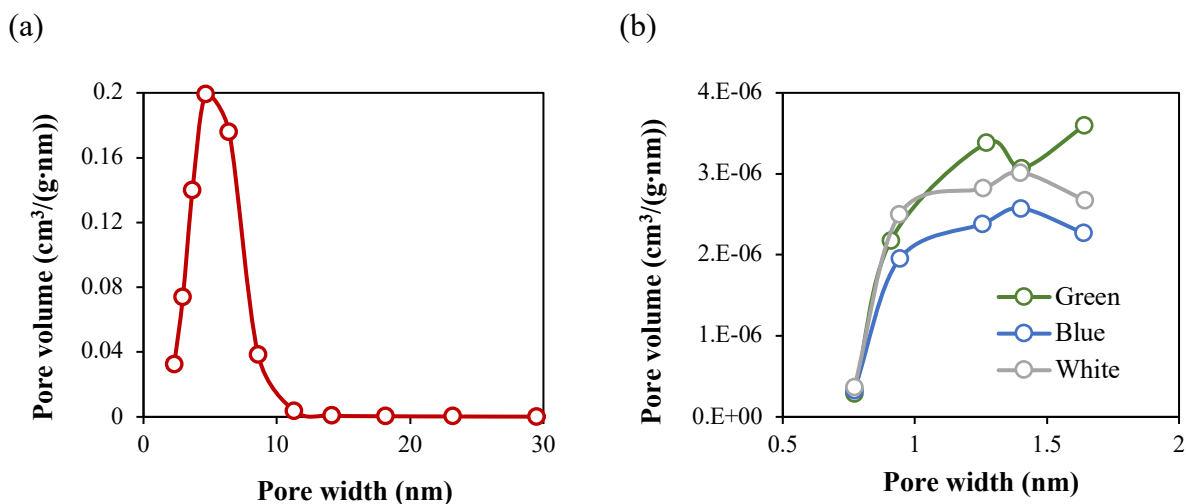
Figure 2.9. Pore size distributions of (a) silica gel (b) green, blue, and white samples.

The silica gel desiccant presented larger pore volumes, which gives an indication of capillary condensation at the higher relative pressures. The average pore width was about 5 nm, indicating a high mesoporosity for multi-layer adsorption. On the other hand, the pore size distributions in Figure 2.9(b), showed that the MS + binder samples are primarily microporous with very small pore volumes. In addition, the pore volumes of the MS + binder samples are much smaller than that of a typical pure MS desiccant due to binder impingement, which is consistent with similar studies in the literature [12], [90].

2.6.2 Equilibrium water vapour sorption

2.6.2.1 *Sorption isotherms*

The water vapour sorption isotherm measurements were conducted as described in Section 2.5.3. over 6 relative humidity step-changes (0 – 95%) and isothermally at 298 K for all 4 samples. The equilibrium sorption uptakes were measured after each relative humidity step-change, for up to 95% during adsorption, then back to 0% during the desorption process. Uncertainty bars are not included in the sorption (*i.e.,* adsorption/desorption) results shown in Figure 2.10 due to the very low uncertainty in the experiment (less than 1% in all cases).

(a)   (b)

(c)   (d)
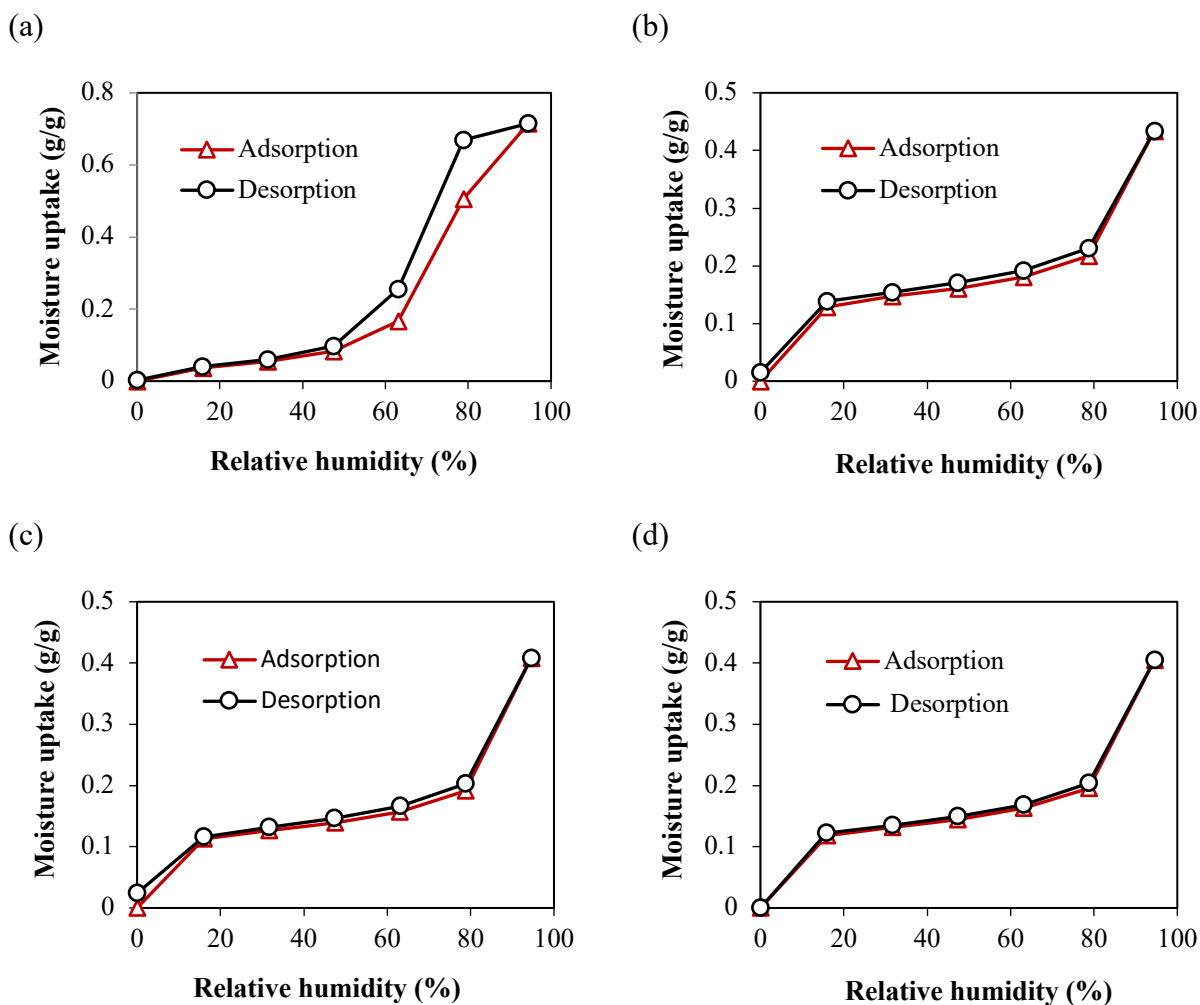
Figure 2.10. Sorption isotherms of (a) silica gel, (b) green, (c) blue, and (d) white desiccants at 298 K.

The sorption results (adsorption/desorption) shown in Figure 2.10 presents multilayer sorption for all 4 desiccant samples. Figure 2.10(a) contains the sorption results for silica gel which shows a type IV isotherm with a steep hysteresis loop. In Figure 2.10(a), the hysteresis which occurred at the higher RH values (50 – 95%) was due to capillary condensation of water vapour into the mesopores. Silica gel showed a distinct difference in moisture uptake between the monolayer formation of water vapour (up to 16% RH) and the subsequent multilayers (up to 95% RH) due to its low microporosity and high mesoporosity, which is also evidenced from its BJH pore size distribution in Figure 2.9(a). As a result of its low microporosity, micropore filling by the water

vapour molecules peaked at a low moisture uptake, thereby allowing mesopore filling to be much more predominant after 16% RH, representing over 90% of the total moisture uptake.

The 3 MS + binder samples in Figures 2.10(b) – (d) exhibited a slightly different sorption isotherm curve from that of a conventional molecular sieve desiccant. The MS + binder samples showed a type II sigmoid-like isotherm curve as opposed to the typical type I isotherm curve of microporous desiccants. This change in isotherm shape was due to the binder material, which created a disproportionate pore blockage and 'clusters' of binder material at the adsorption sites as seen from the SEM images (Figure 2.7). Similar changes in the sorption isotherm curve of a desiccant + binder have been reported in the literature [90]. However, the benefits of using a binder in a desiccant coated exchanger far outweighs any of its drawbacks, since good adhesion between an FBR's plates and desiccant is required [92]. Nevertheless, other techniques such as the sieving method [77], where a spray adhesive (as opposed to a binder) is used may be a better option.

It can also be observed from Figures 2.10(b) – (d) that the characteristic micropore filling stage (*i.e.,* 0 – 16% RH) reached over 25% of the maximum uptake, primarily due to the microporous nature of 3Å molecular sieve. However, due of the significant pore blockages created by binder impingement as observed from the SEM images, water vapour molecules were able to 'condense' on the surface area created by the disproportionate clusters of binder compound. This led to the multilayer adsorption observed by all 3 MS + binder samples. It can also be observed from the adsorption/desorption curves in Figures 2.10(b) – (d) that capillary condensation (*i.e.,* hysteresis) was minimal due to pore blockages by the binder. The maximum moisture uptakes from Figure 2.10 were 0.71 g/g, 0.43 g/g, 0.41 g/g, and 0.40 g/g for silica gel, green, blue and white desiccants respectively. Thus, comparing the moisture uptake results with Table 3, it can be inferred that a higher BET surface area was associated with greater moisture uptakes.

In addition to nitrogen adsorption shown in Section 2.6.1, the water vapour isotherm indicates one of the most vital parameters required to select desiccants for FBR as discussed in Section 2.5.2 – which is the slope of the sorption curve at operating conditions. In this regard, as observed from Figure 2.10(b)-(d), the relative humidity step-changes from 16% - 80% have nearly linear isotherm slopes. However, for silica gel, a linear slope can be seen from the 16% - 47% relative humidity step-changes, which is very acceptable given that a typical operating relative humidity for HVAC

purposes lies within 30% - 50% [92]. This indicates that in FBR, all four samples would have good latent effectiveness performances. Thus, from the above narrative with respect to Figures 2.7 – 2.10, it is also evident that the sorption results presented so far show a direct relationship between the evaluated surface areas via nitrogen adsorption and the moisture uptakes via water vapour adsorption.

2.6.2.2 *Sorption kinetics*

As described in Section 2.5.3, the measurements of water vapour sorption kinetics were conducted simultaneously with the sorption isotherm measurements. As previously discussed, the sorption isotherms were obtained from the equilibrium moisture uptake after each relative humidity step change (relative pressure), while the sorption kinetics were obtained from the transient moisture uptake curves at each relative humidity as shown for the green MS desiccant in Figure 2.11. The data acquisition system in the IGA-002 was set to measure the sorption uptakes at a time interval of 1 s until equilibrium moisture content was reached before proceeding to the next relative humidity step-change.
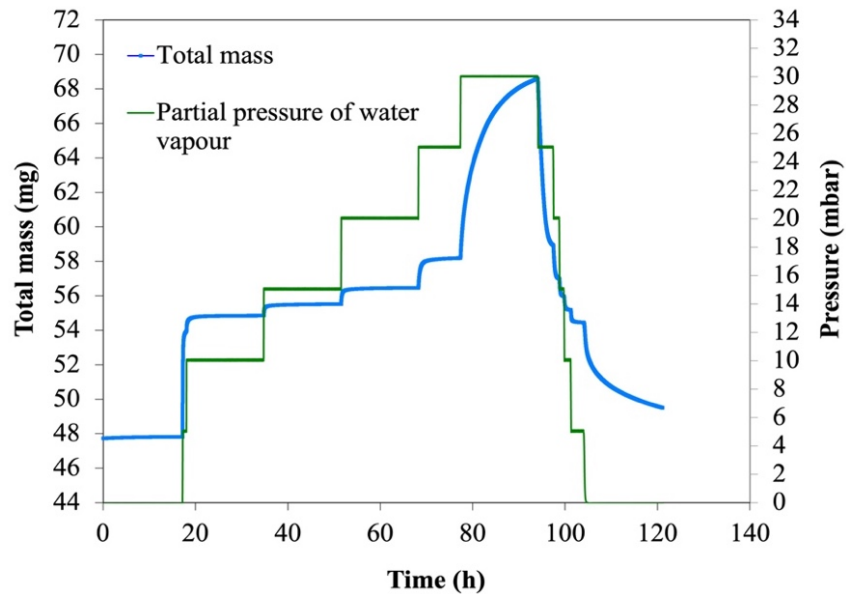
Figure 2.11. Adsorption/desorption evolution curves during step changes in vapour pressure (e.g., green sample) at 298 K.

Figure 2.12 contains the sorption kinetics curves which were obtained by transposing and plotting the transient moisture uptake data at each step-change (*i.e.,* 0-16%, then 16-31%, etc.) against time.

It can easily be observed that the moisture uptakes were greater at the higher RH values, primarily due to the presence of more water vapour molecules in the sample chamber. In terms of their dynamic sorption uptakes at 80% RH, silica gel had the highest after 1h at 0.053 g/g, followed by the green desiccant at 0.022 g/g, then blue and white desiccants at 0.019 g/g and 0.18 g/g respectively. Comparing the trend in the kinetics results with their average pore width in Table 2.5 shows that larger pore sizes are associated with faster kinetics. Thus, it can be inferred from the results so far that the textural properties (*i.e.,* surface area, average pore width) played a significant role in both sorption isotherm and kinetics performance of all four desiccant samples.

The dynamic sorption uptake (or capacity) is a crucial parameter in desiccant-coated exchangers (including FBRs), because it has the potential to affect the moisture transfer in a given cycle. In this regard, given that FBR operates on a 60 second adsorption period usually within a 30 - 50% relative humidity range [77], the desiccant with the highest dynamic sorption uptake during this period and range of RH should be recommended for FBR. At 31% RH, the silica gel had the highest dynamic sorption uptake after 60 s at 0.0015 g/g, followed by the blue sample at 0.0011 g/g, then green and white samples at 0.00095 g/g and 0.00011 g/g respectively. At 47% RH, the blue desiccant had the highest dynamic sorption uptake after the first 60 s at 0.00074 g/g, followed by silica gel at 0.00068 g/g, then the green and white desiccant samples at 0.00060 g/g and 0.00035 g/g respectively. This shows that regardless of the fact that silica gel had a higher dynamic sorption uptake after 1 h, sorption performance during the first 60 s (*i.e.,* the cycle period) is of greater importance for FBR, and as such the blue sample with comparable performance over this period could be the preferred option.

It can be observed from the relative uptake plots that the moisture content increased rapidly during the initial sorption stage and then gradually as the sorption quantity approached equilibrium. This indicates that the higher the sorption rate, the quicker the sorption uptake attains equilibrium capacity, and as such, a better transient performance would be expected. For a more detailed insight into the kinetics of the desiccant samples, curve fitting of the experimental data with the LDF model is presented in the next section in order to quantity the kinetics and derive the sorption rate constants at each relative humidity.
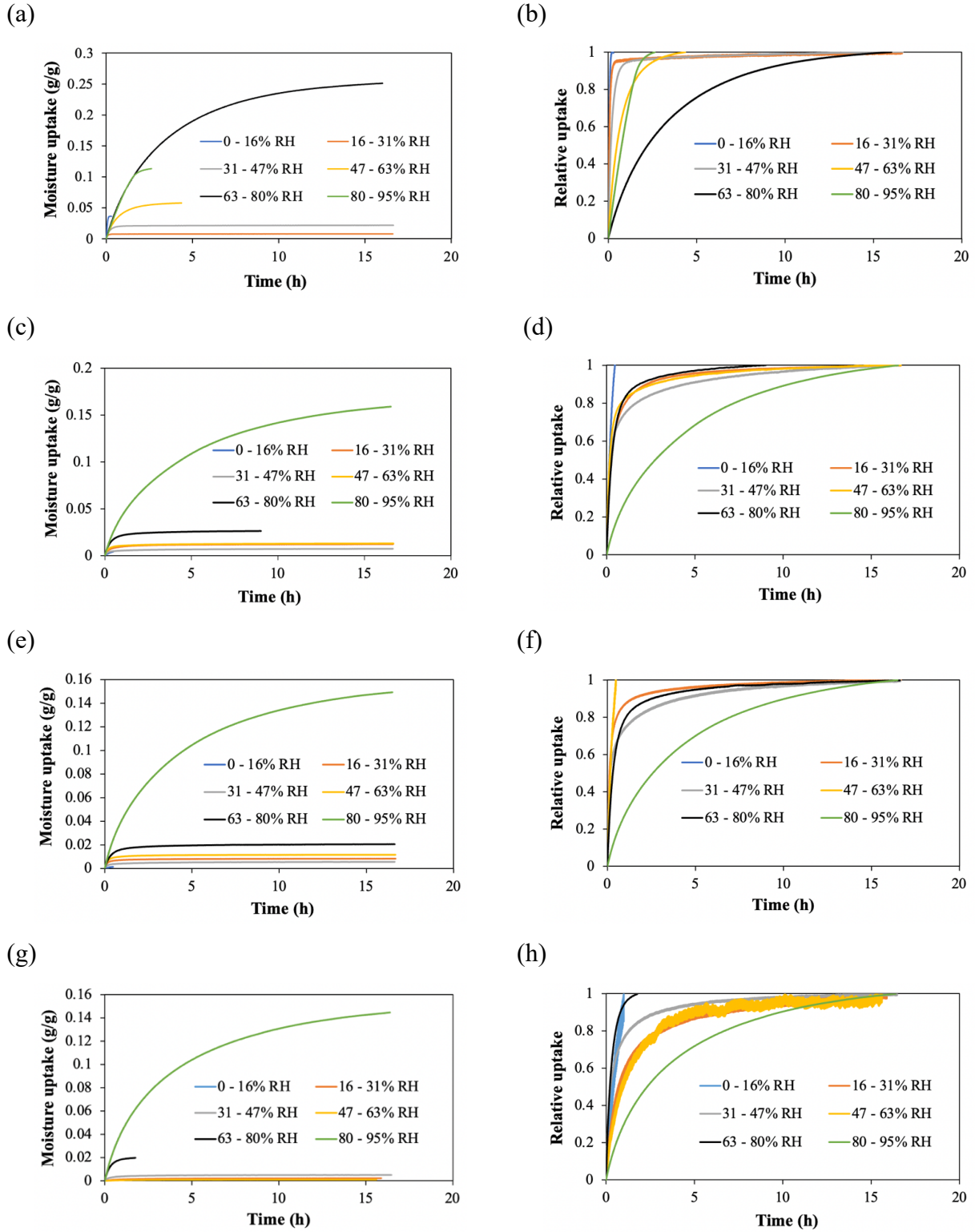
Figure 2.12. Sorption kinetic adsorption curves of (a)-(b) silica gel, (c)-(d) green, (e)-(f) blue, and (g)-(h) white desiccants at 298 K.

41

2.6.2.3 Sorption rate constants

Given that the sorption kinetics curves followed a nearly exponential trend in Figure 2.13, the linear driving force (LDF) model was used to analyze the kinetic results and fit the experimental data as described in Section 2.4.3. Taking into account that FBRs operate within a total cycle of 120 s (*i.e.,* 60 s adsorption and 60 s desorption), the kinetic rate constants were determined using the sorption data for the entire experiment at each step change in RH and using only data from the first 60 seconds of each step change in RH. The curve fits in Figure 2.13 of $-ln\left(1 - \frac{u_t}{u}\right)$ against time were linear, showing a good agreement with R^2 correlation coefficients very close to 1. In Figure 2.13, the first two RH step changes (*i.e.,* $0 - 16\%$ and $16 - 31\%$) were omitted in order to make the graphs more readable and less obscure. Nevertheless, all 6 RH step changes and their sorption rate constants (k) from the curve fits are shown in Figure 2.14.
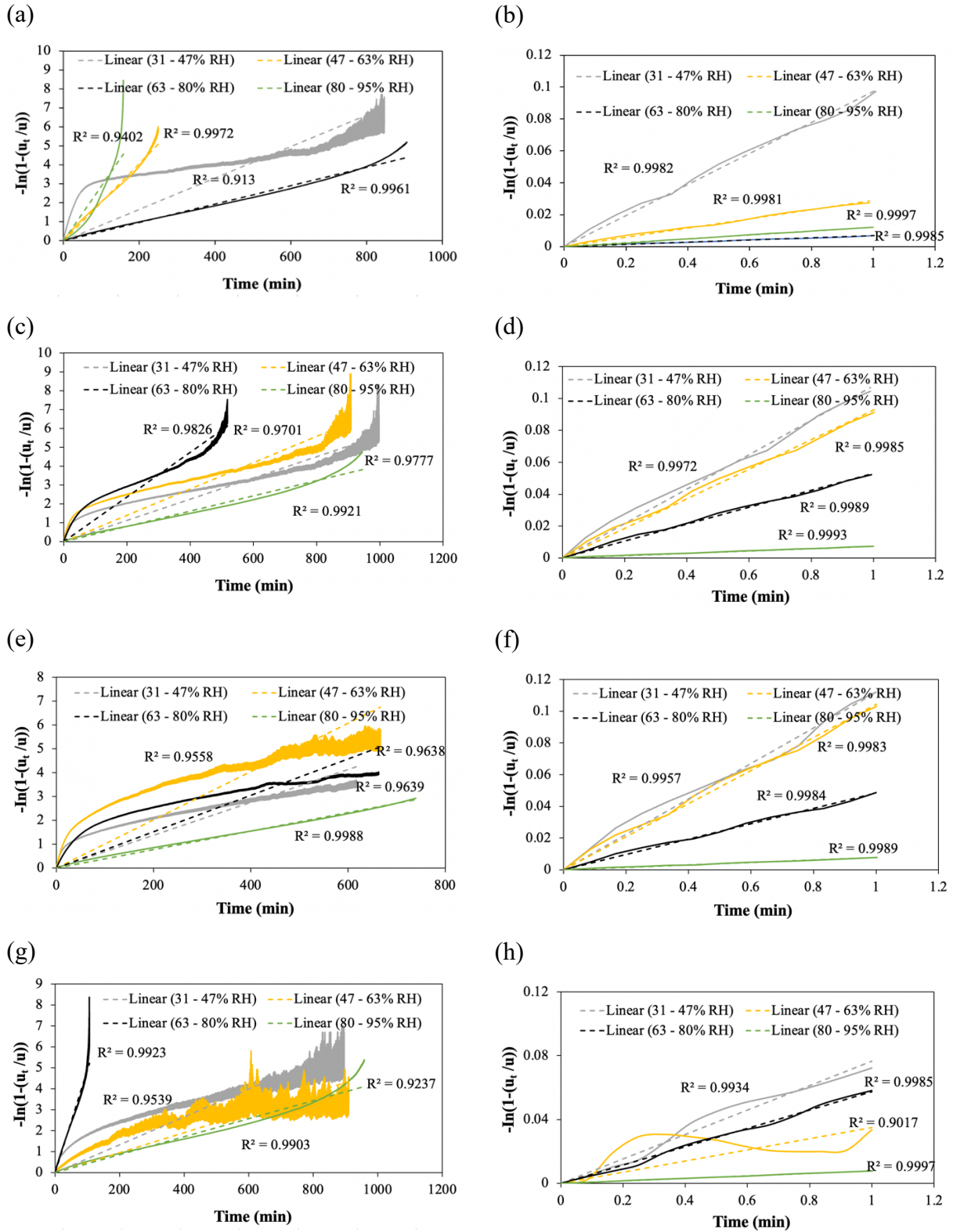
Figure 2.13. LDF curve fitting of (a)-(b) silica gel, (b)-(c) green, (d)-(e) blue, (f)-(g) white desiccant samples during time till equilibrium sorption quantity and 120 seconds operation respectively.

The rate constants (k) are presented for each RH step-change over the entire experimental run and during first 60 second period for all desiccant samples as shown in Figure 2.14. It should be noted that the slopes of the linear plots in Figure 2.13 represent the sorption rate coefficient (k) in units of 1/s as shown in Figure 2.14. It can be observed from Figure 2.14(a) that the rate constants till equilibrium sorption quantity (*i.e.,* using all the sorption data for each RH step change) showed a distinct peak at the first RH step change (0 – 16%). This was associated with the initial micropore/mesopore filling of water vapour molecules which occurs rapidly [93]. After pore filling occurred, the kinetic rate constants dropped to a near steady value between 31% RH to 63% RH. This decrease in the kinetic rate constant may be due to the fact that affinity for adsorbate-adsorbate interactions is usually weaker than adsorbate-adsorbent interactions given that multilayer adsorption occurred at this stage for all samples. After this stage, the silica gel showed a further decline at 80% RH followed by a subsequent increase in the kinetic rate constant at 95% RH due to the high affinity of the samples to water vapour molecules at this step change. On the other hand, the MS + binder samples showed a slight increase in the kinetic rate constant at 80% RH followed by a subsequent decline at 95% RH. This was attributed to the binder compound impingement which created disproportionate pore blockages as seen from the SEM images (Figure 2.7). As a result, most of the adsorption sites were filled after 80% RH, making the kinetic rate constant at 95% RH lower.

Figure 2.14(b) shows the kinetic rate constants during adsorption at the first 60 s. As one would expect, the sorption rates were much higher during the first 60 s as opposed to the sorption process till equilibrium capacity. The trends were also quite different, showing a general decline towards saturation with the silica gel, green and blue samples. The white sample on the other hand, showed a subsequent peak and decline over each RH step change. However, considering that FBRs operate within a 120 s adsorption + desorption cycle, kinetic performance of a desiccant coating during the first 60 s of adsorption may be more important than the kinetic performance over the time till equilibrium capacity. This is because in many cases, the FBR may not reach its equilibrium sorption capacity over several cycle periods.
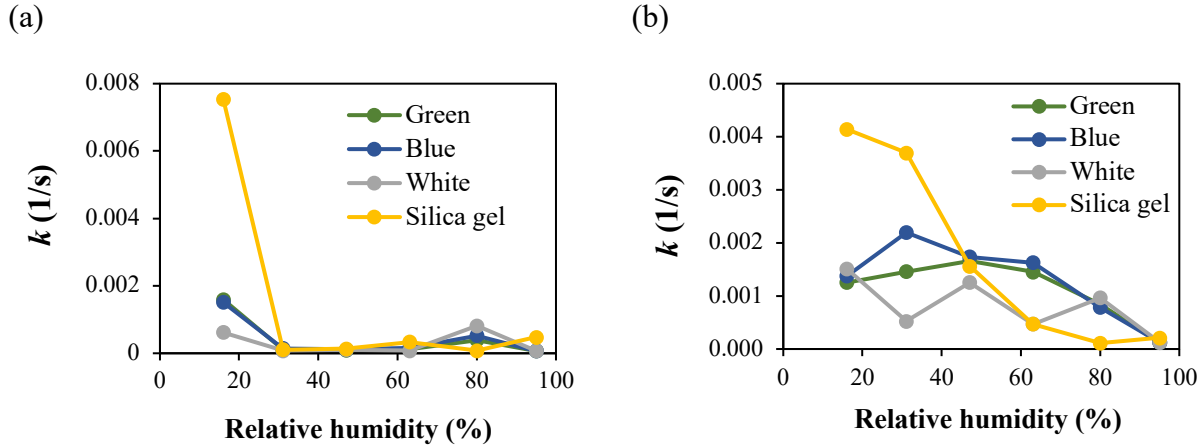
Figure 2.14. Adsorption rate constants (k) of all 4 desiccants determined using data measured over (a) time till equilibrium sorption capacity (b) the first 60 seconds.

In order to provide a better understanding of the kinetic results, the average adsorption rate constants are compared in Figure 2.15. The error bars shown in the figure represent the random uncertainty for a 95% confidence interval, which was less than 4% in all cases for adsorption. It can easily be observed from Figure 2.15(a) that silica gel had the highest average rate constant value over the sorption process till equilibrium capacity, which would naturally be expected given that its dynamic sorption quantities were considerably higher in Figure 2.12. However, over the first 60 seconds of adsorption in Figure 2.15(b), silica gel had comparable results with the blue desiccant. The similar results of silica gel and the blue sample over the first 60 s shows that in recommending desiccants for FBR applications, the sorption rate till equilibrium and equilibrium sorption capacity may not be as vital as the sorption rate for the first 60 seconds. This is because the desiccant coated FBR may never reach equilibrium over cycles of 60 seconds. Thus, estimating FBR performance based solely on an equilibrium process could lead to errors.

(a)

(b)
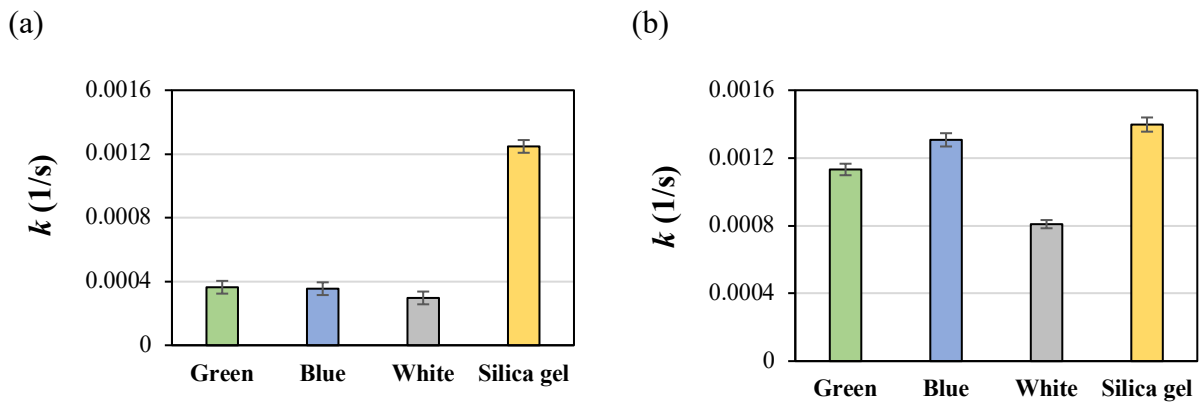
Figure 2.15. Average adsorption rate constants (k) determined using data measured over (a) the time till equilibrium sorption capacity (b) the first 60 seconds. The error bars indicate the 95% confidence interval for the average adsorption rate constant.

On the other hand, Figure 2.16 shows the desorption kinetic rate constants from 95 – 80% RH step change back to 16 – 0% RH step change. It can be observed from Figure 2.16(a) that the rate constants till equilibrium sorption quantity (*i.e.,* using all the sorption data for each RH step change) for the MS + binder samples showed a steady increase from the 95 – 80% RH step-change until it peaked at the 63 – 47% RH step change. From this point, the kinetic rate constant began to decline after most of the moisture had been desorbed, until the final RH step change at 16 – 0%. Similarly, the silica gel desorption rate constant also showed a steady increase from the 95 – 80% RH step-change; however, the peak in this case was at the 31 -16% RH step change before the decline at the 16 – 0% RH step-change. Furthermore, the desorption rate constants for the first 60 s depicted in Figure 2.16(b) showed a similar trend also. However, the kinetic rate constant peaked at the 47 – 31% RH step change for the 3 MS + binder samples, and at the 31 – 16% RH for silica gel. This was because those were the respective step-changes at which most of the moisture was desorbed. After these respective RH step-changes, the desorption kinetic rate constant decreased in succession until the final step change at 16 – 0% RH as seen in all 4 samples.

(a)   (b)
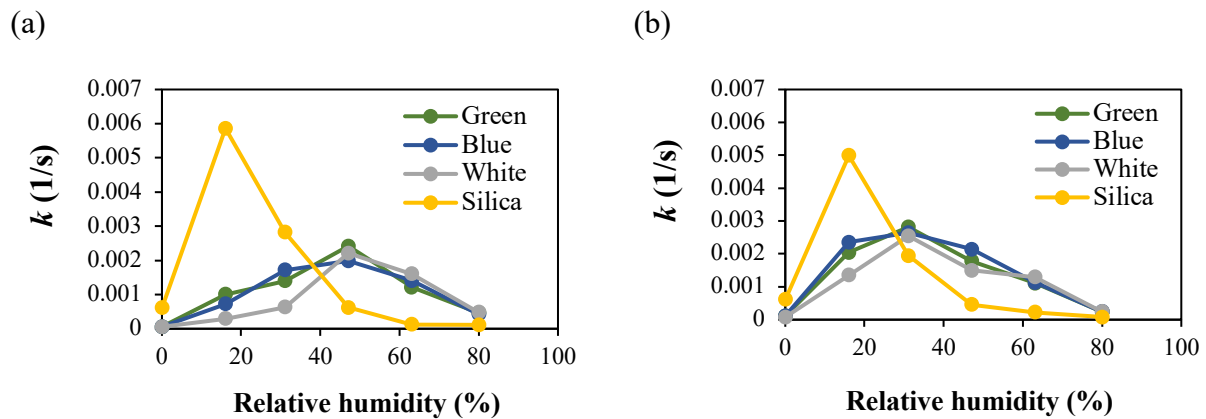
Figure 2.16. Desorption rate constants (k) determined using data measured over (a) time till equilibrium sorption capacity (b) the first 60 seconds.

Figure 2.17 shows the average desorption rate constants for all 4 samples. The error bars shown in the figure represent the random uncertainty for a 95% confidence interval, which was less than 5% in all cases for desorption. It can be observed that similar to Figure 2.15(a), the green and blue samples had a comparable rate constant value over the sorption process till equilibrium as seen in

Figure 2.17(a). Silica gel showed the highest desorption rate constant value while the white desiccant showed the lowest. However, over the first 60 seconds, the blue sample showed a higher average desorption kinetic rate constant as seen in Figure 2.17(b). Thus, by comparing Figures 2.15 and 2.17, it can be inferred that both silica gel and the blue desiccant had better sorption kinetics during the first 60 seconds.

(a)   (b)
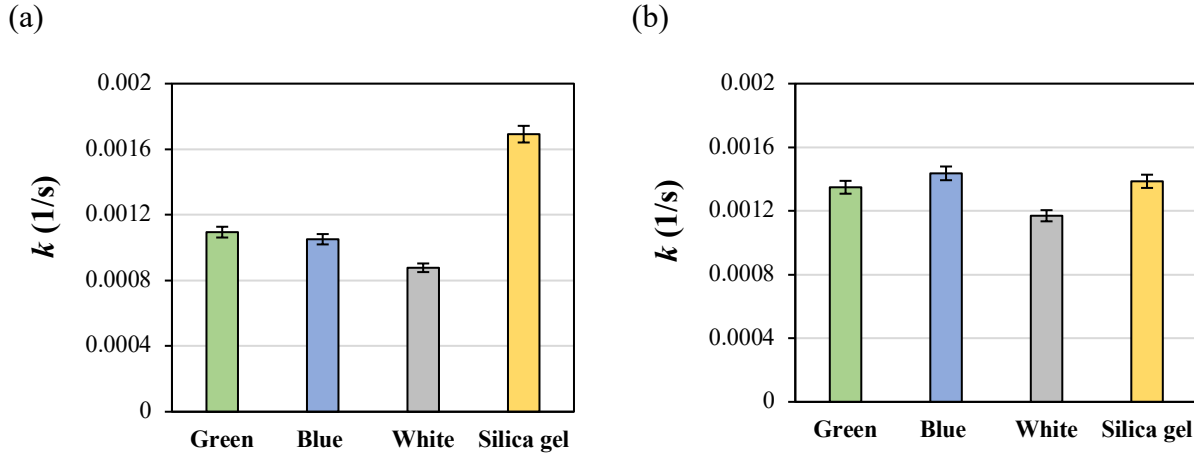
Figure 2.17. Average desorption rate constants (k) determined using data measured over (a) time till equilibrium sorption capacity (b) the first 60 seconds. The error bars indicate the 95% confidence interval for the average desorption rate constant.

A key contribution from this chapter is the identification of crucial parameters (adsorption and desorption rate constants) for kinetics and diffusion (as described by the LDF model) which can be used as inputs for FBR modelling. Thus, this chapter presents a general insight into these vital parameters required in desiccant selection for FBR applications, from which a numerical model can be used to quantify the effects of equilibrium sorption capacity and sorption kinetics of a desiccant coating on FBR performance.

2.7   SUMMARY AND CONCLUSIONS

In this chapter, desiccant properties (textural and sorption) for fixed-bed regenerator (FBR) applications were investigated experimentally. It was observed that textural properties (*i.e.,* surface area and pore size) have a direct influence on the sorption performance (isotherm and kinetics) of desiccants. It was also inferred from the results that in addition to the equilibrium sorption capacity, the dynamic sorption quantity and the rate constant are also important desiccant properties for

FBRs. Thus, in order to recommend desiccants for FBR applications, key findings to be considered from this study are summarised as follows:

1. The impingement of a binder to improve adhesiveness of a desiccant coating on FBR plates may cause disproportionate pore blockages. This was evidenced by alterations in the isotherm shape as seen from the molecular sieve (MS) + binder samples when compared to that of pure molecular sieve (MS) desiccant. However, the 3 MS + binder samples still showed a high affinity for water vapour, presenting sorption results comparable to a conventional silica gel.

2. The textural properties of desiccants affect their sorption performance. Higher surface areas were associated with a higher sorption capacity while larger pore sizes were associated with faster kinetics in all 4 desiccant samples.

3. In addition to the equilibrium sorption capacity from the isotherm, dynamic sorption quantities and rate constant are also crucial parameters for a desiccant coated FBR, given that FBR operates in a total cycle of only 120 seconds.

4. The rate constants for an entire RH step-change and the rate constants over a 60 second period had different values. In this regard, desiccants for FBRs should be selected based on the kinetic performance over a 60 second period as opposed to an equilibrium process. During the 60 second period, silica gel had the highest adsorption rate constant, followed by the blue (6% lower), then the green (19% lower), and lastly the white desiccant (42% lower). Conversely, on desorption during the 60 second period, the blue sample had the highest adsorption rate constant, followed by silica gel (3% lower), then the green (6% lower), and lastly the white desiccant sample (18% lower).

An important contribution in this thesis (from this chapter) is the identification of crucial kinetic parameters which can be used in the modelling of an FBR desiccant coated layer. The sorption parameters (u, and k) of the tested desiccants are used as inputs for the porous media model in Chapter 3 to solve the coupled heat and moisture transfer problem of the desiccant coated layer.

CHAPTER 3

DESICCANT MODELLING FOR FBR APPLICATIONS

3.1   OVERVIEW

This chapter is a continuation of the study presented in Chapter 2, aimed at completing the main objective of this thesis (*i.e., 'develop a method to select desiccants for FBR applications'*). In this regard, this chapter is focused on the second major task of this thesis, which is to develop a numerical model to evaluate desiccant performance for FBR applications using the material input parameters evaluated in Chapter 2.

The model presented in this chapter solves the coupled heat and moisture transfer problem for a desiccant when humid air flows over its surface and is validated with available analytical solutions in the literature. The results in this chapter identified sorption kinetics as a vital parameter for desiccant coated FBRs. Furthermore, key recommendations to be considered when selecting desiccants for FBR applications were also established.

The manuscript presented in this chapter is under internal review for submission to the International Conference on Building Energy & Environment (COBEE, 2022). The first author – Teddy Okolo (M.Sc. student) conducted the research and wrote the manuscript, and the second author – Carey Simonson (Professor) supervised the research and critically reviewed the manuscript.

Transient heat and moisture transfer performance of a desiccant-coated layer for fixed-bed regenerator applications

T.I. Okolo, H. Ramin, G. Annadurai, C.J. Simonson

3.2 ABSTRACT

Desiccants are adsorptive materials used for coating fixed-bed regenerators in order to enable moisture interactions with the process air. This chapter presents a porous media numerical model which solves the coupled heat and moisture transfer problem in a desiccant when humid air flows over its surface. The results for heat and moisture transfer (*i.e.,* temperature and water vapour density profiles) were validated with analytical models in the literature.

The numerical results showed that neglecting sorption kinetics during moisture transfer leads to a significant overestimation in the desiccant moisture content. In addition, the results presented some key recommendations such as selecting desiccants with: (i) higher sorption kinetic rate constants, (ii) smaller particle sizes, and (iii) thinner desiccant coatings. It was also established from the results in this chapter that sorption kinetics must not be neglected in recovery periods less than 60 s when thick coatings are used. The contribution of this thesis chapter is that the results presented will enable HVAC engineers design better desiccant coated FBRs.

3.3 INTRODUCTION

According to the United Nations (UN), sustainability in the consumption of global resources is essential to preserve our ecosystem [94]. One of the key sustainable goals set by the United Nations is to ensure that access to reliable, affordable, and efficient energy is available on a global scale by 2030 [94]. This goal was set due to the challenge posed by the ever increasing global energy consumption, given the continuous progression in urbanization and economic growth [95]. Previously, surveys in Canada showed that 30% of total energy consumption is attributed to buildings, and over 50% of building energy is consumed by heating, ventilating and air-conditioning (HVAC) systems [8]. As a result, the Canadian government recommends the use of energy-efficient HVAC equipment through various buildings codes and standards [96].

Amongst the energy-efficient HVAC technologies, energy recovery ventilators (ERVs) are widely used due to their short payback period, energy efficiency, and ability to maintain adequate indoor air quality (IAQ) [84], [97]. Fixed-bed regenerators (FBRs) are a relatively novel type of ERV as described in detail in Chapter 1 (Section 1.1). This chapter addresses the second objective task of this thesis which is to "*develop and verify a porous media model to determine the heat and moisture transfer performance of a desiccant-coated layer for FBR applications.*"

Desiccants are the primary adsorptive material used in coating FBRs in order to enable moisture interactions with the air stream [37]. Over the past few decades, several studies conducted experimental and numerical investigations into the heat and moisture transfer performance of desiccants for ERV applications [10], [38], [56], [62]–[65]. However, very few of these studies focused on FBRs in particular. Additionally, none of the aforementioned studies presented numerical insights into the effect of sorption kinetics during heat and moisture transfer. Recently, Ramin et al. [15] developed a numerical model for energy recovery in FBR which showed the heat and moisture transfer performance. However, the model only solved the air-side resistance (GSR approach), thereby ignoring desiccant performance during heat and moisture transfer (GSSR approach). This chapter targets the gap in the literature by presenting a GSSR desiccant study approach (porous media model) for FBR applications.

In this chapter, the effect of the measured desiccant properties shown in the previous chapter (sorption isotherm, sorption kinetics, rate constants) are applied as inputs for modelling an FBR desiccant layer. As discussed earlier, sorption kinetics is an important parameter in FBR, given that quicker response times and a high adsorption rate would affect its moisture transfer rate and latent effectiveness during the short cycle of 120 s. From a design perspective, the effect of sorption kinetics and other desiccant properties would enable HVAC designers adequately select promising desiccants based on performance. The numerical results presented in this chapter for heat and moisture transfer are also validated with analytical models in the literature [98].

3.4 PHYSICAL MODEL

Figure 3.1 shows a schematic to illustrate the physical model. The desiccant layer has a thickness of 15 mm. The air stream flowing over its surface is at a constant temperature and relative humidity. The top of the desiccant is in direct contact with the air stream as convective heat and moisture transfer occurs, while the bottom of the desiccant is impermeable and adiabatic. In addition, the vertical sides of the desiccant layer are also assumed to be impermeable and adiabatic. The physical properties of the desiccant (silica gel) used in the model are shown in Table 3.1.
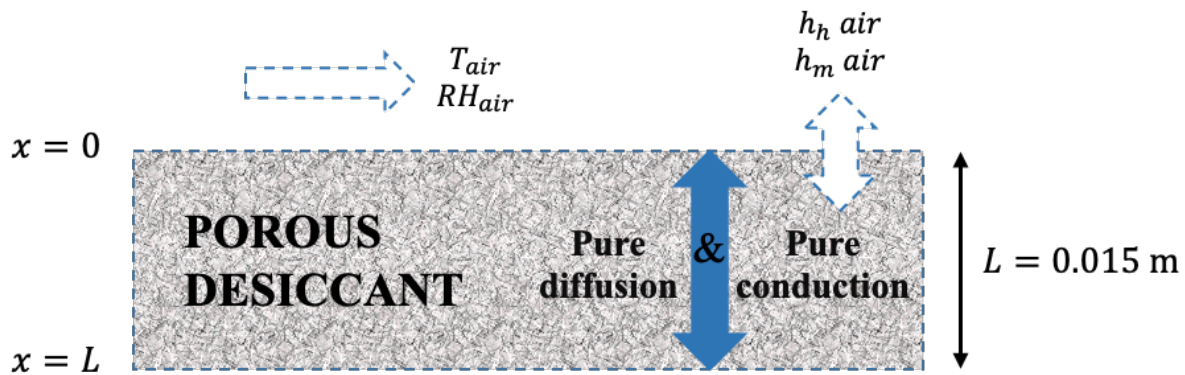
Figure 3.1. A schematic of the heat of moisture transfer between the air stream and desiccant layer.

In this physical model, the transfer of moisture from the humid air to the dry desiccant is assumed to be a transient process where the moisture content in the desiccant is not uniform and in equilibrium with the air stream. This results in a coupling between the sorption kinetics (delay in adsorption) and pure diffusion through the desiccant layer. The porous media numerical model is also assumed to be one-dimensional because in FBR applications, the length and width of the

desiccant coated layer is significantly greater than the thickness. In this model, evaporation/condensation conditions will not be considered since the relative humidity conditions are below 100%. In addition, frosting conditions in the desiccant are also not considered because all temperature conditions in this chapter are above 273.15 K (0°C).

Table 3.1. Input properties for silica gel used in the model [99]–[101].

Density (kg/m^3)	Thermal conductivity (W/(m·K))	Specific heat capacity (J/(kg·K))	Binary diffusion coefficient (m^2/s)	Thickness (mm)	Porosity (-)	Heat of adsorption (J/kg)	Tortuosity (-)
780	0.2	924	2.54×10^{-4}	15	0.55	2.7×10^6	3

3.5 NUMERICAL MODEL

A numerical model was developed to calculate the temperature and humidity profiles in a desiccant layer due to heat and moisture transfer with the air stream. The model is a one-dimensional porous media (GSSR) approach based on the theory of local thermal equilibrium and local volume averaging (details presented in Appendix B). The equations presented in this section are adapted to predict the behaviour of a silica gel desiccant when used in FBR. In order to simplify the solution, some basic assumptions were made which are listed as follows:

1. Heat and moisture transfer through the desiccant is one-dimensional.
2. The air and water vapour are ideal gases.
3. There is no heat source in the porous desiccant except the heat of phase change due to adsorption/desorption.
4. The thermophysical properties of the air and water vapour are constant.
5. The porous desiccant is homogenous.
6. There are no changes in desiccant volume (swelling or shrinkage) due to adsorption/desorption.
7. Fickian diffusion dominates in the desiccant.

3.5.1 Governing Equations

Considering the above-mentioned assumptions, the governing equations presented below are used to calculate the heat and moisture transfer performance of the desiccant (*i.e.,* temperature and vapour density profiles). The schematic of the physical problem is presented in Figure 3.1 and the equations representing the conservation of energy and mass are delineated below [98]:

3.5.1.1 *Energy equation*

$$(\rho c_p)_{eff} \frac{\partial T}{\partial t} - \dot{m} h_{fg} = \frac{\partial}{\partial x}\left(K_{eff} \frac{\partial T}{\partial x}\right)$$

(3.1)

3.5.1.2 *Water vapour diffusion equation*

$$\frac{\partial(\varepsilon_g \rho_v)}{\partial t} + \dot{m} = \frac{\partial}{\partial x}\left(D_{eff} \frac{\partial \rho_v}{\partial x}\right)$$

(3.2)

where D_{eff} represents the effective diffusion during moisture transfer and is related to the binary diffusion of water vapour in air (D_{AB}), and the tortuosity (τ) of the desiccant as shown below:

$$D_{eff} = \frac{\varepsilon_g \cdot D_{AB}}{\tau}$$

(3.3)

3.5.1.3 *Continuity equation:*

$$\frac{\dot{m}}{\rho_l} = \frac{\partial \varepsilon_l}{\partial t}$$

(3.4)

3.5.1.4 *Moisture adsorption equation*

The phase change rate of water vapor ($\dot{m}$) is related to the adsorption/desorption rates as shown in Equation 3.5. It is a function of the dynamic moisture content (u_t) of the desiccant (due to sorption kinetics).

$$\dot{m} = \frac{\partial u_t}{\partial t} \rho_{dry}$$

(3.5)

As illustrated earlier in Section 2.4, the moisture content in the desiccant is not assumed to be uniform and in equilibrium with the air (*i.e.,* instantaneous moisture transfer). Instead, the delay in adsorption due to sorption kinetics is incorporated in the physical model by including the Linear

Driving Force model (LDF). The sorption kinetic rate constant (k) of silica gel which was measured in chapter 2 is used as an input for Equation (3.6).

$$\frac{\partial u_t}{\partial t} = k(u - u_t) \tag{3.6}$$

The equilibrium moisture content (u) in the desiccant is calculated using Equation (3.7). The equation was generated by curve fitting the experimental sorption isotherm data for silica gel (Section 2.6.2). The polynomial equation showed good agreement with the experimental data presenting an R^2 value of 0.9964.

$$u = 0.2227RH^3 + 0.6646RH^2 - 0.1375RH + 0.0154 \tag{3.7}$$

3.5.1.5 *Volumetric constraint equation*

Given that the GSSR numerical model represents a porous desiccant; the physical model during adsorption process consists of a desiccant volume fraction (solid side), gas volume fraction (empty pores filled with air) and liquid volume fraction (adsorbed moisture in the empty pores). Therefore, the volumetric constraint in the porous media is represented by:

$$\varepsilon_d + \varepsilon_g + \varepsilon_l = 1 \tag{3.8}$$

3.5.2 Physical properties

The physical (or material) properties of the desiccant are subjected to changes during heat and moisture transfer, resulting in 'effective parameters' as moisture is adsorbed or desorbed. The effective parameters are calculated as follows:

$$\rho_{eff} = \varepsilon_g(\rho_v + \rho_a) + \varepsilon_l\rho_l + \varepsilon_d\rho_d \tag{3.9}$$

$$c_{p_{eff}} = \frac{\varepsilon_g(\rho_v c_{p,v} + \rho_a c_{p,a}) + \varepsilon_l\rho_l c_{p,l} + \varepsilon_d\rho_d c_{p,d}}{\rho_{eff}} \tag{3.10}$$

$$K_{eff} = \varepsilon_g \cdot \left(\frac{\rho_v K_v + \rho_a K_a}{\rho_v + \rho_a}\right) + \varepsilon_l K_l + \varepsilon_d K_d \tag{3.11}$$

3.5.3 Thermodynamic relationships

The water vapour density of the desiccant in Equation (3.2) can be converted to relative humidity by using the following thermodynamic relationships:

$$P_v = \rho_v R_v T \tag{3.12}$$

$$P_a = \rho_a R_a T \tag{3.13}$$

$$P_a = P_g - P_v \tag{3.14}$$

$$\rho_g = \rho_a + \rho_v \tag{3.15}$$

$$RH = \frac{P_v}{P_{v,sat}}\bigg|_T \tag{3.16}$$

The saturation vapour pressure over liquid water at any given temperature is obtained from a fundamental handbook by the American Society of Heating, Refrigerating and Air-conditioning Engineers (ASHRAE, 2017) [102]. Thus, the saturation vapour pressure is expressed by:

$$P_{v,sat} = \exp\left(\frac{C_1}{T} + C_2 + C_3 T + C_4 T^2 + C_5 T^3 + C_6 \ln T\right) \tag{3.17}$$

where the constants are: C_1 = -5.6745E+03, C_2 = 1.3915, C_3 = -4.8640E-02, C_4 = 4.1765E-05, C_5 = -1.4452E-08, C_6 = 6.5460.

3.5.4 Boundary conditions

According to the physical model explained in Section 3.4, the boundary equations at the top (*i.e.,* $x = 0$) and bottom (*i.e.,* $x = L$) of the desiccant are delineated as follows for heat transfer:

$$h_h(T|_{x=0} - T_a) = K_{eff} \frac{\partial T}{\partial x}\bigg|_{x=0} \tag{3.18}$$

$$\frac{\partial T}{\partial x}\bigg|_{x=L} = 0 \tag{3.19}$$

The boundary equations for moisture transfer are:

$$h_m\left(\rho_v|_{x=0} - \rho_{v,a}\right) = D_{eff}\left.\frac{\partial \rho_v}{\partial x}\right|_{x=0} \tag{3.20}$$

$$\left.\frac{\partial \rho_v}{\partial x}\right|_{x=L} = 0 \tag{3.21}$$

3.5.5 Initial conditions

Initially, the desiccant is assumed to be dry, with humid air flowing over its surface. The values used in the model for the initial conditions are listed in Table 3.2.

Table 3.2. Initial conditions.

Parameters	Unit	Air	Desiccant
Temperature	K	297.15	313.15
Relative humidity	%	50	0
Heat transfer coefficient (h_h)	W/(m²·K)	40 [15]	-
Mass transfer coefficient (h_m)	m/s	0.04 [15]	-

3.5.6 Numerical solution scheme

The governing partial differential equations are discretized using the finite difference method which has a second order accuracy. The time derivative is fully implicit. The spatial nodes are solved using the forward and backward difference at the boundaries, while the central difference scheme is used to solve the interior nodes. The solution is solved using an under relaxed, Gauss-Seidel iteration in order to ensure stability. The numerical solution was assumed to be converged when the dependent variables for heat and moisture transfer (*i.e.*, T, ρ_v) satisfied the convergence criterion shown in Equation (3.22).

$$\left|\frac{\psi^k - \psi^{k-1}}{\psi_\infty - \psi_i}\right| < 1 \times 10^{-7} \tag{3.22}$$

In order to solve the governing equations, a MATLAB code was developed. Details on the computer program and discretized equations are presented in Appendix C. The numerical

algorithm used to calculate the temperature and water vapour density profiles in the desiccant are presented as follows:

1. Input all physical property data and initial conditions.
2. Solve and update the effective parameters of the desiccant.
3. Calculate the temporal and spatial temperatures using the energy equation (*i.e.,* Equation 3.1).
4. Calculate the temporal and spatial vapour density using the water vapour diffusion equation (*i.e.,* Equation (3.2)).
5. Calculate the rate of phase change using the moisture adsorption equation, sorption isotherm and LDF model (*i.e.,* Equations (3.5) – (3.7)).
6. Evaluate the gas volume fraction via the volumetric constraint equation (*i.e.,* Equation (3.8)).
7. Repeat steps 2 to 6 until the convergence criteria is satisfied for both temperature and water vapour density.
8. Repeat steps 2 to 7 for the next time step.

For the results presented in this chapter, a time step of 0.1 s, grid size of 0.0003 m, normalized convergence criteria of 1×10^{-7}, under-relaxation factors of 0.65 for temperature and 0.005 for vapour density were used in the MATLAB code. These values were selected based on a sensitivity study (details presented in Appendix D). Appendix D shows that increasing the grid size, time step and convergence criterion by a factor of 10 had less than a 1% change in the results, with more than a 15% increase in computation time.

3.6 MODEL VALIDATION

The temperature and vapor density results for heat transfer only (no moisture transfer) and moisture transfer only (no heat transfer) were validated with available analytical models in the literature. In addition, the moisture content in the desiccant was validated with the equilibrium sorption data from Chapter 2 for a case of moisture transfer only (no heat transfer).

3.6.1 Heat transfer only (no moisture transfer)

The numerical temperature profiles were compared with the analytical solution (semi-infinite solid assumption) by Incropera et al. [103] for a scenario of heat transfer only (*i.e.,* $u = 0$, $RH_d = 0$ and $h_{fg} = 0$) when cool air flows over a warm desiccant layer. The analytical solution presented in the literature [103] is expressed by:

$$\frac{T - T_d}{T_a - T_d} = erfc\left(\frac{x}{2\sqrt{\alpha t}}\right) - \left[\exp\left(\frac{h_h x}{k} + \frac{h_h^2 \alpha t}{k^2}\right) \times \left[erfc\left(\frac{x}{2\sqrt{\alpha t}} + \frac{h_h\sqrt{\alpha t}}{k}\right)\right]\right] \qquad (3.23)$$

Figures 3.2 and 3.3 represent the numerical and analytical temperature profiles at the surface and for various depths in the desiccant respectively. These validated results make physical sense given that the temperature in the desiccant layer will reduce due to heat transfer with the cold air stream.
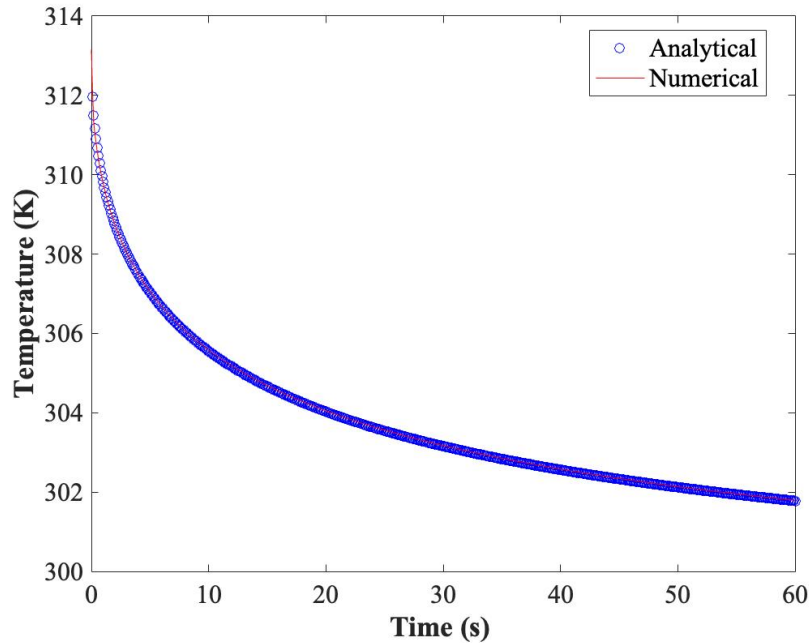
Figure 3.2. Validation of numerical and analytical temperature profiles at the desiccant surface.
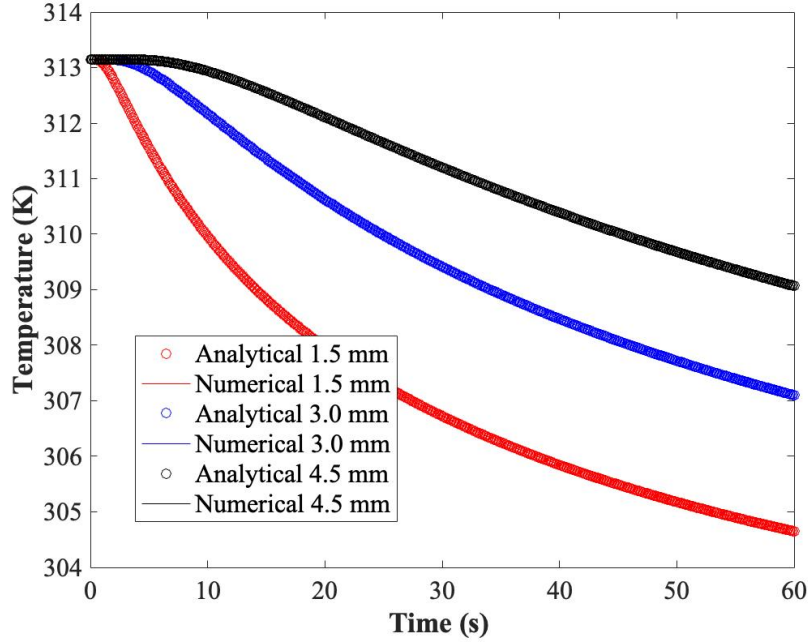
Figure 3.3. Validation of numerical and analytical temperature profiles at depths of 1.5 mm, 3.0 mm and 4.5 mm in the desiccant layer.

3.6.2 Moisture transfer only (no heat transfer)

The numerical water vapor density profiles were compared with an analytical solution (semi-infinite solid assumption) by Olutimayin et al. [98] for a scenario of moisture transfer only (*i.e.,* $T_d = T_a$ and $h_{fg} = 0$) when humid air flows over a dry desiccant layer. The analytical solution presented in the literature [98] is expressed by:

$$
\frac{\rho_v - \rho_{v,d}}{\rho_{v,a} - \rho_{v,d}} = erfc\left(\frac{x}{2\sqrt{\alpha_{m,eff}t}}\right)
$$
$$
-\left[\exp\left(\frac{h_m x}{D_{eff}} + \frac{h_m^2 \alpha_{m,eff}t}{D_{eff}^2}\right)\right.
$$
$$
\left.\times \left[erfc\left(\frac{x}{2\sqrt{\alpha_{m,eff}t}} + \frac{h_m\sqrt{\alpha_{m,eff}t}}{D_{eff}}\right)\right]\right]
$$

(3.24)

Figures 3.4 and 3.5 represent the numerical and analytical vapour density profiles at the surface and at various depths in the desiccant respectively. These validated results also make physical

sense given that the water vapour density in the desiccant layer will increase due to moisture transfer with the humid air stream.
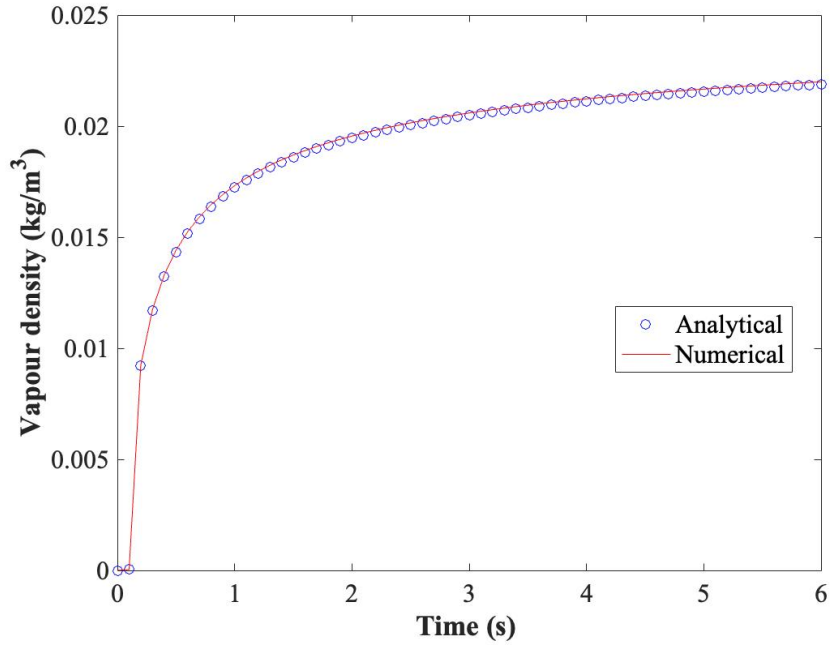
Figure 3.4. Validation of numerical and analytical vapour density profiles on desiccant surface.
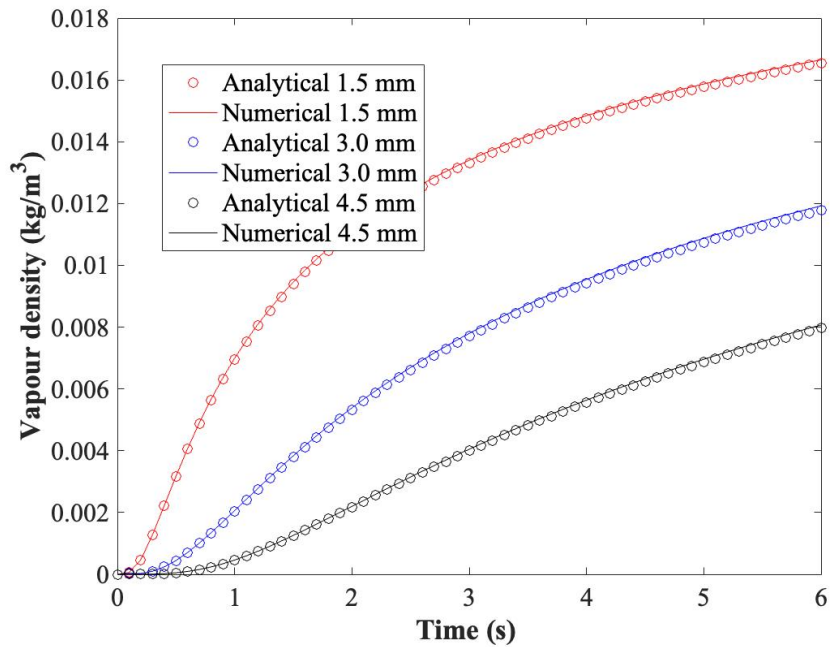
Figure 3.5. Validation of numerical and analytical water vapour density profiles at 1.5 mm, 3.0 mm and 4.5 mm depths in the desiccant layer.

It can be observed visually that the numerical results showed very good agreement with the analytical solutions. The average and maximum errors based on Equation (3.25) were 0.1% and 0.8% for heat transfer and 0.3 and 1.1% for moisture transfer respectively.

$$err = \left| \frac{\psi_{num} - \psi_{anl}}{\psi_a - \psi_d} \right| \times 100 \tag{3.25}$$

The numerical solution for moisture transfer only was also compared with the experimental sorption data (from Chapter 2) as seen in Figure 3.6. The results are shown for a case of moisture transfer only, and at the same process air temperature used in the sorption experiments (*i.e.,* $T_d = T_a = 298$ K). As can easily be observed from the figure, the numerical model shows a very good agreement with the experimental data. In all cases, the maximum difference between the experiments and numerical model was less than 0.01 g/g.
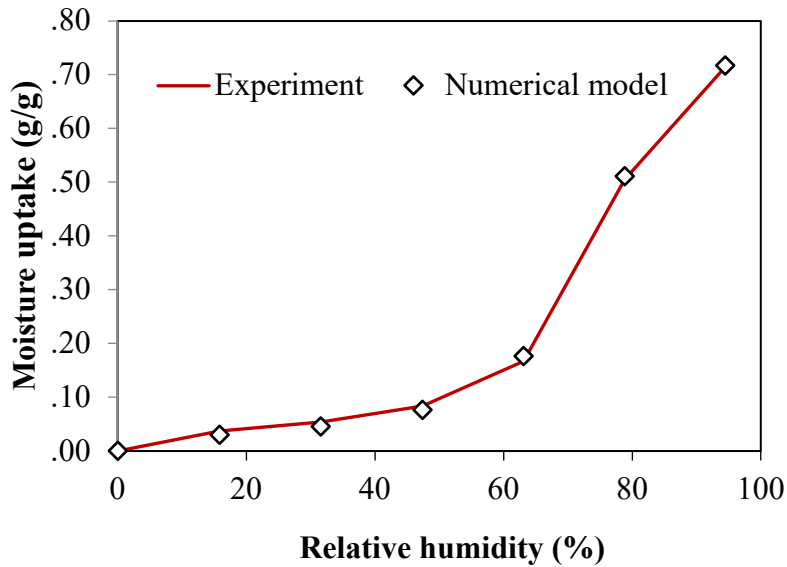
Figure 3.6. Validation of the desiccants' moisture content in the numerical model with experimental data.

3.7   RESULTS AND DISCUSSION

This section contains the numerical results for heat and moisture transfer with the initial conditions presented in Table 3.2. The results in this section were simulated for a silica gel desiccant, however, further comparisons with kinetic rate constants (*k*) of the MS + binder desiccants measured in the previous chapter are shown in Section 3.7.3. In addition, further analysis on silica

gel based on the effect of typical particle sizes used in desiccant coatings are also presented in Section 3.7.3.

3.7.1 Equilibrium model

3.7.1.1 Heat transfer

In order to understand the heat transfer performance of a desiccant layer, the model must determine the temperature profiles at different locations in the desiccant. Figure 3.7 shows the temporal temperature profiles in the desiccant during 60 s of adsorption as cool humid air flows over the desiccant surface. It can be observed that the heat release due to phase change plays a role in increasing the desiccants' temperature during adsorption. This makes physical sense because when $h_{fg} = 0$ J/kg, the desiccant cools with time and along its depth as expected. On the other hand, when $h_{fg} = 2.7 \times 10^6$ J/kg, adsorption releases heat energy and this increases the temperature of the desiccant above air temperature. However, after a certain period, heat transfer begins to dominate at the depths closer to the desiccant surface.

(a)   (b)
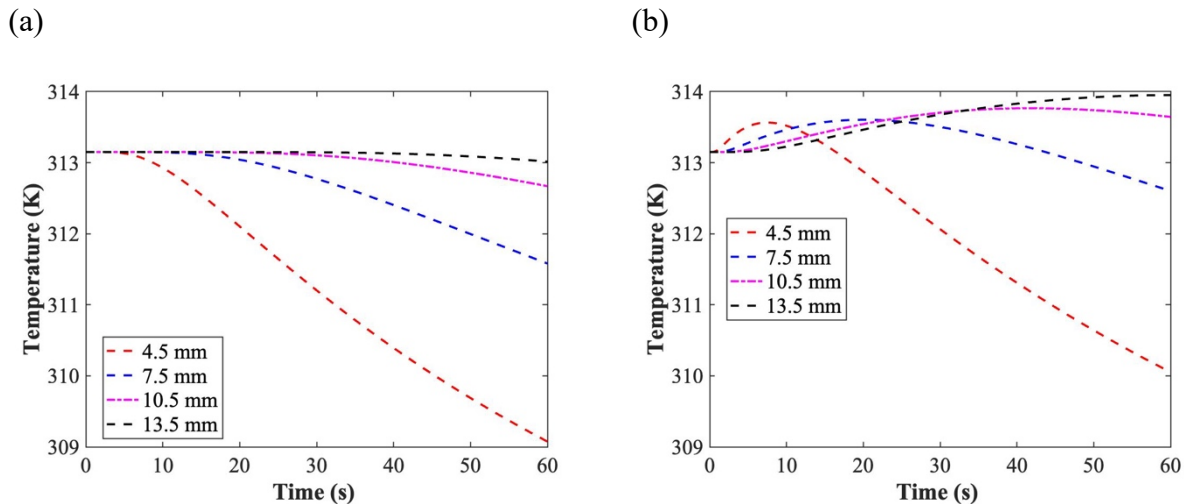
Figure 3.7. Temporal temperature profiles with (a) $h_{fg} = 0$ J/kg, and (b) $h_{fg} = 2.7 \times 10^6$ J/kg.

Figure 3.8 shows the spatial temperature profiles in the desiccant layer. As would be expected, at any given time, the desiccant closer to the cool air at the surface will have a lower temperature than the desiccant closer to the adiabatic boundary at the bottom of the desiccant, due to the transient nature of heat conduction. Comparing Figures 3.8 (a) and (b), it can be observed that there also is a slight increase in the desiccant temperature as a result of the heat release due to phase change. This temperature increase becomes conspicuous at approximate depths of 4 mm

after 15 s, 5 mm after 30 s, 6 mm after 45 s, and 7 mm after 60 s; as heat transfer due to temperature difference slowly begins to dominate.

(a) (b)
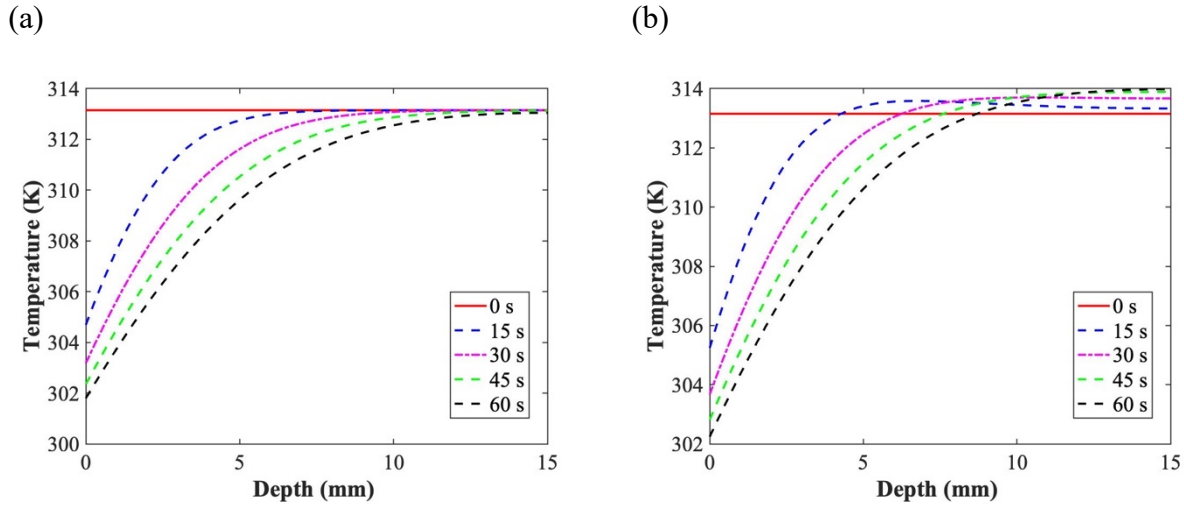
Figure 3.8. Spatial temperature profiles when (a) $h_{fg} = 0$ J/kg, and (b) $h_{fg} = 2.7 \times 10^6$ J/kg.

3.7.1.2 *Moisture transfer*

In this section, the profiles in the desiccant with respect to moisture transfer via the sorption isotherm in Equation (3.7) are analyzed and discussed. Figure 3.9 shows the spatial moisture content, relative humidity and water vapour density profiles in the desiccant using the sorption isotherm of silica gel. As would be expected, the results showed the transient diffusion of water vapour molecules from the desiccant's surface (in contact with humid air) to the bulk of the media. In general, the results showed a higher moisture content at the surface which is due to diffusion of water vapour from the humid air at the desiccant surface.
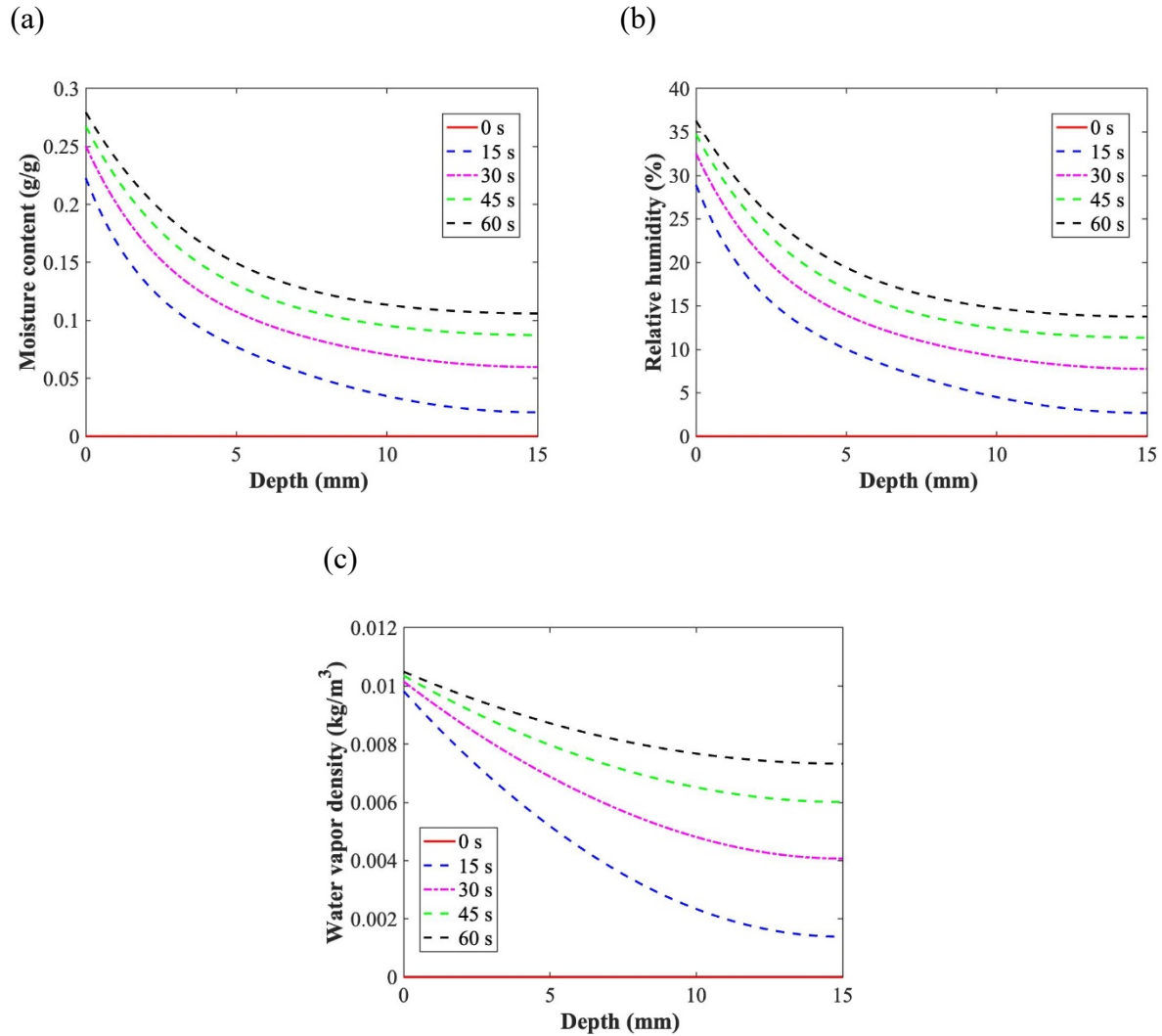
Figure 3.9. Spatial profiles of (a) moisture content, (b) relative humidity, (c) and water vapour density in the desiccant.

3.7.2 Sensitivity studies on the equilibrium model

Sensitivity studies are used to determine and quantify the dependent properties (or parameters) which influence the numerical results. The sensitivity studies presented in this section were conducted for a 25% increase and decrease respectively, to quantify the effect of each parameter on the desiccant's temperature and relative humidity. All sensitivity results delineated in this section were conducted at initial conditions shown in Table 3.2, presenting the profiles at the middle of the desiccant layer (*i.e., L / 2*).

3.7.2.1 Sorption isotherm

The sorption isotherm used in this section is the polynomial curve fit of the experimental data shown in Equation (3.7). Figure 3.10 contains the relative humidity and temperature profiles at position $L / 2$ in the desiccant for $\pm 25\%$ changes in the sorption isotherm. As can be observed from Figure 3.10(a), an increase in the sorption isotherm reduces the relative humidity in the desiccant and vice versa. This phenomenon makes physical sense because increasing the sorption isotherm means greater moisture accumulation, and as such, the vapour density and relative humidity will decrease due to an increased amount of moisture transfer and water vapor molecules in the desiccant. This is because increasing the sorption capacity is analogous to increasing the thermal mass [98], which results in a slower response. On the other hand, the temperature as observed from Figure 3.10(b) increases when the sorption isotherm was increased and vice versa. This is because an increase in adsorption (moisture accumulation) leads to a higher release of phase change heat, which in turn heats up the desiccant and increases its temperature.

(a)　　　　　　　　　　　　　　　　　　　(b)
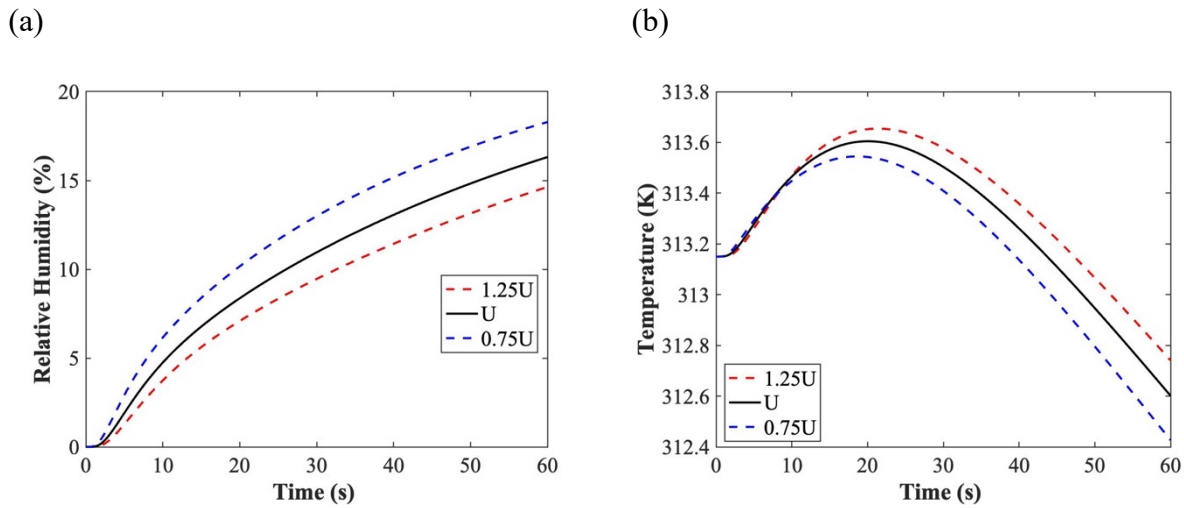
Figure 3.10. Sensitivity study at position $L/2$ showing the (a) relative humidity, and (b) temperature profiles by changing the sorption isotherm by $\pm 25\%$.

3.7.2.2 Effective diffusion coefficient

The effective diffusion used in the model is illustrated by Equation (3.3). The effect of changing effective diffusion for moisture transfer by $\pm 25\%$ is shown in Figure 3.11. As would be expected, the relative humidity in the desiccant increases when the moisture transfer via diffusion is increased. In addition, the temperature in the desiccant also increases due higher diffusion which leads to a higher moisture accumulation, and therefore more phase change energy is released.

(a)   (b)
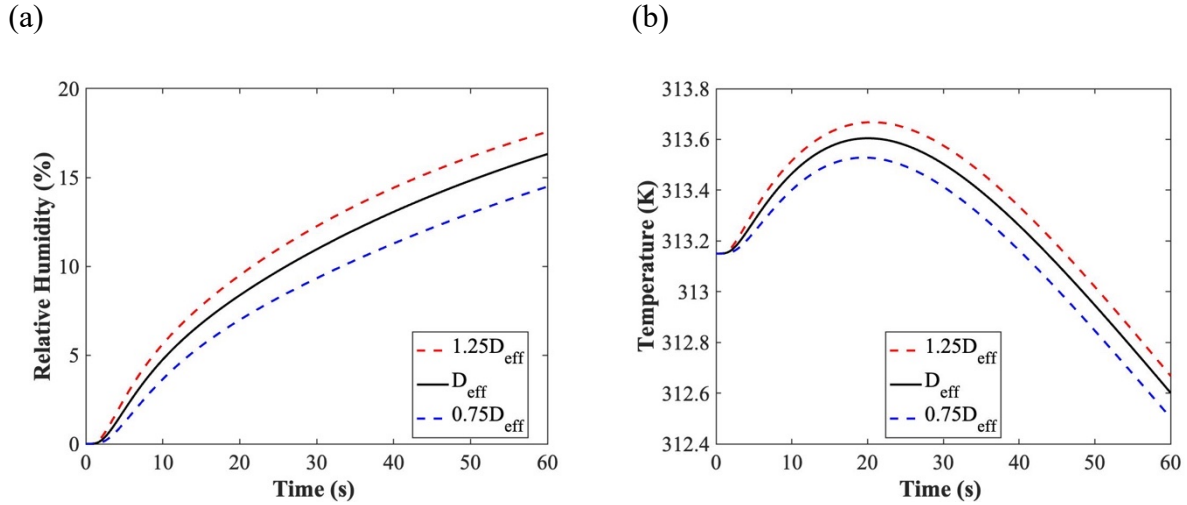
Figure 3.11. Sensitivity study at position $L/2$ showing the (a) relative humidity, and (b) temperature profiles by changing the effective diffusion by $\pm 25\%$.

3.7.2.3 *Heat of adsorption*

The heat of adsorption in the model was assumed to be constant. However, in reality, the heat of adsorption actually varies with moisture content, particularly at the initial stages of adsorption (low moisture content) [85]. Therefore, it is important to quantity the effect of heat release due to water vapour adsorption as shown in Figure 3.12. As can be observed form the figure, an increase in the heat of adsorption value (shown in Table 3.1) increases the temperature in the desiccant due to the higher energy released during phase change and vice versa. On the other hand, there was a negligible decrease in the relative humidity (less than 1%) when the heat of adsorption was increased or decreased, as would be expected.
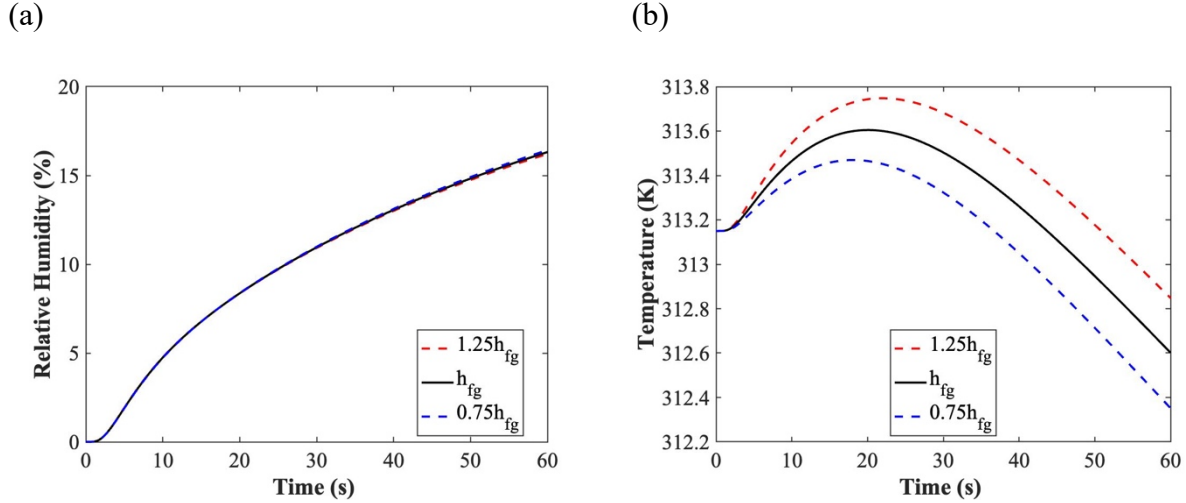
Figure 3.12. Sensitivity study at position $L/2$ showing the (a) relative humidity, and (b) temperature profiles by changing the heat of adsorption (h_{fg}) by $\pm 25\%$.

3.7.2.4 *Summary of sensitivity analysis*

In many core desiccant studies, changes in moisture content are perhaps more valuable than changes in relative humidity and temperature. As such, Figure 3.13 shows the sensitivity of the major desiccant property parameters to moisture content. As can easily be observed from the y-axis range, the parameters in Figure 3.13(a) are less sensitive to changes in moisture content as compared to the parameters in Figure 3.13(b). This shows that changes in the sorption isotherm, thickness of the desiccant layer and effective diffusion coefficient impact the moisture content in the desiccant much more than changes in the thermal conductivity, heat of adsorption and density of the desiccant.
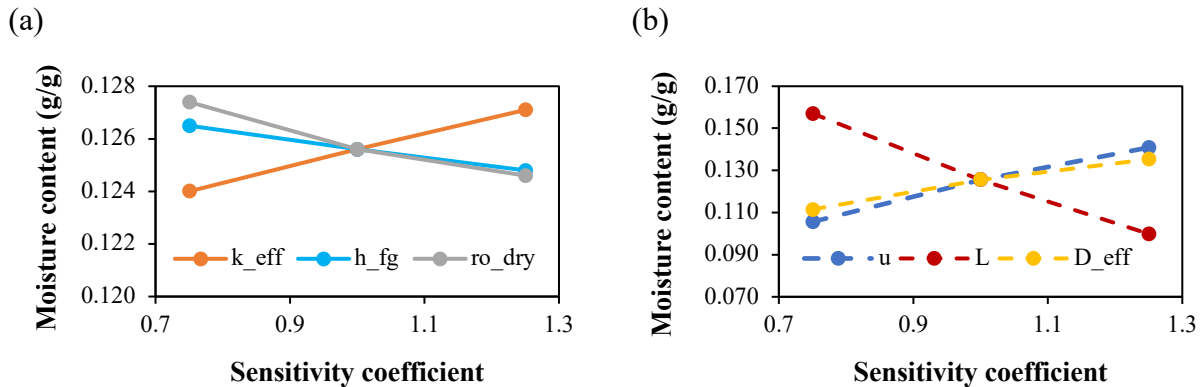
Figure 3.13. Impact of (a) thermal conductivity (K_{eff}), heat of adsorption (h_{fg}), density (ρ_{dry}), (b) sorption isotherm (u), thickness (L), and effective diffusion coefficient (D_{eff}) for a $\pm 25\%$ change in input parameters on the desiccant's moisture content at position $L/2$.

3.7.3 Linear driving force (LDF) model

3.7.3.1 *Effect of rate constant (k)*

Many numerical models for moisture transfer in FBR are based on the assumption that the moisture transfer is instantaneous and the desiccant's moisture content is uniform with the air [15]. However, this assumption does not accurately represent the physical problem. This is because there is a delay in moisture transfer due to the sorption kinetics. As such, the moisture transfer is not instantaneous and the desiccant moisture content cannot be in equilibrium with the air but instead, it is transient and represented by a dynamic sorption quantity (u_t). The dynamic sorption quantities presented in this section were evaluated using Equation (3.6).

As discussed earlier, there is a difference between the equilibrium moisture content (u) via the sorption isotherm and the dynamic moisture content (u_t) as described by the sorption kinetics. Figure 3.14 shows the moisture content at the desiccant surface (silica gel) with the equilibrium and kinetic delay assumptions. Unlike the GSSR solutions (equilibrium and dynamic moisture contents), the GSR solution (*i.e.,* Ramin et al. [15]) showed a steep slope at time $t = 0$ min, indicating no kinetic delay before the equilibrium sorption capacity was reached. On the other hand, the dynamic moisture content showed a more visible delay in the mass transfer process, indicating that the moisture transfer is not instantaneous. This result makes physical sense because it may take several hours for a desiccant to reach equilibrium moisture content for each RH step-change as discussed in Chapter 2 and shown from the sorption kinetics curves in Figure 2.12. Therefore, the assumption of an equilibrium moisture content in the desiccant at any air relative humidity (via the isotherm equation) using either the GSR or GSSR solutions, will falsely represent the actual scenario due to the dynamic adsorption behaviour of desiccants. As a result, sorption kinetics should not be neglected in an FBR model.

Considering that this thesis presents a method to select desiccants, comparison with the kinetic performance of the other desiccants tested in chapter 2 are shown in Figure 3.14(b). For this scenario, a parametric study using their respective rate constants is conducted with the same sorption isotherm and properties of the silica gel desiccant, while changing only the rate constant (k). The result of the simulation supports the key recommendation in Chapter 2, proving that a desiccant with a higher rate constant should be recommended for FBR applications.

(a)

(b)
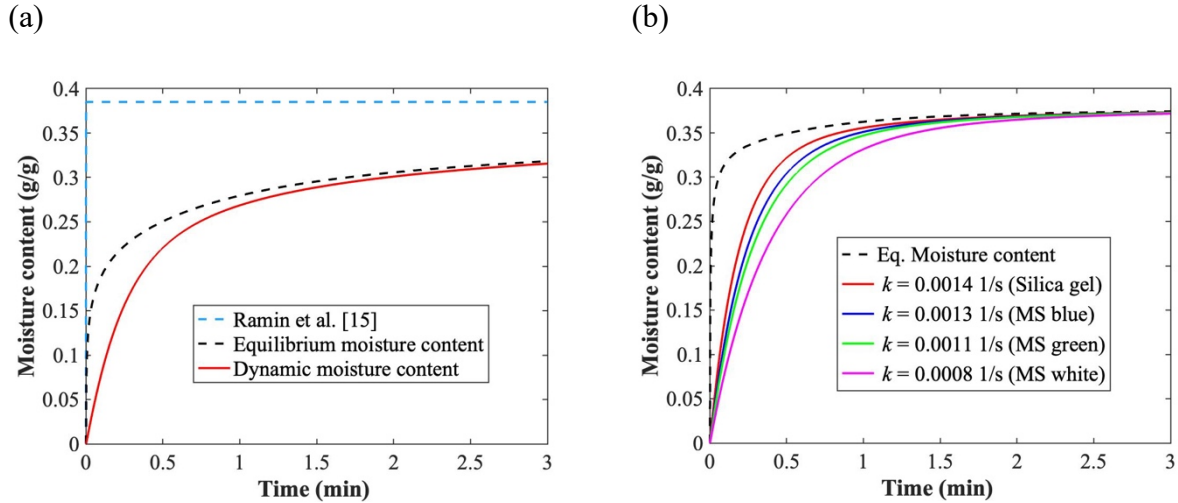
Figure 3.14. Numerical results showing (a) equilibrium (GSR and GSSR solutions) and dynamic moisture contents of silica gel (SG) at $x = 0$, and (b) parametric study on the effect of sorption kinetics using rate constants of silica gel (SG), blue, green and white molecular sieve (MS) desiccants at $x = 0$ after 3 mins of adsorption respectively.

In addition, considering that FBRs operate in a cycle of 120 seconds (*i.e.,* 60 s adsorption, 60 s desorption), the role of the sorption kinetics was analyzed using the rate constants of the tested desiccants during 60 s of adsorption as shown in Figure 3.15. Given that this was a parametric study, all other properties of silica gel were held constant except the rate constant (k). The results show the overestimation when using an equilibrium isotherm in the GSSR model during only 60 s of adsorption. As previously discussed, this is because physically and even under test conditions, adsorption is transient and may take several minutes or hours before equilibrium capacity is reached. As such, estimating FBR desiccant performance based on an equilibrium isotherm can lead to errors. In terms of the average moisture content in the desiccant, the measured kinetic rate constants of silica gel, blue, green, and white samples showed a 21%, 22%, 25%, and 33% lower moisture content in the desiccant respectively in comparison to the equilibrium assumption.
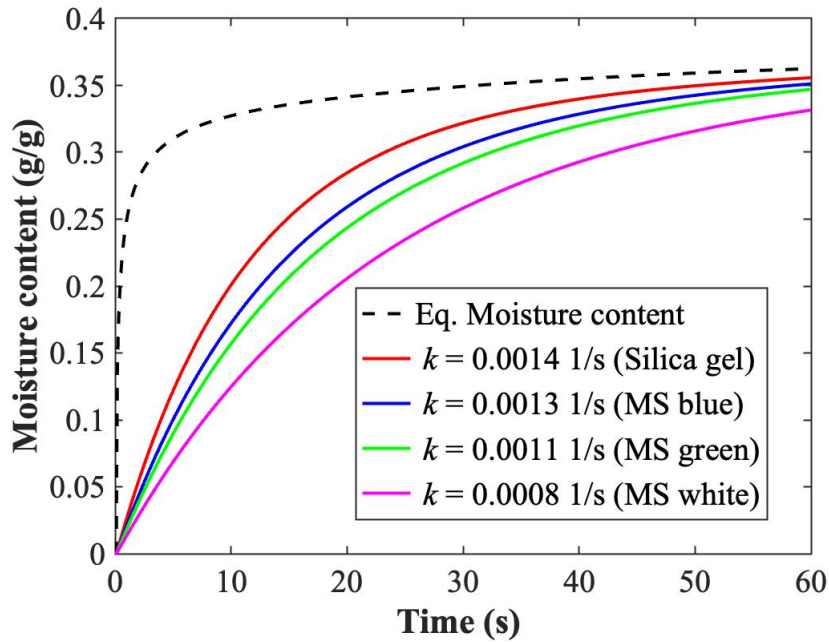
Figure 3.15. Parametric study on the effect of sorption kinetics using k's of silica gel (SG), blue, green and white molecular sieve (MS) desiccants respectively after 60 s of adsorption.

3.7.3.2 *Effect of particle size*

In many applications, desiccant materials used for coating energy exchangers are selected solely based on their sorption isotherm capacity. However, some intrinsic properties of the desiccant such as the particle/mesh size could play a crucial role in terms of energy exchanger performance. In this section, the effect of particle size (*i.e.,* particle radius) on the kinetic performance of a silica gel desiccant layer is investigated in accordance with the LDF approximation for rate constant (k) as shown in Equation (3.29).

$$k = {15D_{eff}}\Big/{R_p^2} \tag{3.26}$$

Figure 3.16 shows the moisture content profile at the surface when three different types of silica gel are used. The particle radii used for this study are IR silica gel (0.08 mm), and RD silica gel (0.2 mm and 0.25 mm types). As observed from the figure, it can be inferred that when a desiccant layer is coated with finer particles, the moisture content in the desiccant increases. This is because the intra-particle mass transfer resistances are weaker when the particle size is smaller. As a result, the sorption kinetics are much faster, thereby increasing the overall mass transfer process. In

quantifiable terms, the 0.2 mm particle radius had a 16% lower average moisture content than the 0.08 mm IR silica gel, while the 0.25 mm particle radius had a 11% lower average than the 0.20 mm RD silica gel. It can also be seen that initially, the moisture transfer is much quicker in the 0.08 mm IR silica gel, making it more suitable for FBRs given their short operating periods.
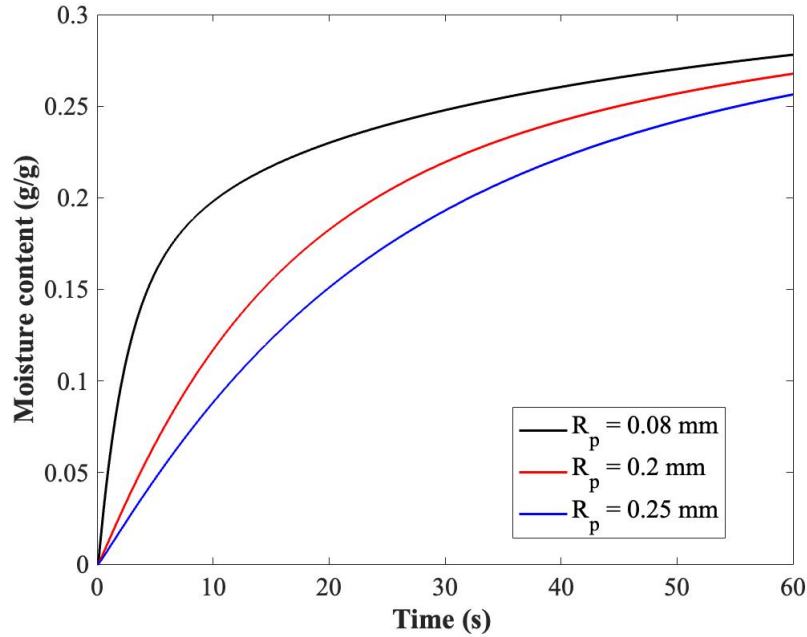
Figure 3.16. Moisture content profiles at desiccant surface with R_p = 0.08 mm, R_p = 0.2 mm, and R_p = 0.25 mm respectively.

3.7.4 Cyclical conditions during moisture transfer

Given that FBR operates in a cycle, it is necessary to investigate the water vapour interactions in the desiccant for each cycle, by virtue of their relative humidity and moisture content profiles. The boundary conditions used for the analysis are shown in Table 3.3. As seen from the table, the desiccant is exposed to isothermal conditions with a periodic change in relative humidity every 60 seconds. In addition, the desiccant is assumed to be dry and at the same temperature as the air initially.

Table 3.3. Cyclical boundary conditions representing FBR operation.

Parameters	Unit	Adsorption period	Desorption period
Temperature	K	313.15	313.15
Relative humidity	%	50	5 [15]
Period	s	60	60 [77]

In order to understand the cyclical moisture transfer performance of the desiccant, a quasi-steady state criterion must first be established, which represents the condition at which the moisture accumulation during the adsorption period equals moisture removal during the desorption period. The change in moisture content for a given period (adsorption or desorption) in each cycle can be evaluated by:

$$\Delta u = u_{ave,final} - u_{ave,start} \tag{3.27}$$

where $u_{ave,final}$ is the average moisture content in the desiccant evaluated at the end of an adsorption or desorption period, while $u_{ave,start}$ is the average moisture content in the desiccant evaluated at the start of an adsorption or desorption period. Numerically, quasi-steady state is assumed to exist when the normalized percentage difference between Δu_{ads} and Δu_{des} is less than 0.1%, which is expressed mathematically as:

$$\frac{\Delta u_{ads} - \Delta u_{des}}{\Delta u_{cycle}} < 0.1\% \tag{3.28}$$

where

$$\Delta u_{cycle} = \frac{\Delta u_{ads} + \Delta u_{des}}{2} \tag{3.29}$$

3.7.4.1 *Moisture transfer with equilibrium model*

Figure 3.17 presents the average values of Δu_{ads} and Δu_{des} for the first 15 cycles and at the boundary conditions shown in Table 3.3. It can easily be observed that the moisture accumulation during adsorption equalled the moisture removal during desorption after about the 10th cycle. However, the numerical value for quasi-steady state condition in Equation (3.28) was not attained until the 15th cycle.
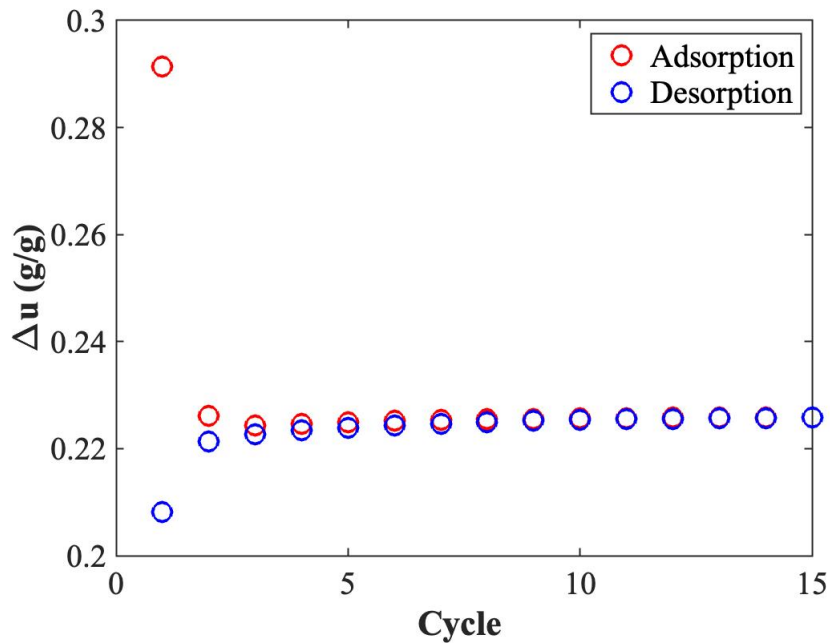
Figure 3.17. Moisture content change in the desiccant during the first 15 adsorption and desorption cycles via the equilibrium model.

Previously, Sections 3.7.2 and 3.7.3 showed that desiccants with smaller thicknesses and particle sizes results in a higher moisture content, and as such better moisture transfer performance would be expected. In addition, a previous experimental study [77] for evaluating performance in desiccant coated FBRs showed high performance with a thin and uniform ca. 1 mm desiccant coat of silica gel. In this regard, the thick 15 mm silica gel coating is compared with a thin 1 mm silica gel coating under the same cyclical conditions as shown in Figure 3.18.

Figure 3.18 shows a 120 second cycle period with 60 seconds of adsorption and desorption respectively. It should be noted that the desorption lines at 120 s also represent adsorption at 0 s, given that the results are shown at quasi-steady state. It can be observed from the figure that the 1 mm thick desiccant has a higher average relative humidity and moisture content profile than the 15 mm thick desiccant. It can also be seen that the 1 mm thick desiccant had a uniform moisture content and relative humidity profiles. This was due to the low mass transfer resistance in the thin desiccant, which in turn makes the relative humidity and moisture content in the entire desiccant nearly in equilibrium with the air. Conversely, this was very different in the thick 15 mm coating, where the adiabatic and impermeable boundary conditions at the bottom depth of the desiccant played a significant role in the profiles. In addition, it can clearly be seen in the thick coating that

the moisture content increases as time increase during the adsorption period and decreases as time increase during the desorption period. In the thin coating on the other hand, this phenomenon is not clearly visible due to the high moisture transfer rates as a result of the low mass transfer resistances.

(a)

(b)

(c)

(d)
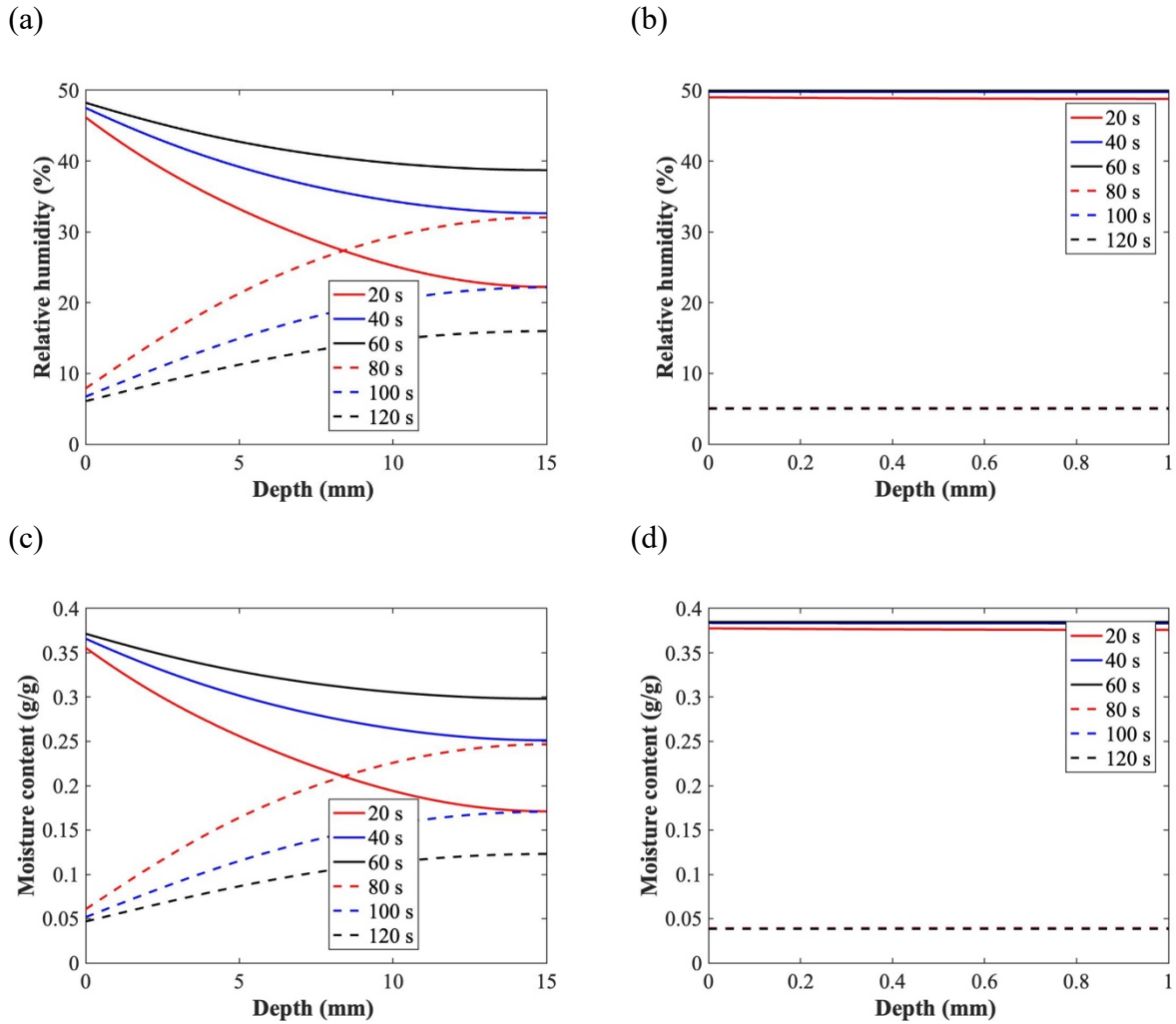
Figure 3.18. Relative humidity profiles of (a) 15 mm, (b) 1 mm, and moisture content profiles of (c) 15 mm, and (d) 1 mm thick desiccant coatings at quasi-steady state respectively.

3.7.4.2   Linear driving force (LDF) model

Figure 3.19 shows the moisture content in the desiccant (15 mm and 1 mm coating) using both the equilibrium and the LDF model with $k = 0.0014$ 1/s. In Figure 3.19, the 1 mm coating (Figure 3.19(b)) has a higher moisture content at the surface than the 15 mm coating (Figure 3.19(a)) due to its lower resistance to moisture transfer. As a result, the 1 mm coating arrives at quasi-steady state after the first cycle. This shows that 60 s of adsorption and desorption in a single cycle was

sufficient for the moisture accumulation to equal the moisture removal in the thin coating. On the other hand, the 15 mm coating attained quasi-steady state after the 15th cycle, due to the greater mass transfer resistances in the thick coating. This indicates that adsorption/desorption periods of more than 60 s would be required for the moisture content in the thick coating to equal that of the thin coating.

The delay due to sorption kinetics in each cycle can also be observed via the dynamic moisture content in Figure 3.19, presenting a slightly lower moisture content than the equilibrium assumption. However, in order to adequately observe the effect of kinetics in the desiccant, the spatial moisture content profiles during adsorption and desorption periods are shown in Figure 3.20 for the thick (15 mm) and thin (1 mm) desiccant coatings.

(a)   (b)
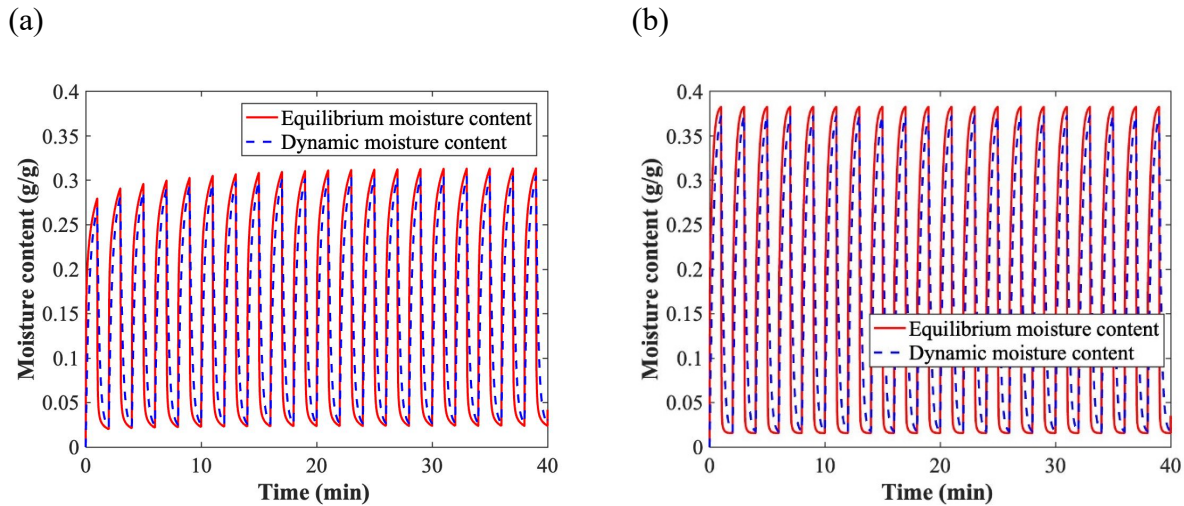
Figure 3.19. Equilibrium and dynamic moisture content ($k = 0.0014$ 1/s) profiles of (a) 15 mm (b) 1 mm thickness of desiccant coating at the surface.

In Figure 3.20, it can be observed that the effect of sorption kinetics in the desiccant was quite substantial, as the kinetics assumption showed a more visible delay given that the change in moisture content during both adsorption and desorption periods was much slower. However, it can also be observed that at the 60 s adsorption and desorption periods, the effect of kinetics (*i.e.,* at Eq. 60 s and Dyn 60 s) was much less for the 1 mm coating in comparison to the 15 mm coating. In addition, it can also be seen in the 15 mm coating that the difference between the dynamic and equilibrium models reduce as the adsorption or desorption periods increase. This indicates that sorption kinetics plays a greater role when FBR recovery periods are shorter as opposed to longer recovery periods. Thus, in order to investigate the conditions at which kinetic effects become

76

minimal for FBR, a parametric study is conducted in Section 3.7.4.3 to determine when sorption kinetics can be neglected.

(a)

(b)

(c)

(d)
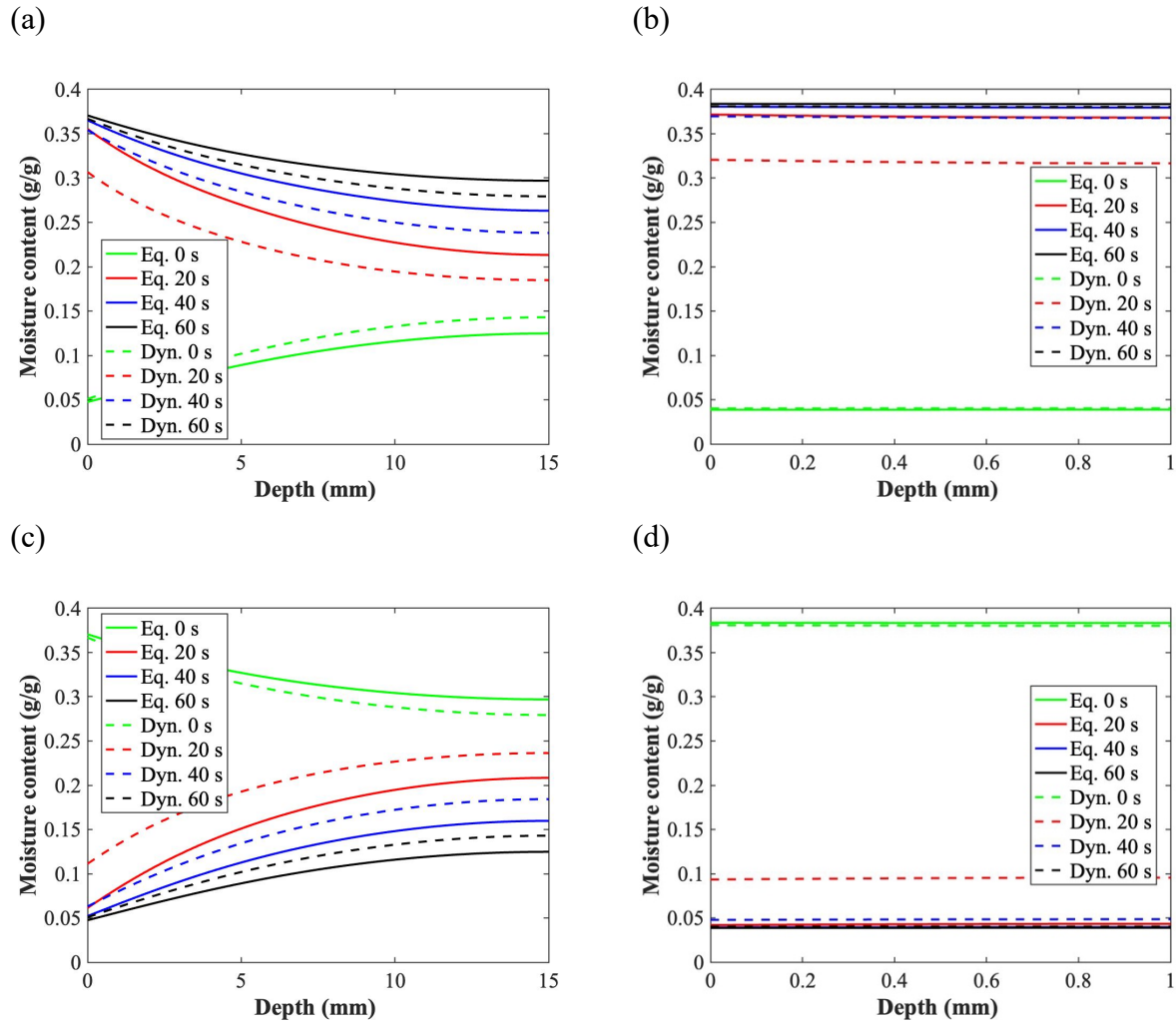
Figure 3.20. Effect of kinetics during adsorption in (a) 15 mm, (b) 1 mm and desorption in (c) 15 mm (d) 1 mm thick desiccant coatings respectively.

3.7.4.3 *Errors in equilibrium model*

From the results presented thus far, it is evident that the delay due to sorption kinetics is substantial during moisture transfer. Based on this narrative, it is vital to identify the conditions and operating parameters for which the effects of kinetics are minimal; thus, indicating when the solution with an equilibrium assumption is accurate to evaluate moisture transfer performance. In this regard, a dimensionless parameter (λ) can be defined as:

$$\lambda = \frac{m_{w,LDF}}{m_{w,equ}} \tag{3.30}$$

where $m_{w,LDF}$ represents the amount of water vapour adsorbed in the desiccant via kinetics assumption, and $m_{w,equ}$ represents the amount of water vapour adsorbed in the desiccant via equilibrium assumption.

The parameter (λ) shown in Equation (3.30) represents the accuracy of the equilibrium solution, where a value close to unity represents a scenario in which the sorption kinetics can be disregarded without any substantial errors. This parameter (λ) is also related to the effectiveness of FBRs, where a value of 0.95 means that the latent effectiveness will be reduced by 5% (relative) due to the sorption kinetics.

Figure 3.21 shows the effectiveness of the equilibrium assumption with respect to changes in kinetic rate constant, desiccant thickness and effective diffusion coefficient. It should be noted that the same coefficients (*i.e.,* 0.1, 0.5, 1, 5 and 10) were used for all 3 properties in the parametric study shown in Figure 3.21. In Figure 3.21(a), as would be expected, an increase in the kinetic rate constant of the desiccant results in an increase in the accuracy of the equilibrium model. This is because the equilibrium assumption of instantaneous moisture transfer becomes more accurate when the kinetic delay decreases (*i.e., $k \approx 1$*).

In Figure 3.21(b), it can be observed that the accuracy of the equilibrium solution increases as the desiccant thickness decreases. This phenomenon makes physical sense because when the desiccant coating becomes sufficiently thin, the ideal assumption which states that the desiccant's moisture content is in equilibrium with the air becomes more accurate. A similar occurrence was observed previously in Figure 3.20, where the moisture content and relative humidity profiles in the 1 mm thin coating were uniform and approximately equal to the kinetic model after 60 s. In Figure 3.21(c), it can be observed that an increase in the effective diffusion coefficient leads to an increase in accuracy of the equilibrium solution. This is because an increase in the moisture accumulation leads to an overall increase in the mass transfer, which makes the sorption kinetic delay negligible due to high water vapour accumulation in the desiccant.
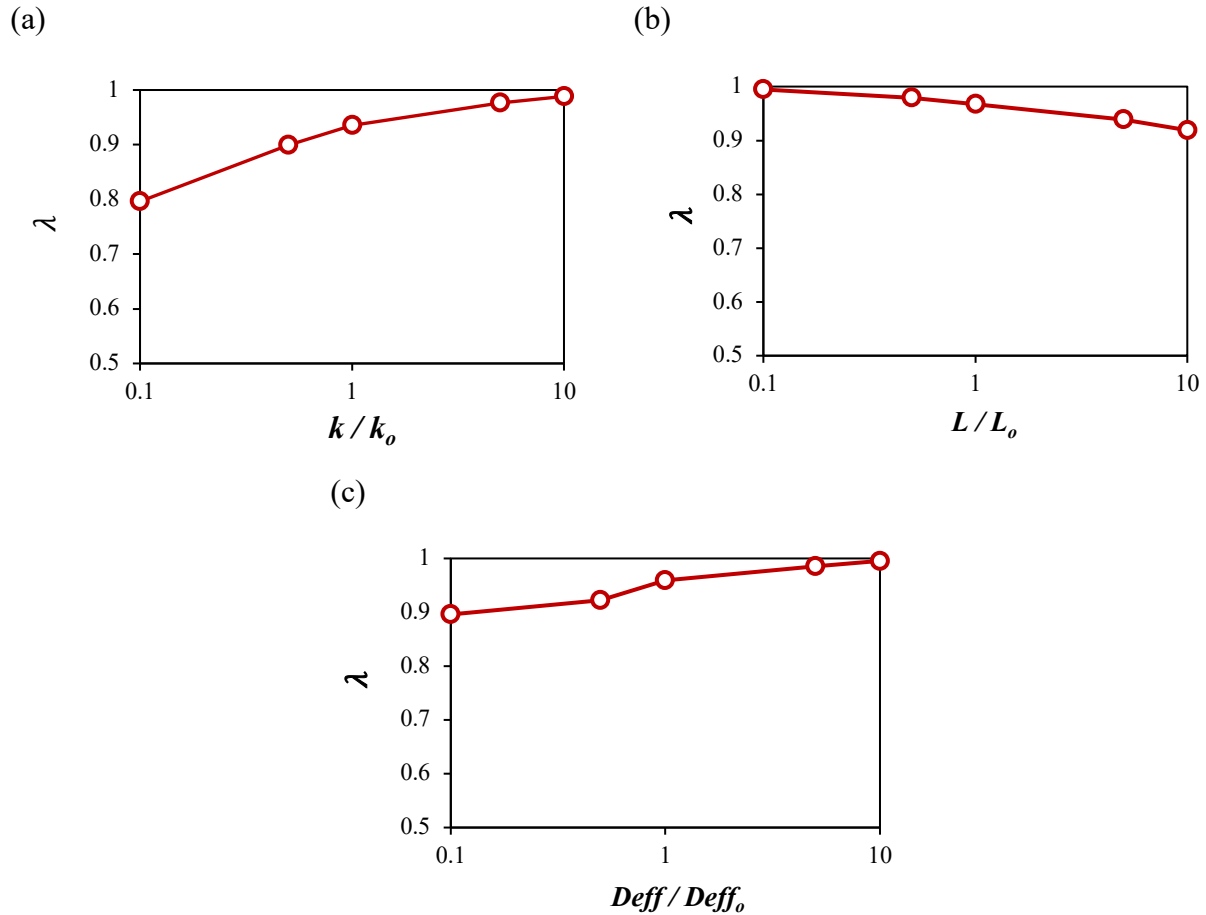
Figure 3.21. Parametric study on the accuracy of the equilibrium assumption due to changes in (a) kinetic rate constant (k), (b) thickness (L), and (c) effective diffusion coefficient (D_{eff}).

Previously, FBRs have shown good performance with a period of 60 s in several studies [15], [16], [77], [104], however, the effect of the sorption kinetic delay has not been studied with respect to FBR periods. Figure 3.22 shows a parametric study on the accuracy of the equilibrium model at different recovery periods. It can easily be observed that as the adsorption/desorption period increases, the effect of the sorption kinetics decreases. This indicates that the delay due to sorption kinetics is much more important during shorter recovery periods, and less significant at longer periods.
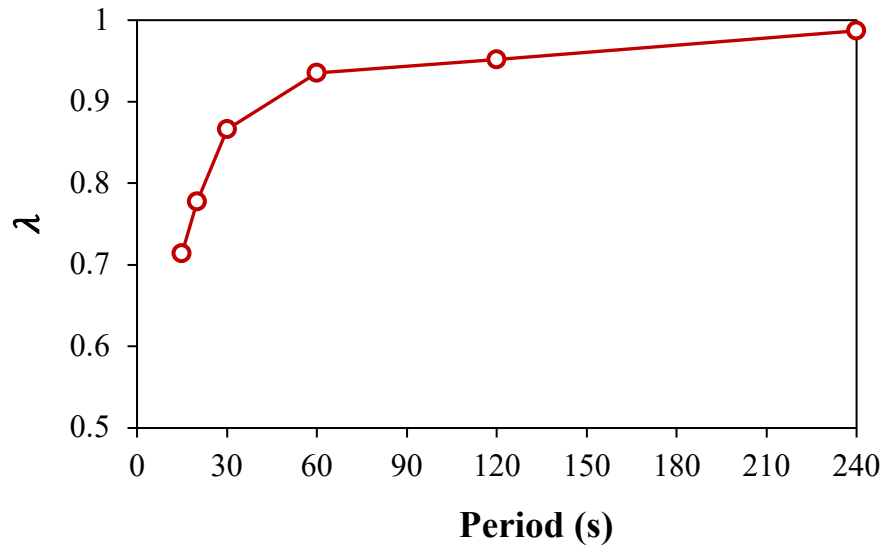
Figure 3.22. Parametric study on the effectiveness of equilibrium assumption due to changes in period at $k = 0.0014$ 1/s.

In order to provide recommendations to researchers and HVAC engineers for desiccant coated FBRs, a benchmark of 0.95 for λ is selected from Figures 3.21 and 3.22. This benchmark of 0.95 represents a 5% relative error for latent effectiveness when the equilibrium assumption is used. In this regard, desiccant parameters such as the rate constant, thickness, effective diffusion coefficient, and period should carefully be selected when using an equilibrium model. In quantifiable terms, the allowable benchmark ($\lambda = 0.95$) is achieved when the rate constant is at least equal to that of the tested silica gel (*i.e.*, $k = 0.0014$ 1/s), for thicknesses of less than 25 mm (*i.e.,* about 1.5 times greater than its original value), and an effective diffusion coefficient of at least 2.9×10^{-5} m^2/s (*i.e.,* about 1.5 times less than its original value). It can also be observed from Figure 3.22 that recovery periods of no less than 60 s should be used in an equilibrium model in order to achieve this benchmark. From the narrative thus far, it can be inferred that higher rate constants, thinner desiccants, higher diffusivities and longer recovery periods can reduce the errors when sorption kinetics is neglected.

3.8   SUMMARY AND CONCLUSIONS

In this chapter, a porous media numerical model was presented which solved the coupled heat and moisture transfer problem between a desiccant layer and an air stream. The results were presented for FBR applications with repeating cycles of adsorption/desorption, and the delay in moisture

transfer due to sorption kinetics was established and discussed. In addition, parametric studies showing the accuracy of the equilibrium model with respect to the kinetics assumption was also presented. The key conclusions from the model can be summarised as follows:

1. The parametric study on kinetics showed that the change in moisture content is higher when the rate constant is higher. As such, desiccants with higher rate constants should be selected for FBR applications as this indicates a higher moisture transfer rate for latent effectiveness.

2. Desiccant coatings with smaller particle sizes have better kinetic performances and higher moisture transfer rates. This shows that FBR coatings should be made with fine and uniform particles.

3. Sensitivity studies showed that the sorption isotherm and coating thickness have the greatest impact on the desiccant. In regard to this, FBRs should be coated in thin layers with desiccants of greater sorption uptakes.

4. In FBRs, the sorption kinetics must not be neglected when short periods (*i.e.,* < 60 s), thick coatings, and low diffusivities are applicable.

An important contribution from this chapter is the key insight which the results provide for HVAC engineers when designing desiccant coated FBRs. The results show that FBR performance can be improved by selecting desiccants with faster kinetics, thin desiccant coatings, and smaller particle sizes. In addition to this, HVAC designers can determine the operating periods and parameters where errors due to sorption kinetic delay are minimal. A benchmark of $\lambda = 0.95$ was established, which represents a 5% relative error in latent effectiveness when an equilibrium model (without sorption kinetics) is used. This benchmark was achieved for a rate constant of at least 0.0014 1/s, thicknesses of up to 25 mm, effective diffusion coefficient of at least 2.9×10^{-5} m^2/s, and cycle periods of at least 60 s.

CHAPTER 4

SUMMARY, CONCLUSIONS AND RECOMMENDATIONS

4.1   SUMMARY

The primary aim of this thesis was to develop a methodology to select desiccants for fixed-bed regenerator applications. In order to meet this objective, a thorough methodology involving both experimental and numerical methods were presented. Two major tasks were defined and carried out sequentially to complete the objective of this thesis. These tasks were to:

1. Measure the relevant properties (textural, sorption isotherm, sorption kinetics) of a few selected desiccants for FBR and determine their uncertainty.
2. Develop and verify a porous media numerical model to determine the heat and moisture transfer performance of a desiccant-coated layer for FBR applications.

Four desiccant samples were tested to measure their textural and sorption properties. The textural properties of all 4 samples had a direct influence on their sorption properties. The sorption properties were measured with a high reproducibility for a total of three experimental runs, with an uncertainty of less than 1% in all cases. In addition to the sorption isotherm, sorption kinetics was identified as an important desiccant property for FBRs given their short operating periods.

A numerical model was developed in this thesis to determine the heat and moisture transfer performance of a desiccant layer. The developed model was a one-dimensional porous media model based on the theories of local thermal equilibrium and local volume averaging. The goal of the model was to investigate conditions where an equilibrium model with the assumptions of instantaneous moisture transfer and uniform moisture content become invalid. In this regard, the model was adapted to incorporate sorption kinetics (delay in moisture transfer), which was measured in the experimental study and compared with the equilibrium model at different

conditions. The model was verified with analytical solutions and was used to determine performance when the desiccant was subjected to cyclical conditions similar to FBRs.

4.2 CONCLUSIONS

This thesis concluded that desiccants for FBRs should be selected based on properties such as: higher kinetic rate constants, smaller particle sizes, and higher sorption isotherm uptakes. The accuracy of the equilibrium model was investigated, and the results showed that an acceptable 5% error in the equilibrium model was achieved for a rate constant of at least 0.0014 1/s, thickness of up to 25 mm, effective diffusion coefficient of at least 2.9×10^{-5} m^2/s, and recovery periods of at least 60 s.

The experiments showed that desiccant textural properties affect their sorption performance. Higher surface areas were associated with greater sorption uptakes and larger pore sizes were associated with quicker kinetics. It was concluded that desiccants should be selected for FBRs based on their rate constant. The results also inferred that for an FBR exposed to cyclical conditions within a 60 s period, desiccants should be selected based on their kinetic performance over the 60 s period as opposed to their kinetic performance over longer periods such as an equilibrium process.

4.3 RECOMMENDATIONS FOR FUTURE WORK

The following areas are useful to investigate for future research:

1. Considering the global COVID-19 pandemic, contaminant transfer in energy exchangers during adsorption and desorption of water vapour molecules is of recent concern. In this regard, a numerical model should be developed to investigate the possibility of contaminant-free energy exchangers. Such a model would investigate the recommendations of using desiccants with pore sizes of 3 Angstroms (*i.e.,* size of a water vapour molecule) in order to avoid adsorption of contaminants into the desiccant pores.

2. A numerical model (incorporating the sorption kinetics) which includes heat transfer at the bottom of the desiccant into the FBR plates should be developed. This would give a more robust understanding into the performance of desiccant coated FBRs.

3. A numerical model investigating the possibility of frosting under extreme climatic conditions and desiccant durability should be developed. This is because in cold climates like Canada, FBRs may be subjected to extreme weather conditions for almost half of an entire year. As a result, frosting could play a major role in reducing performance.

4. Testing and synthesis of high performing desiccants such as composites, polymers and metal organic frameworks (MOFs) should be investigated for FBR applications. This is because improving the sorption properties of a desiccant would directly lead to higher moisture transfer rates and effectiveness.

5. A 3-dimensional numerical model should also be developed to understand desiccant performance in all spatial directions. Such a model will provide a better insight into the performance of desiccant coated FBRs.

REFERENCES

[1]   J. A. Leech, W. C. Nelson, R. T. Burnett, S. Aaron, and M. E. Raizenne, "It's about time: A comparison of Canadian and American time-activity patterns," *Journal of Exposure Analysis and Environmental Epidemiology*, vol. 12, no. 6, pp. 427–432, 2002, doi: 10.1038/sj.jea.7500244.

[2]   World Health organization, "WHO guidelines for air quality.," *Indian Pediatrics*, vol. 35, no. 8, pp. 812–815, 1998.

[3]   S. Liu, Q. Cao, X. Zhao, Z. Lu, and Z. Deng, "Improving indoor air quality and thermal comfort in residential kitchens with a new ventilation system," *Building and Environment*, vol. 180, no. May, p. 107016, 2020, doi: 10.1016/j.buildenv.2020.107016.

[4]   H. Ganesh, K. Seo, H. Fritz, T. Edgar, A. Novoselac, and M. Baldea, "Indoor air quality and energy management in buildings using combined moving horizon estimation and model predictive control," *Journal of Building Engineering*, p. 101552, 2020, doi: 10.1016/j.jobe.2020.101552.

[5]   H. Tsutsumi, S. ichi Tanabe, J. Harigaya, Y. Iguchi, and G. Nakamura, "Effect of humidity on human comfort and productivity after step changes from warm and humid environment," *Building and Environment*, vol. 42, no. 12, pp. 4034–4042, 2007, doi: 10.1016/j.buildenv.2006.06.037.

[6]   J. Zhao and X. Yang, "Photocatalytic oxidation for indoor air purification: A literature review," *Building and Environment*, vol. 38, no. 5, pp. 645–654, 2003, doi: 10.1016/S0360-1323(02)00212-3.

[7]   Statistics Canada, "Report on Energy Supply and Demand in Canada Catalogue no. 57-003-X," 2011. http://www5.statcan.gc.ca/bsolc/olc-cel/olc-cel?catno=57-003-XWE&lang=eng#formatdisp (accessed Aug. 05, 2021).

[8]   NRC, "Energy Efficiency Trends in Canada- 1990 to 2013," *Nrc*, no. March, pp. 1–51,

2016.

[9]   M. Isaac and D. P. van Vuuren, "Modeling global residential sector energy demand for heating and air conditioning in the context of climate change," *Energy Policy*, vol. 37, no. 2, pp. 507–521, 2009, doi: 10.1016/j.enpol.2008.09.051.

[10]   C. E. L. Nóbrega and N. C. L. Brum, "An analysis of the heat and mass transfer roles in air dehumidification by solid desiccants," *Energy and Buildings*, vol. 50, pp. 251–258, 2012, doi: 10.1016/j.enbuild.2012.03.049.

[11]   M. Rasouli, C. J. Simonson, and R. W. Besant, "Applicability and optimum control strategy of energy recovery ventilators in different climatic conditions," *Energy and Buildings*, vol. 42, no. 9, pp. 1376–1385, 2010, doi: 10.1016/j.enbuild.2010.03.006.

[12]   P. Vivekh, M. Kumja, D. T. Bui, and K. J. Chua, "Recent developments in solid desiccant coated heat exchangers – A review," *Applied Energy*, vol. 229, no. April, pp. 778–803, 2018, doi: 10.1016/j.apenergy.2018.08.041.

[13]   CSA Group, "CAN/CSA-439-18: Labaoratory standards of test for rating the performance of heat/energy recovery ventilators," 2018. www.csagroup.org/legal (accessed Jun. 05, 2021).

[14]   C. M. Yang, C. C. Chen, and S. L. Chen, "Energy-efficient air conditioning system with combination of radiant cooling and periodic total heat exchanger," *Energy*, vol. 59, pp. 467–477, 2013, doi: 10.1016/j.energy.2013.07.015.

[15]   H. Ramin, E. N. Krishnan, and C. J. Simonson, "Effectiveness of fixed-bed regenerators for energy recovery in buildings applications," *E3S Web of Conferences*, vol. 172, pp. 1–8, 2020, doi: 10.1051/e3sconf/202017209001.

[16]   E. N. Krishnan, H. Ramin, M. Shakouri, L. D. Wilson, and C. J. Simonson, "Development of a small-scale test facility for effectiveness evaluation of fixed-bed regenerators," *Applied Thermal Engineering*, vol. 174, no. December 2019, p. 115263, 2020, doi:

10.1016/j.applthermaleng.2020.115263.

[17]   R. P. Singh, V. K. Mishra, and R. K. Das, "Desiccant materials for air conditioning applications - A review," *IOP Conference Series: Materials Science and Engineering*, vol. 404, no. 1, 2018, doi: 10.1088/1757-899X/404/1/012005.

[18]   X. Li, Z. Li, Q. Xia, and H. Xi, "Effects of pore sizes of porous silica gels on desorption activation energy of water vapour," *Applied Thermal Engineering*, vol. 27, no. 5–6, pp. 869–876, 2007, doi: 10.1016/j.applthermaleng.2006.09.010.

[19]   Y. An, Q. Fu, D. Zhang, Y. Wang, and Z. Tang, "Performance evaluation of activated carbon with different pore sizes and functional groups for VOC adsorption by molecular simulation," *Chemosphere*, vol. 227, pp. 9–16, 2019, doi: 10.1016/j.chemosphere.2019.04.011.

[20]   I. Langmuir, "The adsorption of gases on plane surfaces of glass, mica and platinum," *Journal of the American Chemical Society*, vol. 40, no. 9, pp. 1361–1403, 1918, doi: 10.1021/ja02242a004.

[21]   S. Brunauer, P. H. Emmett, and E. Teller, "Adsorption of gases in multi-molecular layers," *Journal of the American Chemical Society*, vol. 60, no. 2, pp. 309–319, 1938, doi: 10.1021/ja01269a023.

[22]   K. S. W. Sing, D. H. Everett, R. A. W. Haul, and L. Moscou, "Reporting physisorption data for gas/solid systems with special reference to the determination of surface area and porosity," *Pure and Applied Chemistry*, vol. 57, no. 4, pp. 603–619, 1985, doi: 10.1351/pac198557040603.

[23]   F. Lou, A. Zhang, G. Zhang, L. Ren, X. Guo, and C. Song, "Enhanced kinetics for CO2 sorption in amine-functionalized mesoporous silica nanosphere with inverted cone-shaped pore structure," *Applied Energy*, vol. 264, no. February, p. 114637, 2020, doi: 10.1016/j.apenergy.2020.114637.

[24] M. Thommes, K. Kaneko, A. V. Neimark, J. P. Olivier, and F. Rodriguez-Reinoso, "Physisorption of gases, with special reference to the evaluation of surface area and pore size distribution (IUPAC Technical Report)," *Pure and Applied Chemistry*, vol. 87, no. 9–10, pp. 1051–1069, 2015, doi: 10.1515/pac-2014-1117.

[25] X. Zheng, T. S. Ge, and R. Z. Wang, "Recent progress on desiccant materials for solid desiccant cooling systems," *Energy*, vol. 74, no. 1, pp. 280–294, 2014, doi: 10.1016/j.energy.2014.07.027.

[26] M. Sultan, I. I. El-Sharkawy, T. Miyazaki, B. B. Saha, and S. Koyama, "An overview of solid desiccant dehumidification and air conditioning systems," *Renewable and Sustainable Energy Reviews*, vol. 46, pp. 16–29, 2015, doi: 10.1016/j.rser.2015.02.038.

[27] X. Zheng, T. S. Ge, R. Z. Wang, and L. M. Hu, "Performance study of composite silica gels with different pore sizes and different impregnating hygroscopic salts," *Chemical Engineering Science*, vol. 120, pp. 1–9, 2014, doi: 10.1016/j.ces.2014.08.047.

[28] I. Petrov and T. Michalev, "Synthesis of Zeolite A: A Review," *Proceedings - Chemical Technologies*, no. 51, Book 9.1, pp. 30–35, 2012, [Online]. Available: http://conf.uni-ruse.bg/bg/docs/cp12/9.1/9.1-5.pdf.

[29] C. H. Chen, P. C. Huang, T. H. Yang, Y. C. Chiang, and S. L. Chen, "Polymer/alumina composite desiccant combined with periodic total heat exchangers for air-conditioning systems," *International Journal of Refrigeration*, vol. 67, no. 1, pp. 10–21, 2016, doi: 10.1016/j.ijrefrig.2016.01.003.

[30] N. Hanikel, M. S. Prévot, F. Fathieh, E. A. Kapustin, and H. Lyu, "Rapid cycling and exceptional yield in a metal-organic framework water harvester," *ACS Central Science*, vol. 5, no. 10, pp. 1699–1706, 2019, doi: 10.1021/acscentsci.9b00745.

[31] S. Cui, M. Qin, A. Marandi, V. Steggles, and S. Wang, "Metal-Organic Frameworks as advanced moisture sorbents for energy-efficient high temperature cooling," *Scientific Reports*, vol. 8, no. 1, pp. 2–10, 2018, doi: 10.1038/s41598-018-33704-4.

[32] C. Chen, C. Hsu, C. Chen, and S. Chen, "Silica gel polymer composite desiccants for air conditioning systems," *Energy & Buildings*, vol. 101, pp. 122–132, 2015, doi: 10.1016/j.enbuild.2015.05.009.

[33] I. Girnik, T. Yang, L. Gordeeva, W. Wang, T. Ge, and Y. Aristov, "New adsorption method for moisture and heat exchange in ventilation systems in cold countries: Concept and mathematical simulation," *Energies*, vol. 16, no. 3, 2020, doi: 10.3390/en13061386.

[34] L. F. Leonardo Betiol, R. R. Evangelista, M. A. Ribeiro Sanches, and R. C. Basso, "Influence of temperature and chemical composition on water sorption isotherms for dry-cured ham," *LWT - Food Science and Technology*, vol. 123, no. October 2019, 2020, doi: 10.1016/j.lwt.2020.109112.

[35] K. C. Chan, C. Y. H. Chao, G. N. Sze-To, and K. S. Hui, "Performance predictions for a new zeolite 13X/CaCl 2 composite adsorbent for adsorption cooling systems," *International Journal of Heat and Mass Transfer*, vol. 55, no. 11–12, pp. 3214–3224, 2012, doi: 10.1016/j.ijheatmasstransfer.2012.02.054.

[36] X. Zheng, R. Z. Wang, T. S. Ge, and L. M. Hu, "Performance study of SAPO-34 and FAPO-34 desiccants for desiccant coated heat exchanger systems," *Energy*, vol. 93, pp. 88–94, 2015, doi: 10.1016/j.energy.2015.09.024.

[37] D. B. Jani, M. Mishra, and P. K. Sahoo, "Solid desiccant air conditioning - A state of the art review," *Renewable and Sustainable Energy Reviews*, vol. 60, pp. 1451–1469, 2016, doi: 10.1016/j.rser.2016.03.031.

[38] T. S. Ge, Y. Li, R. Z. Wang, and Y. J. Dai, "A review of the mathematical models for predicting rotary desiccant wheel," *Renewable and Sustainable Energy Reviews*, vol. 12, no. 6, pp. 1485–1528, 2008, doi: 10.1016/j.rser.2007.01.012.

[39] C. R. Ruivo, J. J. Costa, and A. R. Figueiredo, "Validity of pseudo-gas-side-controlled models to predict the behaviour of desiccant matrices," *International Journal of Thermal Sciences*, vol. 48, no. 11, pp. 2171–2178, 2009, doi: 10.1016/j.ijthermalsci.2009.04.004.

[40] C. J. Simonson and R. W. Besant, "Heat and moisture transfer in desiccant coated rotary energy exchangers: Part I. numerical model," *HVAC and R Research*, vol. 3, no. 4, pp. 325–350, 1997, doi: 10.1080/10789669.1997.10391381.

[41] E. Cerrah, "Sorbent based enthalpy recovery ventilator (SERV) in northern building applications," *M.Sc Thesis, Simon Fraser University*, 2019.

[42] G. Klein, "Principles of adsorption and adsorption processes," *Reactive Polymers, Ion Exchangers, Sorbents*, vol. 4, no. 1. p. 62, 1985, doi: 10.1016/0167-6989(85)90037-6.

[43] D. D. Do, "Fundamentals of Diffusion and Adsorption in Porous Media," vol. 2, pp. 337–414, 1998, doi: 10.1142/9781860943829_0007.

[44] A. H. Karoyo, L. Dehabadi, W. Alabi, C. J. Simonson, and L. D. Wilson, "Hydration and sorption properties of raw and milled flax fibers," *ACS Omega*, vol. 5, no. 11, pp. 6113–6121, 2020, doi: 10.1021/acsomega.0c00100.

[45] W. M. Miller, "Energy storage via desiccants for food/agricultural applications," *Energy in Agriculture*, vol. 2, no. C, pp. 341–354, 1983, doi: 10.1016/0167-5826(83)90029-3.

[46] R. D. P. Andrade, L. M. Roberto, and C. E. C. Pérez, "Models of sorption isotherms for food: Uses and limitations," *Vitae*, vol. 18, no. 3, pp. 325–334, 2011.

[47] S. Diblan, B. Gökkaya Erdem, and S. Kaya, "Sorption, diffusivity, permeability and mechanical properties of chitosan, potassium sorbate, or nisin incorporated active polymer films," *Journal of Food Science and Technology*, vol. 57, no. 10, pp. 3708–3719, 2020, doi: 10.1007/s13197-020-04403-8.

[48] W. Won, S. Lee, and K. S. Lee, "Modeling and parameter estimation for a fixed-bed adsorption process for CO 2 capture using zeolite 13X," *Separation and Purification Technology*, vol. 85, pp. 120–129, 2012, doi: 10.1016/j.seppur.2011.09.056.

[49] D. Park, S. H. Hong, K. M. Kim, and C. H. Lee, "Adsorption equilibria and kinetics of silica gel for N2O, O2, N2, and CO2," *Separation and Purification Technology*, vol. 251, no.

March, p. 117326, 2020, doi: 10.1016/j.seppur.2020.117326.

[50]   Y. Bruinen De Bruin, K. Koistinen, S. Kephalopoulos, O. Geiss, S. Tirendi, and D. Kotzias, "Characterisation of urban inhalation exposures to benzene, formaldehyde and acetaldehyde in the European Union: Comparison of measured and modelled exposure data," *Environmental Science and Pollution Research*, vol. 15, no. 5, pp. 417–430, 2008, doi: 10.1007/s11356-008-0013-4.

[51]   M. Das, J. D. Perry, and W. J. Koros, "Effect of processing on carbon molecular sieve structure and performance," *Carbon*, vol. 48, no. 13, pp. 3737–3749, 2010, doi: 10.1016/j.carbon.2010.06.036.

[52]   B. O. Adebayo, S. Lawson, A. A. Rownaghi, and F. Rezaei, "Analysis of equilibrium and dynamic adsorption of benzene vapor over unimodal and bimodal silica-based mixed-metal oxides," *Chemical Engineering Journal*, vol. 396, no. April, p. 125273, 2020, doi: 10.1016/j.cej.2020.125273.

[53]   T. R. Ahammad, S. Z.; Gomes, J.; Sreekrishnan, "Waste water treatment for production of H2S - free biogas," *Journal of Chemical Technology & Biotechnology*, vol. 83, no. May, pp. 1163–1169, 2008, doi: 10.1002/jctb.

[54]   C. J. Simonson and R. W. Besant, "Heat and moisture transfer in energy wheels during sorption, condensation, and frosting conditions," *Journal of Heat Transfer*, vol. 120, no. 3, pp. 699–708, 1998, doi: 10.1115/1.2824339.

[55]   C. J. Simonson and R. W. Besant, "Energy wheel effectiveness: Part II - correlations," *International Journal of Heat and Mass Transfer*, vol. 42, no. 12, pp. 2171–2185, 1999, doi: 10.1016/S0017-9310(98)00327-5.

[56]   F. Fathieh, M. Nezakat, R. W. Evitts, and C. J. Simonson, "Effects of physical and sorption properties of desiccant coating on performance of energy wheels," *Journal of Heat Transfer*, vol. 139, no. 6, pp. 1–14, 2017, doi: 10.1115/1.4035650.

[57] W. O. Alabi, A. H. Karoyo, E. N. Krishnan, L. Dehabadi, L. D. Wilson, and C. J. Simonson, "Comparison of the moisture adsorption properties of starch particles and flax fiber coatings for energy wheel applications," *ACS Omega*, 2020, doi: 10.1021/acsomega.0c00762.

[58] N. Agarwal, C. S. Meena, B. P. Raj, L. Saini, and A. Kumar, "Indoor air quality improvement in COVID-19 pandemic: Review," *Sustainable Cities and Society*, vol. 70, no. December 2020, p. 102942, 2021, doi: 10.1016/j.scs.2021.102942.

[59] P. O. Fanger, "What is IAQ?," *Indoor Air*, vol. 16, no. 5, pp. 328–334, 2006, doi: 10.1111/j.1600-0668.2006.00437.x.

[60] W. Zheng, J. Hu, Z. Wang, J. Li, and J. Yan, "COVID-19 impact on operation and energy consumption of heating, ventilation and air-conditioning (HVAC) systems," *Advances in Applied Energy*, vol. 3, no. March, p. 100040, 2021, doi: 10.1016/j.adapen.2021.100040.

[61] A. M. Elsaid and M. S. Ahmed, "Indoor air quality strategies for air-conditioning and ventilation systems with the spread of the global coronavirus (COVID-19) epidemic: Improvements and recommendations," *Environmental Research*, vol. 199, no. May, p. 111314, 2021, doi: 10.1016/j.envres.2021.111314.

[62] C. J. Simonson and R. W. Besant, "Energy wheel effectiveness: Part I - development of dimensionless groups," *International Journal of Heat and Mass Transfer*, vol. 42, no. 12, pp. 2161–2170, 1999, doi: 10.1016/S0017-9310(98)00325-1.

[63] C. J. Simonson and R. W. Besant, "Heat and moisture transfer in desiccant coated rotary energy exchangers: Part II. validation and sensitivity studies," *HVAC and R Research*, vol. 3, no. 4, pp. 351–368, 1997, doi: 10.1080/10789669.1997.10391382.

[64] J. D. Chung, D. Y. Lee, and S. M. Yoon, "Optimization of desiccant wheel speed and area ratio of regeneration to dehumidification as a function of regeneration temperature," *Solar Energy*, vol. 83, no. 5, pp. 625–635, 2009, doi: 10.1016/j.solener.2008.10.011.

[65] C. C. Chang, J. De Liang, and S. L. Chen, "Performance investigation of regenerative total

heat exchanger with periodic flow," *Applied Thermal Engineering*, vol. 130, pp. 1319–1327, 2018, doi: 10.1016/j.applthermaleng.2017.11.024.

[66] Micromeritics, "ASAP 2020 Operator's Manual," *Micromeritics*, vol. 4, pp. 1–458, 2006.

[67] M. Kudasik, "The manometric sorptomat - An innovative volumetric instrument for sorption measurements performed under isobaric conditions," *Measurement Science and Technology*, vol. 27, no. 3, 2016, doi: 10.1088/0957-0233/27/3/035903.

[68] M. Hävecker, S. Wrabetz, J. Kröhnert, L. I. Csepei, and R. Naumann D'Alnoncourt, "Surface chemistry of phase - pure M1 MoVTeNb oxide during operation in selective oxidation of propane to acrylic acid," *Journal of Catalysis*, vol. 285, no. 1, pp. 48–60, 2012, doi: 10.1016/j.jcat.2011.09.012.

[69] E. P. Barrett, L. G. Joyner, and P. P. Halenda, "The determination of pore volume and area distributions in porous substances," *Journal of the American Chemical Society*, vol. 73, no. 1, pp. 373–380, Jan. 1951, doi: 10.1021/ja01145a126.

[70] S. Storck, H. Bretinger, and W. F. Maier, "Characterization of micro- and mesoporous solids by physisorption methods and pore-size analysis," *Applied Catalysis A: General*, vol. 174, no. 1–2, pp. 137–146, 1998, doi: 10.1016/S0926-860X(98)00164-1.

[71] E. Glueckauf, "Theory of chromatography. Part 10.—Formulæ for diffusion into spheres and their application to chromatography," *Transactions of the Faraday Society*, vol. 51, no. 0, pp. 1540–1551, 1955, doi: 10.1039/TF9555101540.

[72] I. I. El-Sharkawy, "On the linear driving force approximation for adsorption cooling applications," *International Journal of Refrigeration*, vol. 34, no. 3, pp. 667–673, 2011, doi: 10.1016/j.ijrefrig.2010.12.006.

[73] H. Liu and K. Nagano, "Numerical simulation of an open sorption thermal energy storage system using composite sorbents built into a honeycomb structure," *International Journal of Heat and Mass Transfer*, vol. 78, pp. 648–661, 2014, doi:

10.1016/j.ijheatmasstransfer.2014.07.034.

[74]   R. Chauveau, G. Grévillot, S. Marsteau, and C. Vallières, "Values of the mass transfer coefficient of the linear driving force model for VOC adsorption on activated carbons," *Chemical Engineering Research and Design*, vol. 91, no. 5, pp. 955–962, 2013, doi: 10.1016/j.cherd.2012.09.019.

[75]   S. Jribi, T. Miyazaki, B. B. Saha, S. Koyama, and A. Maalej, "Equilibrium and kinetics of CO2 adsorption onto activated carbon," *International Journal of Heat and Mass Transfer*, vol. 108, pp. 1941–1946, 2017, doi: 10.1016/j.ijheatmasstransfer.2016.12.114.

[76]   Z. Li and R. T. Yang, "Concentration profile for linear driving force model for diffusion in a particle," *AIChE Journal*, vol. 45, no. 1, pp. 196–200, 1999, doi: 10.1002/aic.690450118.

[77]   E. N. Krishnan, H. Ramin, A. Gurubalan, and C. J. Simonson, "Experimental methods to determine the performance of desiccant coated fixed-bed regenerators (FBRs)," *International Journal of Heat and Mass Transfer*, vol. 182, p. 121909, 2022, doi: 10.1016/j.ijheatmasstransfer.2021.121909.

[78]   T. Higashi, M. Yamaguchi, N. Nakagawa, C. Dang, and E. Hihara, "Gravimetric method for sorption performance measurement of desiccant wheel and desiccant coated heat exchanger," *Applied Thermal Engineering*, vol. 144, no. May, pp. 639–646, 2018, doi: 10.1016/j.applthermaleng.2018.05.079.

[79]   M. Kudasik, "Results of comparative sorption studies of the coal-methane system carried out by means of an original volumetric device and a reference gravimetric instrument," *Adsorption*, vol. 23, no. 4, pp. 613–626, 2017, doi: 10.1007/s10450-017-9881-6.

[80]   C. J. Webb and E. M. Gray, "Analysis of uncertainties in gas uptake measurements using the gravimetric method," *International Journal of Hydrogen Energy*, vol. 39, no. 13, pp. 7158–7164, 2014, doi: 10.1016/j.ijhydene.2014.02.154.

[81]   Y. Gensterblum, P. van Hemert, P. Billemont, A. Busch, and D. Charriére, "European inter-

laboratory comparison of high pressure CO2 sorption isotherms. I: Activated carbon," *Carbon*, vol. 47, no. 13, pp. 2958–2969, 2009, doi: 10.1016/j.carbon.2009.06.046.

[82] Y. Gensterblum, P. van Hemert, P. Billemont, E. Battistutta, and A. Busch, "European inter-laboratory comparison of high pressure CO2 sorption isotherms II: Natural coals," *International Journal of Coal Geology*, vol. 84, no. 2, pp. 115–124, 2010, doi: 10.1016/j.coal.2010.08.013.

[83] K. E. Hurst, T. Gennett, J. Adams, M. D. Allendorf, and R. Balderas-Xicohténcatl, "An international laboratory comparison study of volumetric and gravimetric hydrogen adsorption measurements," *ChemPhysChem*, vol. 20, no. 15, pp. 1997–2009, 2019, doi: 10.1002/cphc.201900166.

[84] F. Fathieh, "A novel transient testing method for heat/energy wheel components," *PhD Thesis, University of Saskatchewan*, no. July, 2016, [Online]. Available: https://harvest.usask.ca/bitstream/handle/10388/7381/FATHIEH-DISSERTATION-2016.pdf?sequence=1&isAllowed=y.

[85] P. Talukdar, S. O. Olutmayin, O. F. Osanyintola, and C. J. Simonson, "An experimental data set for benchmarking 1-D, transient heat and moisture transfer models of hygroscopic building materials. Part I: Experimental facility and material property data," *International Journal of Heat and Mass Transfer*, vol. 50, no. 23–24, pp. 4527–4539, 2007, doi: 10.1016/j.ijheatmasstransfer.2007.03.026.

[86] H. Isochema, "IGA systems user manual," vol. 44, pp. 1–347, 2007.

[87] R. B. Abernethy, R. P. Benedict, and R. B. Dowdell, "Asme measurement uncertainty.," *American Society of Mechanical Engineers (Paper)*, vol. 107, no. 83, 1983.

[88] Joint Committee For Guides In Measurements, "Evaluation of measurement data — Guide to the expression of uncertainty in measurement," *International Organization for Standardization Geneva ISBN*, vol. 50, no. September, p. 134, 2008, [Online]. Available: http://www.bipm.org/en/publications/guides/gum.html.

[89]   C. X. Jia, Y. J. Dai, J. Y. Wu, and R. Z. Wang, "Experimental comparison of two honeycombed desiccant wheels fabricated with silica gel and composite desiccant material," *Energy Conversion and Management*, vol. 47, no. 15–16, pp. 2523–2534, 2006, doi: 10.1016/j.enconman.2005.10.034.

[90]   A. Li, K. Thu, A. Bin Ismail, M. W. Shahzad, and K. C. Ng, "Performance of adsorbent-embedded heat exchangers using binder-coating method," *International Journal of Heat and Mass Transfer*, vol. 92, pp. 149–157, 2016, doi: 10.1016/j.ijheatmasstransfer.2015.08.097.

[91]   L. Pino, Y. Aristov, G. Cacciola, and G. Restuccia, "Composite materials based on zeolite 4A for adsorption heat pumps," *Adsorption*, vol. 3, no. 1, pp. 33–40, 1997, doi: 10.1007/BF01133005.

[92]   P. Vivekh, M. Kumja, D. T. Bui, and K. J. Chua, "Recent developments in solid desiccant coated heat exchangers – A review," *Applied Energy*, vol. 229, no. April, pp. 778–803, 2018, doi: 10.1016/j.apenergy.2018.08.041.

[93]   Y. S. Bae and C. H. Lee, "Sorption kinetics of eight gases on a carbon molecular sieve at elevated pressure," *Carbon*, vol. 43, no. 1, pp. 95–107, 2005, doi: 10.1016/j.carbon.2004.08.026.

[94]   United Nations, "Sustainable development goals | United Nations (UN) development programme." 2015, [Online]. Available: https://www.undp.org/sustainable-development-goals.

[95]   L. Pérez-Lombard, J. Ortiz, and C. Pout, "A review on buildings energy consumption information," *Energy and Buildings*, vol. 40, no. 3, pp. 394–398, 2008, doi: 10.1016/j.enbuild.2007.03.007.

[96]   National Research Council, "National Energy Code of Canada for Buildings," *Canadian Commission on Building and Fire Codes*. 2017, [Online]. Available: https://nrc.canada.ca/en/certifications-evaluations-standards/codes-canada/codes-canada-

publications/national-energy-code-canada-buildings-2017.

[97] M. Fauchoux, "The effect of energy recovery on indoor climate, air quality and energy consumption using computer simulations," *M.Sc Thesis, University of Saskatchewan*, pp. 1–154, 2006, [Online]. Available: http://ecommons.usask.ca/xmlui/bitstream/handle/10388/etd-06222006-162448/Thesis_Melanie_Fauchoux.pdf?sequence=1.

[98] S. O. Olutimayin and C. J. Simonson, "Measuring and modeling vapor boundary layer growth during transient diffusion heat and moisture transfer in cellulose insulation," *International Journal of Heat and Mass Transfer*, vol. 48, no. 16, pp. 3319–3330, 2005, doi: 10.1016/j.ijheatmasstransfer.2005.02.024.

[99] M. R. Manila, S. Mitra, and P. Dutta, "Studies on dynamics of two-stage air cooled water/silica gel adsorption system," *Applied Thermal Engineering*, vol. 178, no. May, p. 115552, 2020, doi: 10.1016/j.applthermaleng.2020.115552.

[100] L. Liu, Y. Bai, Z. He, and L. Deng, "Numerical investigation of mass transfer characteristics for the desiccant-coated dehumidification wheel in a dehumidification process," *Applied Thermal Engineering*, vol. 160, no. November 2018, p. 113944, 2019, doi: 10.1016/j.applthermaleng.2019.113944.

[101] A. Chakraborty, B. B. Saha, and Y. I. Aristov, "Dynamic behaviors of adsorption chiller: Effects of the silica gel grain size and layers," *Energy*, vol. 78, no. 3, pp. 304–312, 2014, doi: 10.1016/j.energy.2014.10.015.

[102] ASHRAE, "ASHRAE fundamentals (SI)," *ASHRAE fundamental handbook*, pp. 7.10, 11.11, 2017.

[103] F. Incropera, D. Dewitt, T. Bergman, and A. Lavine, "Fundamentals of heat and mass transfer," *Fluid Mechanics and its Applications*, vol. 112, pp. 321–338, 2015, doi: 10.1007/978-3-319-15793-1_19.

[104] H. Ramin, E. Krishnan, and C. J. Simonson, "Fixed bed regenerators for HVAC applications," *Proceedings - CANCAM*, vol. 23, no. 1, pp. 1–4, 2019, doi: 10.3390/proceedings2019023004.

[105] M. Kaviany, "Principles of Heat Transfer in Porous Media," *Mechanical Engineering Series*, vol. 53, no. 9, pp. 1–726, 1995, [Online]. Available: http://www.springerlink.com/index/10.1007/978-1-4612-4254-3.

[106] S. Whitaker, "Volume averaging of transport equations," *Advances in Fluid Mechanics*, vol. 13, pp. 1–60, 1997.

APPENDIX A

UNCERTAINTY ANALYSIS OF THE IGA-002 INSTRUMENT

The uncertainty of the IGA-002 instrument for water vapour sorption measurements was not specified by the manufacturer. However, given that the instrument measures the amount of adsorbed water vapour at any given time via an increase in sample mass, the equation for water vapour adsorption can thus be expressed by [79]:

$$\beta_{IGA} = \frac{P_s \cdot V_m}{z \cdot R \cdot T} \cdot \frac{((m_t - m_o) + F_B)}{m_o \cdot \rho} \tag{A.1}$$

where F_B represents the corrections in the measurement due to buoyant forces, z is the compressibility factor, and V_m is the molar volume.

However, the major uncertainty contribution in the IGA-002 is the buoyant force compensation (F_B). The equation is expressed by:

$$F_B = \frac{m_o \cdot P \cdot M}{\rho_s \cdot z \cdot R \cdot T}, \tag{A.2}$$

Thus, using uncertainty propagation rule:

$$u(F_B) = F_B \cdot \sqrt{\left(\frac{u(m)}{m}\right)^2 + \left(\frac{u(P)}{P}\right)^2 + \left(\frac{u(\rho_s)}{\rho_s}\right)^2 + \left(\frac{u(T)}{T}\right)^2} \tag{A.3}$$

However, considering that the resolution of the IGA-002 microbalance is 0.1 µg in the measurement range 0 – 200 mg, the uncertainty in mass measurements can be neglected in relation to the other parameters.

As such, the IGA-002 uncertainty becomes:

$$\gamma_{IGA} = u(F_B) = \frac{m_o \cdot p \cdot M}{\rho_s \cdot R \cdot T} \cdot \sqrt{\left(\frac{u(P)}{P}\right)^2 + \left(\frac{u(\rho_s)}{\rho_s}\right)^2 + \left(\frac{u(T)}{T}\right)^2} \tag{A.4}$$

APPENDIX B

LOCAL VOLUME AVERAGING AND LOCAL THERMAL EQUILIBRIUM

TECHNIQUES

This appendix section presents the methods of local volume averaging and local thermal equilibrium, which were used to model the porous desiccant in Chapter 3. These methods provide useful and physically realistic approximations to define the solid-fluid interfacial boundary area in a porous media [105]. Thus, eliminating the complexity of solving the heat and moisture transfer equations for both solid and fluid phases simultaneously.

In local volume averaging (LVA), the assumption requires selecting a representative elementary volume (REV) which would result in statistically meaningful averaged properties [106]. This REV is such that it represents the smallest differential volume which describes all local volume averaged properties. In simpler terms, it is the smallest representation of the porous media, by which increasing its volume does not change the local averaged properties. Figure B.1 shows a porous desiccant and its representative elementary volume.
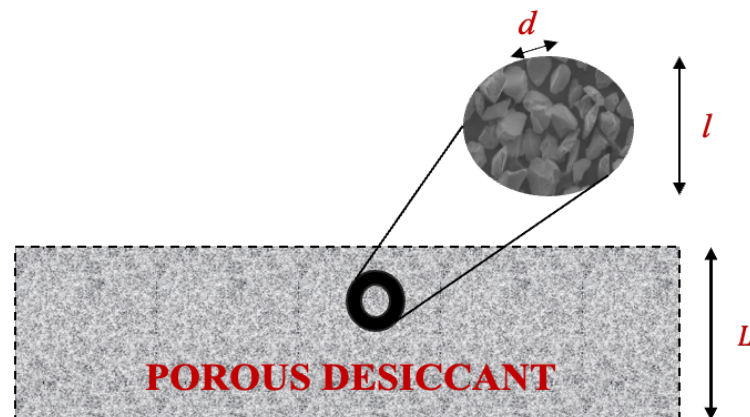
Figure B. 1. Schematic of a porous desiccant and its representative elementary volume.

In order to the implement the LVA method in the porous media model, the condition in Equation (B.1) must be satisfied. As observed from Figure B.1, it can easily be seen that the condition is satisfied given that the diameter (d) of the desiccant particle is much smaller than the representative characteristic length (l), which in turn is much smaller than the thickness (L) of the desiccant layer.

$$d < l \ll L \qquad\qquad\qquad (B.1).$$

On the other hand, the local thermal equilibrium (LTE) technique is of the assumption that the temperature difference across the established length scales satisfies the condition in Equation (B.2) [105]. Given that the temperature values in the numerical model satisfied Equation (B.2), one energy equation was used to represent both the solid and fluid phases as seen in Chapter 3.

$$\Delta T_d < \Delta T_l \ll \Delta T_L \qquad\qquad\qquad (B.2).$$

APPENDIX C

DISCRETIZED EQUATIONS AND COMPUTER SIMULATION PROGRAM

This appendix section contains the discretized equations for the porous media numerical model presented in Chapter 3. Furthermore, the computer simulation program used to solve the porous media model is also presented in this appendix. The computer program was written in MATLAB R2020b.

C.1   DISCRETIZED EQUATIONS

The discretized equations used in the porous media model are presented in this sub-section. It should be noted that symbols i and n represent the spatial node and time step respectively. The central difference scheme was used for the spatial nodes in the desiccant and the fully implicit scheme was used for the time derivative. In addition, the forward and backward difference schemes were used for the top and bottom boundaries respectively. The discretized equations are presented as follows:

Energy transport equation:

$$
\begin{aligned}
(\rho(i,n)c_p(i,n))_{eff} \cdot & \frac{T(i,n) - T(i,n-1)}{\Delta t} - \dot{m}(i,n) \cdot h_{fg} \\
&= \left(\frac{k_{eff}(i+1,n) - k_{eff}(i-1,n)}{2\Delta x} \right) \cdot \left(\frac{T(i+1,n) - T(i-1,n)}{2\Delta x} \right) \\
&+ \left(k_{eff}(i,n) \cdot \frac{T(i+1,n) - 2T(i,n) + T(i-1,n)}{\Delta x^2} \right)
\end{aligned}
\tag{C.1}
$$

Water vapour diffusion equation:

$$\rho_v(i,n)\frac{\varepsilon_g(i,n) - \varepsilon_g(i,n-1)}{\Delta t} + \varepsilon_g(i,n)\frac{\rho_v(i,n) - \rho_v(i,n-1)}{\Delta t} + \dot{m}(i,n) \tag{C.2}$$

$$= \left(\frac{D_{eff}(i+1,n) - D_{eff}(i-1,n)}{2\Delta x}\right)$$

$$\cdot \left(\frac{\rho_v(i+1,n) - \rho_v(i-1,n)}{2\Delta x}\right)$$

$$+ \left(D_{eff}(i,n) \cdot \frac{\rho_v(i+1,n) - 2\rho_v(i,n) + \rho_v(i-1,n)}{\Delta x^2}\right)$$

where

$$D_{eff} = \frac{\varepsilon_g(i,n) \cdot D_{AB}}{\tau} \tag{C.3}$$

Continuity equation:

$$\frac{\dot{m}(i,n)}{\rho_l} = \frac{\varepsilon_l(i,n) - \varepsilon_l(i,n-1)}{\Delta t} \tag{C.4}$$

Phase change rate equation:

$$\dot{m}(i,n) = \frac{u_t(i,n) - u_t(i,n-1)}{\Delta t}\rho_{eff,dry}(i,n) \tag{C.5}$$

LDF equation:

$$\frac{u_t(i,n) - u_t(i,n-1)}{\Delta t} = k(u(i,n) - u_t(i,n)) \tag{C.6}$$

Volumetric constraint equation:

$$\varepsilon_d + \varepsilon_g(i,n) + \varepsilon_l(i,n) = 1 \tag{C.7}$$

Effective parameters:

$$\rho_{eff}(i,n) = \varepsilon_g(i,n) \cdot (\rho_v(i,n) + \rho_a(i,n)) + \varepsilon_l(i,n)\rho_l + \varepsilon_d(i,n)\rho_d \tag{C.8}$$

$$c_{p_{eff}}(i,n) = \frac{\varepsilon_g(i,n)\big(\rho_v(i,n)c_{p,v} + \rho_a(i,n)c_{p,a}\big) + \varepsilon_l(i,n)\rho_l c_{p,l} + \varepsilon_d \rho_d c_{p,d}}{\rho_{eff}(i,n)} \tag{C.9}$$

$$k_{eff}(i,n) = \varepsilon_g(i,n) \cdot \left(\frac{\rho_v(i,n)k_v + \rho_a(i,n)k_a}{\rho_v(i,n) + \rho_a(i,n)}\right) + \varepsilon_l(i,n)k_l + \varepsilon_d k_d \tag{C.10}$$

Thermodynamic relationships:

$$P_v(i,n) = \rho_v(i,n)R_v T(i,n) \tag{C.11}$$

$$P_a(i,n) = \rho_a(i,n)R_a T(i,n) \tag{C.12}$$

$$P_a(i,n) = P_g(i,n) - P_v(i,n) \tag{C.13}$$

$$\rho_g(i,n) = \rho_a(i,n) + \rho_v(i,n) \tag{C.14}$$

$$RH(i,n) = \left.\frac{P_v(i,n)}{P_{v,sat}(i,n)}\right|_T \tag{C.15}$$

where:

$$P_{v,sat}(i,n) = \exp\left(\frac{C_1}{T(i,n)} + C_2 + C_3 T(i,n) + C_4 T^2(i,n) + C_5 T^3(i,n) \right. \tag{C.16}$$
$$\left. + C_6 \ln T(i,n)\right)$$

Boundary conditions:

At $x = 0$ (*i.e.,* convective heat and mass transfer)

$$h_h(Ti,n) - T_\infty) = k_{eff}\left(\frac{-3T(i,n) + 4T(i+1,n) - T(i+2,n)}{2\Delta x}\right) \tag{C.17}$$

$$h_m(\rho_v(i,n) - \rho_{v,\infty}) = D_{eff}\left(\frac{-3\rho_v(i,n) + 4\rho_v(i+1,n) - \rho_v(i+2,n)}{2\Delta x}\right) \tag{C.18}$$

At $x = L$ (*i.e.,* adiabatic and impermeable)

$$-3T(i,n) \; + \; 4T(i+1,n) \; - \; T(i+2,n) \; = \; 0 \qquad\qquad \text{(C.19)}$$

$$-3\rho_v(i,n) \; + \; 4\rho_v(i+1,n) \; - \; \rho_v(i+2,n) \; = \; 0 \qquad\qquad \text{(C.20)}$$

C.2   COMPUTER SIMULATION PROGRAM

The computer simulation program presented in this section is written using MATLAB R2020b. The code presented in this section is the general program used by the author. However, it should be noteworthy that modifications were made as required in order to generate many other results (*i.e.,* effect of kinetics, particle size, etc.).

```
% Teddy Okolo
% 16 Feb 2021
% Transient 1D porous media model for heat and moisture transfer
% Warm and humid air flows over the top of the desiccant bed
% Convective heat and mass transfer boundary conditions at the top
% No heat and mass transfer at the bottom and sides of the bed

clear
clc
tic

%===================================================
% Physical data
%===================================================

L = 0.015;              % (m) Bed thickness

T_a = 297.15;           % (K) Warm air temperature
T_d = 313.15;           % (K) Cold desiccant bed surface temperature

RH_a = 0.5;             % RH of the humid air
RH_d = 0;               % RH in the dry desiccant layer

Cp_d = 921;             % (J/kgK) Specific heat capacity of desiccant
Cp_a = 1005;            % (J/kgK) Specific heat capacity of air
Cp_v = 1864;            % (J/kgK) Specific heat capacity of water vapour
Cp_l = 4180;            % (J/kgK) Specific heat capacity of liquid water

k_d = 0.2;              % (W/mK) Thermal conductivity of desiccant
k_a = 0.0262;           % (W/mK) Thermal conductivity of air
k_v = 0.019;            % (W/mK) Thermal conductivity of water vapour
k_l = 0.6048;           % (W/mK) Thermal conductivity of liquid water

ro_des = 700;           % (kg/m^3) Density of dry desiccant
ro_air = 1.188;         % (kg/m^3) Density of humid air
ro_liq = 997.3;         % (kg/m^3) Density of liquid water
```

```matlab
R_a = 287;                  % (J/kgK) Gas constant of air
R_v = 461.5;                % (J/kgK) Gas constant of water vapour

hfg = 2600E3;               % (J/kg) Latent heat of phase change (i.e. 2590E3)

D_ab = 2.54E-4;             % (m^2/s) Binary diffusion coefficient

tau = 3.0;                  % (-) Tortuosity of the desiccant

h_h = 40.0;                 % (W/m^2K) Heat transfer coefficient
h_m = 0.04;                 % (m/s) Mass transfer coefficient

Bi_hh = (h_h * L)/k_d;      % (-) Heat transfer Biot number
Bi_hm = (h_m * L)/k_d;      % (-) Mass transfer Biot number

P_total = 1.01325E5;        % (Pa) Total pressure

k = 0.001397222;            % (s^-1) Sorption rate constant from LDF model
0.001397222
kg = 0.001132;
kb = 0.001307;
kw = 0.000809;
kzw = 00012;
k2 = 1.44*k;
k3 = 0.64*k;

C1 = -5.8002206 * 10^3; % Constants for calculating Pv,sat
C2 =  1.3914993;
C3 = -4.8640249 * 10^-2;
C4 =  4.1764768 * 10^-5;
C5 = -1.4452093 * 10^-8;
C6 =  6.5459673;

% Saturation vapour pressure for 0 < T < 200 K
Pv_sat1 = exp(C1/T_a + C2 + C3*T_a + (C4*T_a^2) + (C5*T_a^3) + C6*log(T_a));
% (Pa) Saturation air vapor pressure
Pv_sat2 = exp(C1/T_d + C2 + C3*T_d + (C4*T_d^2) + (C5*T_d^3) + C6*log(T_d));
% (Pa) Saturation vapor pressure in desiccant layer

%================================================================
% Numerical paramaters
%================================================================

iMax = 51;                 % (-) Total grid nodes
nMax = 601;                % (-) Total time steps
dz = L/(iMax-1);           % (m) Grid size
dt = 0.1;                  % (s) Time step
conv = 1E-7;               % (-) Convergence criterion
relax_T = 0.65;            % (-) Relaxation factor for temperature
relax_Ro = 0.002;          % (-) Relaxation factor for vapor density


%================================================================
% Main Preallocation
%================================================================

P_v1 = RH_a * Pv_sat1;              % (Pa) Air vapor pressure
ro_v1 = P_v1/(R_v * T_a);           % (kg/m^3) Air vapor density
```

```matlab
P_v2 = RH_d * Pv_sat2;              % (Pa) Vapor pressure in the desiccant
layer
ro_v2 = P_v2/(R_v * T_d);           % (kg/m^3) Vapor density in the desiccant
layer

ep_l = zeros(iMax,nMax);
ep_g = zeros(iMax,nMax);
ro_v = zeros(iMax,nMax);
ro_g = zeros(iMax,nMax);
ro_a = zeros(iMax,nMax);
ro_dry = ones(iMax,nMax);
ro_eff = zeros(iMax,nMax);
Cp_eff = zeros(iMax,nMax);
k_eff = zeros(iMax,nMax);
D_eff = zeros(iMax,nMax);
T = zeros(iMax,nMax);
M = zeros(iMax,nMax);
U = zeros(iMax,nMax);               % (g/g) equilibrium sorption quantity or
uniform moisture content
U_T = zeros(iMax,nMax);             % (g/g) dynamic sorption quantity at time
't' (LDF Model)
M_old = zeros(iMax,nMax);
time = zeros(1,nMax);
dDv_dz = zeros(1,iMax);
depg_dt = zeros(1,iMax);
dk_dz = zeros(1,iMax);
RH = zeros(iMax,nMax);
RH_old = zeros(1,iMax);
T_old = zeros(1,iMax);
ro_old = zeros(1,iMax);
Pv = zeros(1,iMax);
Pv_sat = zeros(1,iMax);
ro_v_sat = zeros(1,iMax);
space = zeros(1,iMax);
A = zeros(iMax-1,iMax-1);
R_A  = zeros(1,iMax-1);
B = zeros(iMax-1,iMax-1);
R_B = zeros(1,iMax-1);
error_T = zeros(1,iMax);
error_Ro = zeros(1,iMax);
res_t = zeros(iMax,nMax);
res_ro = zeros(iMax,nMax);
q_air = zeros(1,nMax);
q_des = zeros(iMax,nMax);
q_balance = zeros(1,nMax);
m_air = zeros(1,nMax);
m_balance = zeros(1,nMax);

for n = 1:nMax
    time(n) = (n-1) * dt;
end

for i = 1:iMax
    space(i) = (i-1) * dz;
end
```

```matlab
%=======================================================
% Initial conditions
%=======================================================

for i = 1:iMax
    T(i,1) = T_d;
    ro_v(i,1) = ro_v2;
    ro_old(i) = ro_v2;
    RH(i,1) = RH_d;
    RH_old(i) = RH_d;
    ep_d = 0.55;
    ep_g(i,1) = 1 - ep_d;
    ep_l(i,1) = 0;
    M(i,1) = 0;
    U_T(i,1) = 0;
    U(i,1) = 0;
    ro_dry(i,1) = ep_d*ro_des;
end


%=======================================================
% Main code
%=======================================================

% Initializing step n in one loop

for n = 2:nMax

    for i = 1:iMax
        T(i,n) = T(i,n-1);
        ro_v(i,n) = ro_v(i,n-1);
        ep_g(i,n) = ep_g(i,n-1);
    end

    count_err = 0;
    max_err = 1;

% Inner convergence loop for specific time

    while (max_err) > conv

        for i= 1:iMax
            Pv_sat(i,n) = exp(C1/T(i,n) + C2 + C3*T(i,n) + (C4*(T(i,n)^2)) +
(C5*(T(i,n)^3)) + C6*log(T(i,n)));

            ro_v_sat(i,n) = Pv_sat(i,n) / (R_v * T(i,n));
            Pv(i,n) = ro_v(i,n) * R_v * T(i,n);
            RH(i,n) = Pv(i,n) / Pv_sat(i,n);
            U(i,n) = (0.2227*(RH(i,n).^3)) + (0.6646*(RH(i,n).^2)) -
(0.1375.*RH(i,n)) + 0.0154;
            M(i,n) = ((U(i,n) - U(i,n-1)) * ro_dry(i,n)) / dt;
        end


        for i = 1:iMax
            ep_l(i,n) = ep_l(i,n-1) + (M(i,n) * dt / ro_liq);
            ep_g(i,n) = 1.0 - ep_l(i,n) - ep_d;

    % Calculation of effective paramters
```

```
        Pa = P_total – Pv(i);
        ro_a(i,n) = Pa / (R_a * T(i,n));
        ro_g(i,n) = ro_a(i,n) + ro_v(i,n);
        ro_eff(i,n) = (ep_d * ro_des) + (ep_l(i,n) * ro_liq) + (ep_g(i,n)
* ro_g(i,n));
        Cp_g = (Cp_v * ro_v(i,n) + Cp_a * ro_a(i,n)) / ro_g(i,n);
        Cp_eff(i,n) = ((ep_d * ro_des * Cp_d) + (ep_l(i,n) * ro_liq *
Cp_l) + (ep_g(i,n) *ro_g(i,n) * Cp_g)) / ro_eff(i,n);
        k_eff(i,n) = ((ep_d * k_d) + (ep_l(i,n) * k_l)) + (ep_g(i,n) * (
ro_a(i,n) * k_a + ro_v(i,n)* k_v) / ro_g(i,n));
        D_eff(i,n) = (ep_g(i,n) * D_ab) / tau;
    end

% Solving the Temperature field

    for i = 2:iMax-1
        dk_dz(i) = (k_eff(i+1,n) – k_eff(i-1,n)) / (2*dz);
    end

    i = 1;
    A(i,i) = –3 – ((2*dz*h_h) / k_eff(i,n));
    A(i,i+1) = 4;
    A(i,i+2) = –1;
    R_A(i) = –2 * dz * (h_h / k_eff(i,n)) * T_a;

    i = iMax;
    A(i,i) = –3;
    A(i,i-1) = 4;
    A(i,i-2) = –1;
    R_A(i) = 0;

    for i = 2:iMax-1
        A(i,i) = –(2*k_eff(i,n)/(dz^2) + ro_eff(i,n)*Cp_eff(i,n)/dt);
        A(i,i+1) = (dk_dz(i)/(2*dz) + k_eff(i,n)/(dz^2));
        A(i,i-1) = (–dk_dz(i)/(2*dz) + k_eff(i,n)/(dz^2));
        R_A(i) =  –(hfg * M(i,n)) – ((ro_eff(i,n) * Cp_eff(i,n)/dt) *
T(i,n-1));
    end
        T_result = A\R_A';

    for i = 1:iMax
        T(i,n) = T(i,n) + (relax_T * (T_result(i) – T(i,n)));
    end

% Updating properties...
    for i= 1:iMax
        Pv_sat(i,n) = exp(C1/T(i,n) + C2 + C3*T(i,n) + (C4*(T(i,n)^2)) +
(C5*(T(i,n)^3)) + C6*log(T(i,n)));

        ro_v_sat(i,n) = Pv_sat(i,n) / (R_v * T(i,n));
        Pv(i,n) = ro_v(i,n) * R_v * T(i,n);
        RH(i,n) = Pv(i,n) / Pv_sat(i,n);
        U(i,n) = (0.2227*(RH(i,n).^3)) + (0.6646*(RH(i,n).^2)) –
(0.1375.*RH(i,n)) + 0.0154;
        M(i,n) = ((U(i,n) – U(i,n-1)) * ro_dry(i,n)) / dt;
    end
```

```matlab
        for i = 1:iMax
            ep_l(i,n) = ep_l(i,n-1) + (M(i,n) * dt / ro_liq);
            ep_g(i,n) = 1.0 - ep_l(i,n) - ep_d;

    % Calculation of effective paramters

            Pa = P_total - Pv(i);
            ro_a(i,n) = Pa / (R_a * T(i,n));
            ro_g(i,n) = ro_a(i,n) + ro_v(i,n);
            ro_eff(i,n) = (ep_d * ro_des) + (ep_l(i,n) * ro_liq) + (ep_g(i,n)
 * ro_g(i,n));
            Cp_g = (Cp_v * ro_v(i,n) + Cp_a * ro_a(i,n)) / ro_g(i,n);
            Cp_eff(i,n) = ((ep_d * ro_des * Cp_d) + (ep_l(i,n) * ro_liq *
Cp_l) + (ep_g(i,n) *ro_g(i,n) * Cp_g)) / ro_eff(i,n);
            k_eff(i,n) = ((ep_d * k_d) + (ep_l(i,n) * k_l)) + (ep_g(i,n) * ((
ro_a(i,n) * k_a + ro_v(i,n)* k_v) / ro_g(i,n)));
            D_eff(i,n) = (ep_g(i,n) * D_ab) / tau;
        end

    % Solving the vapour density field

        for i=2:iMax-1
            dDv_dz(i) = (D_eff(i+1,n) - D_eff(i-1,n)) / (2*dz);
            depg_dt(i) = (ep_g(i,n) - ep_g(i,n-1)) / dt;
        end

        i = 1;
        B(i,i) = -3 - ((2 * dz * h_m) /D_eff(i,n));
        B(i,i+1) = 4;
        B(i,i+2) = -1;
        R_B(i) = -2*dz * (h_m/D_eff(i,n)) * ro_v1;

        i = iMax;
        B(i,i) = -3;
        B(i,i-1) = 4;
        B(i,i-2) = -1;
        R_B(i) = 0;

        for i=2:iMax-1
            B(i,i) = (-2*D_eff(i,n)/(dz^2)) - depg_dt(i) - (ep_g(i,n)/dt);
            B(i,i+1) = (dDv_dz(i)/(2*dz)) + (D_eff(i,n)/(dz^2));
            B(i,i-1) = (-dDv_dz(i)/(2*dz)) + (D_eff(i,n)/(dz^2));
            R_B(i) = M(i,n) - ((ep_g(i,n) * ro_v(i,n-1))/dt);
        end

        ro_result = B\R_B';

        for i=1:iMax
            if RH(i,n) < 1
                ro_v(i,n) = ro_v(i,n) + (relax_Ro * (ro_result(i) -
ro_v(i,n)));
            end
        end

    % Calculating error estimates for temperature and vapour density fields

        for i = 1:iMax
            if T_old(i) ~= 0 && ro_old(i) ~= 0
```

```
                    error_T(i,n) = abs(T_old(i) - T(i,n));
                    error_Ro(i,n) = abs(ro_old(i) - ro_v(i,n));
                end
            end

        max_err = max(max(error_T(:,n),error_Ro(:,n)));

        for i = 1:iMax
            T_old(i) = T(i,n);
            ro_old(i) = ro_v(i,n);
            M_old(i) = M(i,n);
        end

    % End of while loop

    count_err = count_err + 1;

    end

    for i = 1:iMax
        RH_old(i) = RH(i,n);
    end

    % Solving for residuals in energy equation and water balance equation

    for i = 2:iMax-1
        dk_dz(i) = (k_eff(i+1,n) - k_eff(i-1,n)) / (2*dz);
        res_t(i,n) = ((ro_eff(i,n)*Cp_eff(i,n)/dt)*(T(i,n) - T(i,n-1))) -
(M(i,n)*hfg) - ((dk_dz(i)/(2*dz)) * ((T(i+1,n) - T(i-1,n))/(2*dz))) -
((k_eff(i,n)/(dz^2)) * (T(i+1,n) - (2*T(i,n)) + T(i-1,n)));

        dDv_dz(i) = (D_eff(i+1,n) - D_eff(i-1,n)) / (2*dz);
        depg_dt(i) = (ep_g(i,n) - ep_g(i,n-1)) / dt;
        res_ro(i,n) = (((depg_dt(i)/dt) * ro_v(i,n)) + ((ep_g(i,n)/dt) *
(ro_v(i,n) - ro_v(i,n-1))) + M(i,n) - ((dDv_dz(i)/(2*dz)) * (ro_v(i+1,n) -
ro_v(i-1,n))) - ((D_eff(i,n)/(dz^2)) * (ro_v(i+1,n) - (2*ro_v(i,n)) + ro_v(i-
1,n))));
    end

    resid_T = max(abs(res_t));
    resid_Ro = max(abs(res_ro));



%========================================================================
    % ENERGY AND MASS BALANCE
%========================================================================

    % Energy balance
    q_air(n) = h_h * (T_a - T(1,n));

    for i=1:iMax
        q_des(i,n) = (hfg * M(i,n) + ((ro_eff(i,n) * Cp_eff(i,n)) / dt) *
(T(i,n) - T(i,n-1)));
    end

        q_stored = mean(q_des);
        q_balance(n) = q_air(n) + q_stored(n);
```

```matlab
    % Mass balance

        m_air(n) = h_m * (ro_v1 - ro_v(1,n));
        m_stored = mean(M);
        m_balance(n) =  m_air(n) + m_stored(n);


    % END OF MAIN LOOP
end

toc
TIME = toc;
disp(datestr(datenum(0,0,0,0,0,TIME),'HH:MM:SS'))
```

SENSITIVITY STUDIES ON NUMERICAL PARAMETERS

In order to investigate the reliability of the numerical solution, sensitivity studies are conducted on the numerical parameters (time step, grid size and convergence criterion) to determine their respective impacts on the numerical results. This sensitivity was done at position $x = L/2$ in the desiccant and at the initial conditions shown in Chapter 3, to select suitable numerical parameters for the simulations. Figures D.1 – D.3 contain the numerical results for temperature and moisture content in the desiccant as a function of time step, grid size and convergence criterion respectively.


(a) (b)
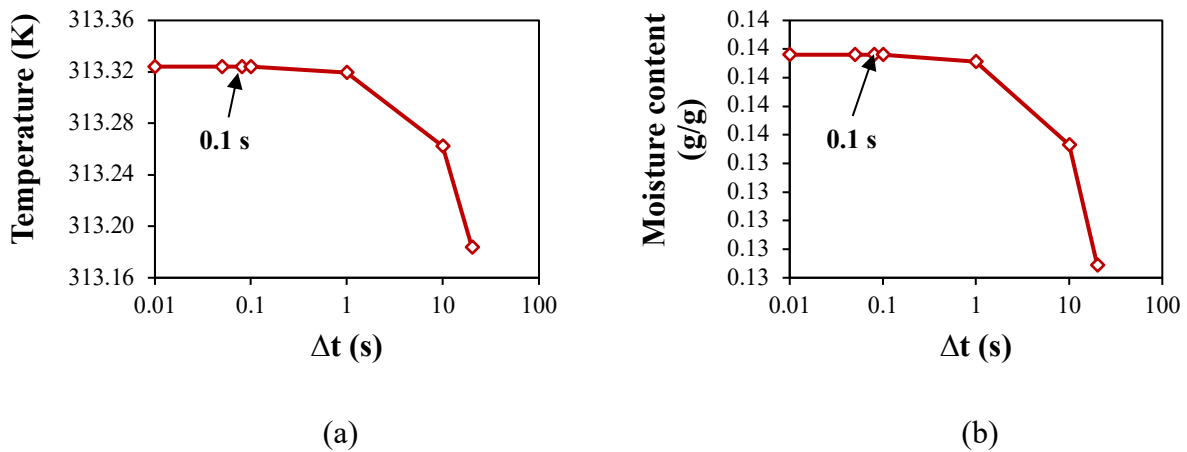
Figure D. 1. Sensitivity study showing the effect of time step on (a) temperature, and (b) moisture content in the desiccant at position $L/2$.


(a) (b)
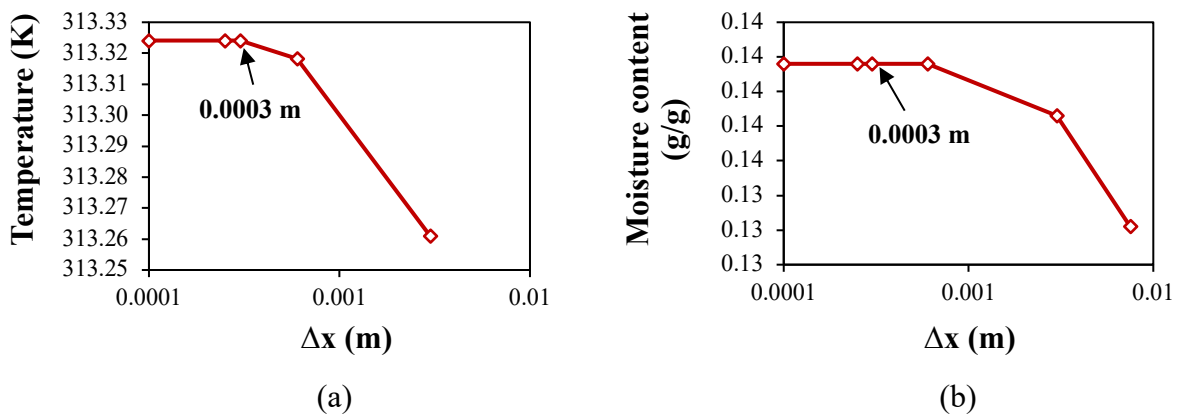
Figure D. 2. Sensitivity study showing the effect of grid size on (a) temperature, and (b) moisture content in the desiccant at position $L/2$.
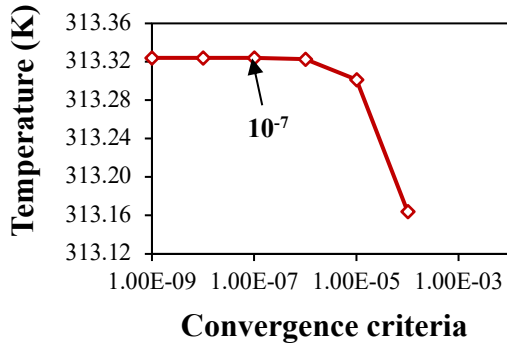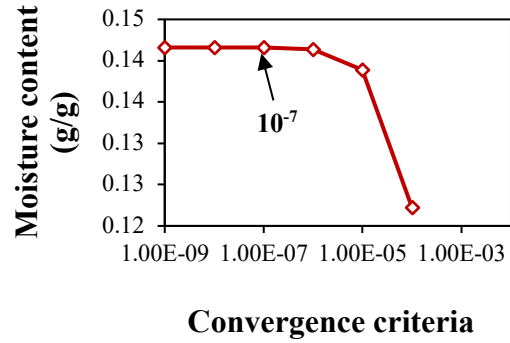
Figure D. 3. Sensitivity study showing the effect of convergence criterion on (a) temperature, and (b) moisture content in the desiccant at position $L/2$.

As observed form Figures D.1 – D.3, for all cases of coupled heat and moisture transfer, the appropriate time step, grid size and convergence criterion were 0.1 s, 0.0003 m and 1×10^{-7} respectively. As such, these were the numerical values used in all cases for the MATLAB simulations.